

**DESARROLLO DE MATERIALES AVANZADOS A PARTIR DE
NANOCELULOSA DE FIQUE**

**SERGIO ANDRÉS OVALLE SERRANO
B.S. CHEMISTRY**

**UNIVERSIDAD INDUSTRIAL DE SANTANDER
FACULTAD DE CIENCIAS
ESCUELA DE QUÍMICA
DOCTORADO EN QUIMICA
BUCARAMANGA
2018**

**DESARROLLO DE MATERIALES AVANZADOS A PARTIR DE
NANOCELULOSA DE FIQUE**

SERGIO ANDRÉS OVALLE SERRANO

**A doctoral dissertation submitted in partial fulfillment of the requirements for
the Doctor degree in Chemistry**

Advisors

Dr. Marianny Yajaira Combariza Montañez

Dr. Cristian Blanco Tirado

UNIVERSIDAD INDUSTRIAL DE SANTANDER

FACULTAD DE CIENCIAS

ESCUELA DE QUÍMICA

DOCTORADO EN QUIMICA

BUCARAMANGA

2018

TABLE OF CONTENTS

	Pág.
INTRODUCTION	13
1. EXPLORING THE COMPOSITION OF RAW AND DELIGNIFIED COLOMBIAN FIQUE FIBERS, TOW AND PULP	17
1.1 ABSTRACT	17
1.2 INTRODUCTION	18
1.3 EXPERIMENTAL	24
1.3.1 Materials	24
1.3.2 Sample pretreatment	24
1.3.3 Alkaline hydrogen peroxide (AHP) treatment	25
1.3.4 Characterization methods	25
1.4 RESULTS AND DISCUSSION	27
1.4.1 Raw Fique fibers, tow and pulp characterization	27
1.4.2 Delignified Fique fibers, tow and pulp characterization	34
1.4.3 Experimental designs: optimal conditions	43
1.5 CONCLUSIONS	45
2. ISOLATION AND CHARACTERIZATION OF CELLULOSE NANOFIBRILS FROM COLOMBIAN FIQUE DECORTICATION BY-PRODUCTS	47
2.1 ABSTRACT	47
2.2 INTRODUCTION	47
2.3 EXPERIMENTAL	53
2.3.1 Materials	53
2.3.2 Tow pretreatment	53
2.3.4 TEMPO-mediated oxidation of Fique tow	54
2.3.5 Mechanical disintegration	54
2.3.6 Conversion to free carboxyl groups	55
2.3.7 Characterization	55
2.3.8 Conductimetry	56

2.4 RESULTS AND DISCUSSION	57
2.5 CONCLUSIONS	73
3. POST-OXIDATION AND HIDROFOBIZATION OF CELLULOSE NANOFIBRILS FROM COLOMBIAN FIQUE TOW	75
3.1 ABSTRACT	75
3.2 INTRODUCTION	75
3.3 EXPERIMENTAL	81
3.3.1 Materials	81
3.3.2 Fique tow treatment, delignification and TOCN extraction	81
3.3.3 Post-oxidation with NaClO ₂	82
3.3.4 Conversion to free carboxyl groups	83
3.3.5 Hydrofobization	83
3.3.6 Conductimetry	84
3.3.7 Solubility Tests	85
3.3.8 Characterization	85
3.4 RESULTS AND DISCUSSION	86
3.5 CONCLUSIONS	107
4. PREPARATION OF FUNCTIONAL HYDRO/AEROGELS FROM COLOMBIAN FIQUE TOW CELLULOSE NANOFIBRILS	108
4.1 ABSTRACT	108
4.2 INTRODUCTION	108
4.3 EXPERIMENTAL	113
4.3.1 Materials	113
4.3.2 Fique tow treatment, delignification and TOCN extraction	113
4.3.3 Preparation of hydro/aerogels	114
4.3.4 Characterization	115
4.4 RESULTS AND DISCUSSION	116
4.5 CONCLUSIONS	130
5. CONCLUSIONES	131
BIBLIOGRAFIA	134

LIST OF FIGURES

	Pàg.
Figure 1. (a) Fique fibers, (b) Fique decortication residues, (c) Clean Fique tow, and (d) Clean Fique pulp	21
Figure 2. (a) IR spectra and (b) XRD patterns of Fique fibers, tow and pulp.	29
Figure 3. SEM images of (a) Fique fibers, (b) Fique tow and (c) Fique pulp.	34
Figure 4. Optical images of (a) raw and (b) delignified Fique fibers/tow. (c) IR spectra, (d) XRD patterns and FESEM images of (e) raw and (f) delignified Fique fibers/tow.	37
Figure 5. Optical images of (a) raw and (b) delignified Fique pulp. (c) IR spectra and (d) XRD patterns of cellulosic filaments (blue trace) and leaf epidermis (green trace) in delignified Fique pulp. FESEM images of (e) cellulosic filaments and (f) leaf epidermis in delignified Fique pulp.	38
Figure 6. TGA and DTG thermograms of (a) raw and (b) delignified fibers/tow and DSC thermograms (c) for raw and delignified fibers/tow.	40
Figure 7. Crystallinity index as a function of H ₂ O ₂ concentration and reaction time using (a) 1% w/v and (b) 8% w/v loadings.	44
Figure 8. Images of (a) untreated and (b) delignified Fique tow. FESEM images of (c) untreated and (d) delignified Fique tow.	60
Figure 9. (a) Delignified Fique tow TOCN aqueous suspension (0.5 %wt.), (b) gel-like appearance of TOCN in free acid form and (c) Optical phenomena of birefringence.	61
Figure 10. Fique tow TOCN: (a) ζ potential and carboxylate contents, (b) FESEM image.	65
Figure 11. (a) IR-ATR spectra and (b) XRD patterns of untreated, delignified, TOCN-COO ⁻ Na ⁺ and TOCN-COOH Fique tow.	69
Figure 12. (a) TGA curves and (b) DTG curves for raw Fique tow, delignified Fique tow and TOCN.	71

Figure 13. Images of (a) untreated and (b) delignified Fique tow, (c) TOCN in water and (d) TOCN-ODA in toluene.	87
Figure 14. TEMPO-mediated oxidation of primary hydroxyls to carboxyl groups.	88
Figure 15. FESEM images of (a) untreated and (b) delignified Fique tow, (c) TOCN, (d) TOCN-P, (e) TOCN-ODA and (f) TOCN-P-ODA.	92
Figure 16. 'One-pot' TBTU amidation mechanism for TOCN surface modification. Adapted from Gómez et al.	94
Figure 17. (a) Complete and (b) zoomed IR-ATR spectra of Fique tow: untreated, delignified, TOCN, TOCN-P, TOCN-ODA and TOCN-P-ODA and representation of their chemical structure.	96
Figure 18. X-ray diffraction profiles of Fique tow: untreated, delignified, TOCN, TOCN-P, TOCN-ODA and TOCN-P-ODA.	99
Figure 19. Images of (a) TOCN/water (b) TOCN/toluene (c) TOCN-ODA/water (d) TOCN-ODA/toluene and e) Light transmittance spectra of TOCN-(P) in water and TOCN-(P)-ODA in toluene dispersions.	102
Figure 20. Thermogravimetical behavior of Fique tow: untreated, delignified, TOCN, TOCN-P, TOCN-ODA and TOCN-P-ODA. (a) TG and (b) DTG curves.	105
Figure 21. Contact angle for a) TOCN, b) TOCN-P, c) TOCN-ODA and d) TOCN-P-ODA films.	106
Figure 22. Optical images of (a) raw and (b) delignified Fique tow, (c) TOCN aqueous suspension, (d) TOCN aerogel, (e) TOCN-Ag NPs hydrogel and (f) TOCN-Ag NPS aerogel.	118
Figure 23. Scheme for the synthesis of Ag NPs in TOCN suspensions.	120
Figure 24. UV-Vis spectra of TOCN suspensions and TOCN-Ag NPs hydrogels prepared at 60 °C.	123
Figure 25. FESEM images of (a) raw and (b) delignified Fique tow, (c) air-dried TOCN suspension, (d) TOCN aerogels and (e) and (f) TOCN-Ag NPs aerogels.	125
Figure 26. (a) IR spectra and (b) XRD patterns of Raw and delignified Fique tow, TOCN suspensions and TOCN-Ag NPs hydrogels.	128

Figure 27. (a) TGA curves and (b) DTG curves for raw Figue tow, delignified Figue tow, TOCN and TOCN-Ag NPs hydrogels.

129

LIST OF TABLES

	Pàg.
Table 1. Experimental matrix for Fique fibers/tow delignification.	25
Table 2. Chemical composition of Fique pulp, tow and fibers (this work) compared to other pulp and fibers sources.	27
Table 3. Elemental analyses by XRF for Fique fibers, tow and bagasse.	32
Table 4. Effects on crystallinity index after AHP process.	44
Table 5. Degree of oxidation (DO), degree of coupling after amidation process (DC), carboxylate content (σ) (by conductimetric titration and methylene blue adsorption (MBA)) and ζ -potential of Fique tow: untreated, delignified, TOCN, TOCN-R, TOCN-ODA and TOCN-R-ODA.	101

RESUMEN

Título: Desarrollo de materiales avanzados a partir de nanocelulosa de fique*¹

Autor: Sergio Andrés Ovalle Serrano**²

Palabras clave: fique, nanocelulosa, fibras naturales, nanopartículas, materiales funcionales

Descripción

Las fibras de fique son extraídas de las hojas de *Furcraea spp*, representando un 5% en peso de sus hojas. Sin embargo, los subproductos, correspondientes a jugo, bagazo y estopa, representan el 95% restante y son considerados desechos. En este trabajo se estudiaron y reportaron, por primera vez, las propiedades espectroscópicas, microscópicas y térmicas de las fibras, estopa y bagazo de fique. Además, estos materiales se sometieron a un proceso de deslignificación con peróxido de hidrógeno alcalino para remover materiales amorfos (lignina y hemicelulosa). Los productos deslignificados también fueron estudiados en términos de composición química, estructura y morfología. La celulosa obtenida se usó para la extracción de nanofibras de celulosa (NFC) mediante una reacción de oxidación con TEMPO, asistida con ultrasonido, seguida de una desintegración mecánica, proceso aplicado por primera vez sobre la estopa de fique. Las NFC presentaron diámetros de 60-100 nm, densidad de carga superficial de 1.6 mmol COOH/g celulosa y alta estabilidad coloidal debido a un alto potencial ζ (-53 mV).

Por otro lado, se investigó el efecto de la postoxidación de las NFC y su hidrofobización mediante reacción de amidación 'one-pot'. La alta densidad de carga superficial fue decisiva en el acoplamiento de largas cadenas alifáticas en la superficie de las NFC para formar el producto amidado. Se observó que entre más hidrofílico fuera el material de partida, más hidrofóbico sería el producto amidado. Finalmente, en este trabajo también se reporta un método 'one-pot', amigable con el medio ambiente para la preparación de hidro/aerogeles funcionales mediante la síntesis de nanopartículas de plata en suspensiones de NFC extraídas de estopa de fique, usando sólo agua como solvente. Los resultados mostraron que, a mayores concentraciones de sal precursora, mayor cantidad de nanopartículas de plata formadas y mayor estabilidad del hidrogel formado.

* Tesis doctoral

** Facultad de ciencias. Escuela de Química. Doctorado en Química. Directora: Marianny Yajaira Combariza Montañez, Ph.D. Codirector: Cristian Blanco Tirado, Ph.D.

ABSTRACT

Title: Advanced materials from fique nanocellulose*³

Author: Sergio Andrés Ovalle Serrano**⁴

Keywords: fique, nanocellulose, natural fibers, nanoparticles, functional materials

Description

Fique fibers are extracted from *Furcraea spp* leaves, with 5% average mass yield, using mechanical decortication. Juice, pulp and tow, the by-products of this process, amount 95% of the leaf weight and are considered waste. In this work is studied and reported, for the first time, the spectroscopic, microscopic and thermal properties of raw Fique fibers, tow and pulp. In addition, these materials were subjected to ultrasound-assisted alkaline hydrogen peroxide treatment (AHP) to remove amorphous materials (hemicellulose and lignin). The delignified products were also studied to determine composition, structure and morphology and to determine the effect of the AHP treatment on the original biomass. Additionally, this contribution reported for the first time the extraction and characterization of nanocellulose from fique tow by chemical methods. Cellulose nanofibrils (CNF) were extracted via ultrasound-assisted TEMPO followed by mechanical disintegration with sonication. Fique CNF exhibit diameters in the range of 60-100 nm, surface charge density of 1.6 mmol COOH/g cellulose and high colloidal stability due to a high ζ potential (-53 mV).

Furthermore, the effect of post-oxidation of CNF produced from delignified Fique tow and its hydrophobization by means of a 'one-pot' amidation reaction was investigated in the present work. The high surface charge density was decisive in the coupling of long aliphatic chains on the surface of CNF to form the amidated product. It showed that the more hydrophilic the starting material became, the more hydrophobic the amidated product. Finally, in this work is reported an environmentally benign 'one-pot' method for the production of functional hydro/aerogels by synthesizing silver nanoparticles in suspensions of CNF extracted from fique tow, using only water as solvent. Results showed that higher precursor amounts increased the amount of silver nanoparticles and added some stability to the hydrogel.

* Doctoral thesis

** Faculty of Science. School of Chemistry. Doctorate in Chemistry. Director: Marianny Yajaira Combariza Montañez, Ph.D. Codirector: Cristian Blanco Tirado, Ph.D.

INTRODUCTION

Cellulose, the most abundant biopolymer on Earth, has attracted the interest of the research community for being a renewable resource available in vast quantities with extraordinary features, making it a competing and sustainable engineering material.⁵ Cellulose is the main structural component in cell walls of most plants but is also produced by algae, bacteria and animals (tunicate)⁶. Together with hemicelluloses and lignin, cellulose assemble a hierarchical fiber-like structure responsible for the high strength, stability, and durability of plants⁷.

In recent times, governments and industries have been attempting to decrease the use of petroleum-derived products due to their negative environmental impact. In this fashion, many studies have been focusing on the use of natural materials because of their economical and environmental advantages compared to traditional products. Natural fibers are a good example of natural materials. They are characterized by their biodegradability, availability, low density, thermal stability and mechanical properties⁸.

In Colombia, the quintessential natural fiber is the Fique fiber. Colombia is the largest producer of Fique fibers in the world, with a net production of at least 30,000 tons per year. These fibers are commonly used in the manufacture of ropes, cordages and packaging materials such as coffee sacks⁹. However, the fiber extraction

⁵ Hamou K Ben, Kaddami H, Dufresne A, et al (2018) Impact of TEMPO-oxidization strength on the properties of cellulose nanofibril reinforced polyvinyl acetate nanocomposites. *Carbohydr Polym* 181:1061–1070 . doi: 10.1016/j.carbpol.2017.11.043

⁶ Stelte W, Sanadi AR (2009) Preparation and Characterization of Cellulose Nanofibers from Two Commercial Hardwood and Softwood Pulps. *Ind Eng Chem Res* 48:11211–11219 . doi: 10.1021/ie9011672

⁷ Isogai A, Bergström L (2018) Preparation of cellulose nanofibers using green and sustainable chemistry. *Curr Opin Green Sustain Chem* 12:15–21 . doi: 10.1016/j.cogsc.2018.04.008

⁸ Senthil Muthu Kumar T, Rajini N, Obi Reddy K, et al (2018) All-cellulose composite films with cellulose matrix and Napier grass cellulose fibril fillers. *Int J Biol Macromol* 112:1310–1315 . doi: 10.1016/j.ijbiomac.2018.01.167

⁹ Peinado JE, Ospina LF, Rodríguez L, et al (2006) Guía Ambiental del Subsector Fiquero. Cadena Productiva Nacional del Fique, Bogotá

process produces not only the widely known fiber (5% wt.), but also by-products such as juice, pulp and tow (95% wt.). Tow and pulp, catalogued as secondary cellulosic sources, represent around 25% wt. of the Fique leaf weight and are currently considered (and treated) as waste, being left to decompose in the crop or discarded in bodies of surface water¹⁰.

The amount of studies focusing on the use of agro-industrial wastes is growing at a high rate. Most of them are working on the production of valuable materials using the main components in the biomass: cellulose, hemicellulose and lignin, since they would give an added value to waste products and would take advantage of their inherent properties such as biodegradability, low density, non-toxicity, and excellent mechanical/thermal properties. With cellulose content being usually the highest among the main components in biomass, most of the reports are towards its extraction, depolymerization, functionalization, etc¹¹.

Despite the interesting features of native cellulose, its applications are somehow limited. Thus, the improvement of its performance and long-term durability becomes necessary based on the final applications. For this purpose, cellulose first is usually purified (removal of waxes, hemicelluloses and lignin) and then subjected to mechanical, biological and/or chemical process to obtain nanocellulose. Nanocellulose is the focus of many researchers nowadays due to unique properties such as very high surface area-to-volume ratio, high mechanical/thermal performance and suitability for surface functionalization. This explains its wide range of applications, since based on the surface modification (or even without any

¹⁰ Ovalle-Serrano SA, Blanco-Tirado C, Combariza MY (2018) Exploring the composition of raw and delignified Colombian fique fibers, tow and pulp. *Cellulose* 25:151–165 . doi: 10.1007/s10570-017-1599-9

¹¹ Collazo-Bigliardi S, Ortega-Toro R, Chiralt Boix A (2018) Isolation and characterisation of microcrystalline cellulose and cellulose nanocrystals from coffee husk and comparative study with rice husk. *Carbohydr Polym* 191:205–215 . doi: 10.1016/j.carbpol.2018.03.022

modification at all) can be used in medical, pharmaceutical, paper manufacturing and catalysis fields, functional materials, among others¹².

Agro-industrial biomass residues are an attractive alternative for the production of biomaterials since they are cellulose-rich and, compared to wood by-products, have lower contents of lignin and hemicelluloses. However, it is well known that chemical composition in biomass varies according to the plant species, so that it becomes necessary to study each species first, in order to know in depth its physicochemical properties and develop new applications and materials¹³.

Chapter 1 focuses on the product (fibers) and by-products (tow and bagasse) from the Fique fiber extraction process. It is given a general physicochemical characterization of these materials by means of chemical composition, spectroscopic, microscopic and thermal characterization. Additionally, Fique fibers, tow and pulp are subjected to delignification through an alkaline hydrogen peroxide process, removing up to 90% of lignin and leaving cellulose microfibrils exposed. To this extent, this is the first in-depth report on Fique by-products characterization.

Chapter 2 studies the extraction of cellulose nanofibrils from Fique tow, via an ultrasound-assisted TEMPO reaction followed by mechanical disintegration with sonication. The resultant cellulose nanofibrils had diameters around 100 nm and were analyzed through spectroscopic, microscopic and thermal characterization, as well as conductimetric titration to measure the carboxylate content and ζ potential to determine their stability in aqueous suspensions. At this regard, it is addressed the role of delignified samples as starting materials and the effects of the ultrasound during the reaction.

¹² Hamou K Ben, Kaddami H, Dufresne A, et al (2018) Impact of TEMPO-oxidization strength on the properties of cellulose nanofibril reinforced polyvinyl acetate nanocomposites. *Carbohydr Polym* 181:1061–1070 . doi: 10.1016/j.carbpol.2017.11.043

¹³ Wang B, Sain M, Oksman K (2007) Study of Structural Morphology of Hemp Fiber from the Micro to the Nanoscale. *Appl Compos Mater* 14:89–103 . doi: 10.1007/s10443-006-9032-9

Chapter 3 discusses in more depth the importance of carboxylate content in the cellulose nanofibrils, through a post-oxidation reaction of the cellulose nanofibrils obtained following the procedure in Chapter 2. It also deals with a novel procedure for the functionalization of cellulose by means of a 'one-pot' amidation reaction of cellulose nanofibrils extracted from Fique tow. The amidation reaction led to a substantial increase in the hydrophobicity of cellulose nanofibrils.

Finally, Chapter 4 presents a green 'one-pot' procedure for the preparation of functional hydro/aerogels starting from cellulose nanofibrils extracted from Fique tow and silver nanoparticles. Along this lines are discussed their physicochemical properties by spectroscopic, microscopic and thermal characterizations. The results showed the importance of parameters such assonication, temperature and salt concentration.

1. EXPLORING THE COMPOSITION OF RAW AND DELIGNIFIED COLOMBIAN FIQUE FIBERS, TOW AND PULP

1.1 ABSTRACT

As worldwide agricultural production rises, agro-industrial biomass becomes an abundant raw source for uses in energy and materials production. In Colombia Fique plants (*Furcraea spp*) are traditionally used to extract hard cellulosic fibers using mechanical decortication. Juice, pulp and tow, the by-products of this process, represent almost 95% of the Fique leaf weight and are produced in large quantities. Data on these materials is scarce and greatly needed to guide and fuel Fique agro-industrial development in Colombia. In this chapter, the physicochemical properties of Fique fibers and by-products (tow and pulp) are studied, before and after alkaline hydrogen peroxide treatment (AHP), using spectroscopic and microscopic techniques. Raw Fique tow is similar in structure and composition to Fique fibers with average cellulose, hemicellulose and lignin contents of 52.6%, 23.8% and 23.6%; in this by-product cellulose exists as a highly ordered structure with crystallinity index of 57%. Raw Fique pulp, composed of cellulose filaments from secondary cell walls and leaf epidermis, has average cellulose, hemicellulose and lignin contents of 30.5%, 29.7% and 9.6%, respectively, with cellulose exhibiting an amorphous structure with a crystallinity index of 35%. The AHP treatment of these by-products effectively removed non-cellulosic compounds such as hemicellulose and lignin. After AHP lignin content in Fique tow decreases to 2.8% while crystallinity index increases up to 73%. Likewise, Fique pulp shows a reduction in lignin to 2.1% and an increase in crystallinity index up to 47%. IR spectroscopic analyses, after AHP, show a decrease of signals attributed to hemicellulose and lignin and FESEM images show a disruption of the lamellar structure in the macro fiber by the removal of hemicellulose, lignin and ground tissue, leaving cellulose microfibrils exposed. As the first in-depth report on Fique by-products characterization, these results indicate

that pulp and tow are interesting lignocellulosic materials due to their significant content of crystalline and amorphous cellulose.

1.2 INTRODUCTION

Trends in sustainable development such as the Circular Economy concept promote the use of residual materials or wastes as raw sources for new products, in an effort to change the current Linear Economy model. Within this framework lignocellulosic biomass, derived from intensive agro-industrial activity, emerges as an attractive raw material because of its wide availability and low cost¹⁴. Biomass is catalogued depending upon the final product; for instance primary biomass sources (wood, soft and hard fibers) are used mainly for paper or textile manufacture, while secondary (bark, leaves, straw or by-products from food/agricultural/forestry) and tertiary sources (pulp, food residues, and wastes from treatments of cellulosic biomass) are used as livestock feed and raw materials for biofuel and compost production¹⁵. However, interest in secondary and tertiary biomass sources as raw materials, specifically for cellulose production, is steadily growing. Examples of successful applications based on cellulose extracted from alternative lignocellulosic sources abound in the scientific literature. For instance, production of activated carbon from by-products (leaves) from carnauba wax transformation, from macauba seeds oil extraction (endocarp), from pine nut production (shell) and from sisal fiber waste¹⁶. Also, pectin extraction from sisal waste^{17 18}; dyes adsorption from aqueous effluents

¹⁴ Malucelli LC, Lacerda LG, Dziedzic M, da Silva Carvalho Filho MA (2017) Preparation, properties and future perspectives of nanocrystals from agro-industrial residues: a review of recent research. *Rev Environ Sci Bio/Technology* 16:131–145. doi: 10.1007/s11157-017-9423-4

¹⁵ García A, Gandini A, Labidi J, et al. (2016) Industrial and crop wastes: A new source for nanocellulose biorefinery. *Ind Crops Prod* 93:26–38. doi: 10.1016/j.indcrop.2016.06.004

¹⁶ da Silva Lacerda V, López-Sotelo JB, Correa-Guimarães A, et al. (2015) Rhodamine B removal with activated carbons obtained from lignocellulosic waste. *J Environ Manage* 155:67–76. doi: 10.1016/j.jenvman.2015.03.007

¹⁷ Santos JDG, Espeleta AF, Branco A, de Assis SA (2013) Aqueous extraction of pectin from sisal waste. *Carbohydr Polym* 92:1997–2001. doi: 10.1016/j.carbpol.2012.11.089

¹⁸ Maran JP, Priya B (2015) Ultrasound-assisted extraction of pectin from sisal waste. *Carbohydr Polym* 115:732–738. doi: 10.1016/j.carbpol.2014.07.058

using cellulose extracted from banana and orange peels¹⁹, and the use of jute by-products in the manufacture of pulp and paper, rayon, and cardboard, among others²⁰.

In Colombia, Fique plants (*Furcraea spp*) are traditionally used to extract hard cellulosic fibers. Tunosa común (*Furcraea gigantea*), uña de águila (*Furcraea macrophylla*), ceniza (*Furcraea cabuya*), bordo de oro (*Furcraea castilla*) and rabo de chucha (*Furcraea andina*) are amongst the most common species grown in Colombia for agro-industrial purposes²¹. The fiber extraction process, which involves mechanical decortication, results not only in fiber production (Figure 1.a) but also in by-products such as juice, pulp and tow (Figure 1.b). These by-products, catalogued as secondary cellulosic sources and currently considered (and treated) as waste, represent almost 95% of the Fique leaf weight; with current handling practices, they are left to decompose in the crop or discarded in bodies of surface water resulting in an environmental pollution problem^{22 23}. Juice, pulp and tow are generated in large quantities, since Colombia produces approximately 30.000 tons of Fique fibers per year. Although some information is available in literature about the structure and

¹⁹ Annadurai G, Juang R-S, Lee D-J (2002) Use of cellulose-based wastes for adsorption of dyes from aqueous solutions. *J Hazard Mater* 92:263–274. doi: 10.1016/S0304-3894(02)00017-1

²⁰ Gopal M, Mathew MD (1986) The scope for utilizing jute wastes as raw materials in various industries: A review. *Agric Wastes* 15:149–158. doi: 10.1016/0141-4607(86)90046-6

²¹ Peinado JE, Ospina LF, Rodríguez L, et al. (2006) *Guía Ambiental del Subsector Fiquero*. Cadena Productiva Nacional del Fique, Bogotá

²² Gañán P, Mondragon I (2002) Surface modification of Fique fibers. Effect on their physico-mechanical properties. *Polym Compos* 23:383–394. doi: 10.1002/pc.10440

²³ Castellanos D. OF, Torres P. LM, Rojas L. JC (2009) *Agenda prospectiva de investigación y desarrollo tecnológico para la cadena productiva de Fique en Colombia*. Ministerio de agricultura y desarrollo rural, Bogotá

composition of the Fique fiber^{24 25 26 27 28 29}, very limited reports are published about the by-products³⁰.

Long fibers in Fique plants (Figure 1.a) represent only 4-5% of the leaf total weight, while Fique decortication residues, with a sludge-like appearance (Figure 1.b), contain juice, tow and pulp, correspond to the remaining 70%, 8% and 17%, respectively³¹. Despite of the significant content of cellulose in Fique fibers, tow and pulp, only the fibers are commonly used, for instance, in the manufacture of ropes, cordages, textiles and packaging materials such as coffee sacks. Tow (Figure 1.c) and pulp (Figure 1.d) are only occasionally employed in traditional constructions or as raw materials for paper pulp³². Hence, alternative uses for Fique by-products such as pulp and tow could strengthen Fique fibers agro-industrial cycle, improve crop profitability and have a positive impact on socio-economic issues.

²⁴ Gañán P, Mondragon I (2002) Surface modification of Fique fibers. Effect on their physico-mechanical properties. *Polym Compos* 23:383–394. doi: 10.1002/pc.10440

²⁵ Hoyos CG, Alvarez V a., Rojo PG, Vázquez A (2012) Fique fibers: Enhancement of the tensile strength of alkali treated fibers during tensile load application. *Fibers Polym* 13:632–640. doi: 10.1007/s12221-012-0632-8

²⁶ Castellanos LJ, Blanco-Tirado C, Hinestroza JP, Combariza MY (2012) In situ synthesis of gold nanoparticles using Fique natural fibers as template. *Cellulose* 19:1933–1943. doi: 10.1007/s10570-012-9763-8

²⁷ Chacón-Patiño ML, Blanco-Tirado C, Hinestroza JP, Combariza MY (2013) Biocomposite of nanostructured MnO₂ and Fique fibers for efficient dye degradation. *Green Chem* 15:2920. doi: 10.1039/c3gc40911b

²⁸ Ovalle-Serrano SA, Blanco-Tirado C, Combariza MY (2013) Síntesis in situ de nanopartículas de plata sobre fibras de Fique. *Rev Colomb Química* 42:30–37.

²⁹ Ovalle-Serrano SA, Carrillo VS, Blanco-Tirado C, et al. (2015) Controlled synthesis of ZnO particles on the surface of natural cellulosic fibers: effect of concentration, heating and sonication. *Cellulose* 22:1841–1852. doi: 10.1007/s10570-015-0620-4

³⁰ Quintero M, Castro L, Ortiz C, et al. (2012) Enhancement of starting up anaerobic digestion of lignocellulosic substrate: Fique's bagasse as an example. *Bioresour Technol* 108:8–13. doi: 10.1016/j.biortech.2011.12.052

³¹ Peinado JE, Ospina LF, Rodríguez L, et al. (2006) Guía Ambiental del Subsector Fiquero. Cadena Productiva Nacional del Fique, Bogotá

³² *Ibíd.*

Figure 1. (a) Fique fibers, (b) Fique decortication residues, (c) Clean Fique tow, and (d) Clean Fique pulp



In hard cellulosic fibers, such as Fique, cellulose, hemicelluloses and lignin self-assemble to form a natural composite held together by strong interactions, such as covalent and hydrogen bonds, and weak forces of the van der Waals type^{33 34}. The robust and layered nature of these fibers requires strong chemical and mechanical

³³ Habibi Y, Lucia LA, Rojas OJ (2010) Cellulose nanocrystals: chemistry, self-assembly, and applications. *Chem Rev* 110:3479–3500.

³⁴ Oudiani a. El, Chaabouni Y, Msahli S, Sakli F (2011) Crystal transition from cellulose I to cellulose II in NaOH treated *Agave americana* L. fibre. *Carbohydr Polym* 86:1221–1229. doi: 10.1016/j.carbpol.2011.06.037

treatments to utilize the cellulose within them. Particularly, the presence of lignin (10–25%) in these hard fibers hinders access to cellulose³⁵; consequently, a wide variety of pretreatment methods have been developed for delignification. These treatments include acid/alkaline treatment, steam explosion, organosolv and even the use of ionic liquids. Nonetheless, most of these methods are energetically intensive and use expensive chemicals also difficult to produce, handle or dispose^{36 37 38}. Therefore, new pretreatments have been put forward to remove lignin and hemicellulose from lignocellulosic biomass with high efficiency and low environmental and economic impact. Among these, the use of hydrogen peroxide under alkaline conditions (AHP, alkaline hydrogen peroxide treatment) and ultrasonic irradiation stands out^{39 40 41 42 43 44}.

³⁵ Liu C-F, Ren J-L, Xu F, et al. (2006) Isolation and characterization of cellulose obtained from ultrasonic irradiated sugarcane bagasse. *J Agric Food Chem* 54:5742–5748. doi: 10.1021/jf060929o

³⁶ Bussemaker MJ, Xu F, Zhang D (2013) Manipulation of ultrasonic effects on lignocellulose by varying the frequency, particle size, loading and stirring. *Bioresour Technol* 148:15–23. doi: 10.1016/j.biortech.2013.08.106

³⁷ Subhedar PB, Gogate PR (2014) Alkaline and ultrasound assisted alkaline pretreatment for intensification of delignification process from sustainable raw-material. *Ultrason Sonochem* 21:216–25. doi: 10.1016/j.ultsonch.2013.08.001

³⁸ Heidarian P, Behzad T, Karimi K (2016) Isolation and characterization of bagasse cellulose nanofibrils by optimized sulfur-free chemical delignification. *Wood Sci Technol* 1–18. doi: 10.1007/s00226-016-0820-6

³⁹ Sun RC, Fang JM, Tomkinson J (2000) Delignification of rye straw using hydrogen peroxide. *Ind Crops Prod* 12:71–83. doi: 10.1016/S0926-6690(00)00039-X

⁴⁰ Sun JX, Sun R, Sun XF, Su Y (2004) Fractional and physico-chemical characterization of hemicelluloses from ultrasonic irradiated sugarcane bagasse. *Carbohydr Res* 339:291–300. doi: 10.1016/j.carres.2003.10.027

⁴¹ Liu C-F, Ren J-L, Xu F, et al. (2006) Isolation and characterization of cellulose obtained from ultrasonic irradiated sugarcane bagasse. *J Agric Food Chem* 54:5742–5748. doi: 10.1021/jf060929o

⁴² Bussemaker MJ, Zhang D (2013) Effect of ultrasound on lignocellulosic biomass as a pretreatment for biorefinery and biofuel applications. *Ind Eng Chem Res* 52:3563–3580. doi: 10.1021/ie3022785

⁴³ Subhedar PB, Gogate PR (2014) Alkaline and ultrasound assisted alkaline pretreatment for intensification of delignification process from sustainable raw-material. *Ultrason Sonochem* 21:216–25. doi: 10.1016/j.ultsonch.2013.08.001

⁴⁴ Perez-Pimienta JA, Poggi-Varaldo HM, Ponce-Noyola T, et al. (2016) Fractional pretreatment of raw and calcium oxalate-extracted agave bagasse using ionic liquid and alkaline hydrogen peroxide. *Biomass and Bioenergy* 91:48–55. doi: 10.1016/j.biombioe.2016.05.001

Ultrasonic waves produce mechanoacoustic and sonochemical effects that can physically and chemically assist the delignification process, respectively^{45 46 47 48 49}. On the other hand, the hydroperoxide ion (HOO^-), formed in the presence of hydrogen peroxide under alkaline conditions, is a strong nucleophile with the ability to attack ethylenic and carbonylic groups in lignin (such as quinones, cinnamaldehyde and ketones) transforming them into nonchromophoric species. In addition alkaline conditions are critical to form hydroxyl ($\text{HO}\cdot$) and superoxide anion ($\text{O}_2^{\cdot-}$) radicals in high concentrations, which in turn are vital to disrupt intermolecular bonds between lignin and cellulose thus facilitating the dissolution of lignin and hemicelluloses^{50 51 52 53}. Radicals produced during cavitation and hydrogen peroxide under alkaline conditions are effective to cleave phenolic α -O-4 linkages, non-phenolic β -O-4 linkages, and to remove residual lignin fractions usually by cleavage of carbon-carbon linkages or carbohydrate degradation, releasing lignin-carbohydrate fractions⁵⁴. Hence, the final product of the AHP treatment would be ideally cellulose free from hemicelluloses and lignin.

⁴⁵ Sul'man EM, Sul'man MG, Prutenskaya EA (2011) Effect of ultrasonic pretreatment on the composition of lignocellulosic material in biotechnological processes. *Catal Ind* 3:28–33. doi: 10.1134/S2070050411010120

⁴⁶ Iskalieva A, Yimmou BM, Gogate PR, et al. (2012) Cavitation assisted delignification of wheat straw: a review. *Ultrason Sonochem* 19:984–93. doi: 10.1016/j.ultsonch.2012.02.007

⁴⁷ Bussemaker MJ, Xu F, Zhang D (2013) Manipulation of ultrasonic effects on lignocellulose by varying the frequency, particle size, loading and stirring. *Bioresour Technol* 148:15–23. doi: 10.1016/j.biortech.2013.08.106

⁴⁸ Subhedar PB, Gogate PR (2014) Alkaline and ultrasound assisted alkaline pretreatment for intensification of delignification process from sustainable raw-material. *Ultrason Sonochem* 21:216–25. doi: 10.1016/j.ultsonch.2013.08.001

⁴⁹ Brahim M, El Kantar S, Boussetta N, et al. (2016) Delignification of rapeseed straw using innovative chemo-physical pretreatments. *Biomass and Bioenergy* 95:92–98. doi: 10.1016/j.biombioe.2016.09.019

⁵⁰ Sun RC, Fang JM, Tomkinson J (2000) Delignification of rye straw using hydrogen peroxide. *Ind Crops Prod* 12:71–83. doi: 10.1016/S0926-6690(00)00039-X

⁵¹ Sun JX, Sun R, Sun XF, Su Y (2004) Fractional and physico-chemical characterization of hemicelluloses from ultrasonic irradiated sugarcane bagasse. *Carbohydr Res* 339:291–300. doi: 10.1016/j.carres.2003.10.027

⁵² Liu C-F, Ren J-L, Xu F, et al. (2006) Isolation and characterization of cellulose obtained from ultrasonic irradiated sugarcane bagasse. *J Agric Food Chem* 54:5742–5748. doi: 10.1021/jf060929o

⁵³ Yu H, You Y, Lei F, et al. (2015) Comparative study of alkaline hydrogen peroxide and organosolv pretreatments of sugarcane bagasse to improve the overall sugar yield. *Bioresour Technol* 187:161–166. doi: 10.1016/j.biortech.2015.03.123

⁵⁴ Sun R, Tomkinson J (2002) Comparative study of lignins isolated by alkali and ultrasound-assisted

Considering not only the abundance but also the vast variety of secondary and tertiary biomass sources worldwide, characterization of these materials becomes vital to determine end uses and applications. In this chapter is studied and reported, for the first time, the spectroscopic, microscopic and thermal properties of raw Fique fibers, tow and pulp. In addition, these materials were subjected to ultrasound-assisted alkaline hydrogen peroxide treatment (AHP) to remove amorphous materials (hemicellulose and lignin). The delignified products were also studied to determine composition, structure and morphology and to determine the effect of the AHP treatment on the original biomass.

1.3 EXPERIMENTAL

1.3.1 Materials. Fique fibers, tow and pulp were sampled from Fique crops in the rural area of San Joaquín, Santander, Colombia. The decortication residues were collected directly on-site during the fiber extraction from the leaves, stored at low temperature and transported to the lab for immediate analysis. Hydrogen peroxide (H_2O_2) and sodium hydroxide (NaOH), were purchased from Merck (Darmstadt, Germany) and used as received without further purification. Aqueous solutions were prepared using distilled water.

1.3.2 Sample pretreatment. Fique fibers, tow and pulp were filtered and washed thoroughly with distilled water to remove residues of Fique juice that remained after the mechanical decortication process used to extract fibers from the Fique leaves. 120 g of each sample was sonicated in 6 L of distilled water in a Bransonic Ultrasonic Bath (130 W, 40 kHz) at 40 °C for 60 minutes. Finally, the samples were dried at 60 °C for 24 hours.

1.3.3 Alkaline hydrogen peroxide (AHP) treatment. The delignification process was adapted from the report by Sun et al.⁵⁵ as follows: pretreated Fique tow samples (which normally range from 10 to 30 cm in length and 0.1 to 0.2 mm in width) were cut into pieces of about 1 cm; 8 g of tow were immersed in a H₂O₂ 10% w/w solution brought to pH 11.5 by dropwise addition of NaOH 4 N. The mixture was allowed to react for 2 h. Finally, the delignified product was filtrated, washed thoroughly with distilled water and dried a 60 °C for 24 h. For Fique pulp delignification, the parameters used were the same as described above. However, for Fique pulp the maximum load used was 5% w/v because at higher loads increasing froth production made it difficult to maintain the reaction volume. This effect was due to the high-surface area of the material since pulp has a particle size ranging from 5 to 10 mm. The reported delignification conditions for Fique tow and pulp were selected from a factorial experimental design (2³) as seen in Table 1.

Table 1. Experimental matrix for Fique fibers/tow delignification.

Exp	Biomass load [% w/v]	H ₂ O ₂ concentration [% w/w]	Reaction time [min]
E1	1.0	10.0	30.0
E2	1.0	10.0	120.0
E3	4.5	5.5	75.0
E4	1.0	1.0	120.0
E5	8.0	10.0	30.0
E6	8.0	1.0	120.0
E7	1.0	1.0	30.0
E8	8.0	10.0	120.0
E9	8.0	1.0	30.0

1.3.4 Characterization methods. Cellulose, hemicellulose and lignin percentages were determined according to the Kürschner and Höffer method⁵⁶, Jayme-Wise's

⁵⁵ Sun RC, Fang JM, Tomkinson J (2000) Delignification of rye straw using hydrogen peroxide. *Ind Crops Prod* 12:71–83. doi: 10.1016/S0926-6690(00)00039-X

⁵⁶ Browning BL (1967) No Title. *Methods Wood Chem. Vol II.* John Wiley & Sons, New York, USA,

chlorite method⁵⁷ and Klason method (Tappi T 222 om-88), respectively. Attenuated total reflectance infrared spectroscopy (ATR-IR) analyses were carried out on a Bruker Tensor 27 (Billerica, MA) FTIR instrument equipped with a Platinum Diamond ATR unit A225/Q (Billerica, MA). ATR-IR spectra were recorded at a resolution of 2 cm⁻¹ and 32 scans were accumulated for each spectrum. For X-ray diffraction measurements were performed on a Bruker D8 DISCOVER X-ray diffractometer (Billerica, MA) with a DaVinci geometry equipped with a CuK α 1 radiation source (40 kV and 30 mA), an area detector VANTEC-500, and a poly(methyl methacrylate) sample holder. The Segal method was used to calculate the crystallinity index of cellulose with the following equation:

$$C_I = \frac{I_{200} - I_{am}}{I_{200}} \times 100$$

Where I_{200} is the height of the 2 0 0 peak representing both crystalline and amorphous materials and I_{am} is the minimum between the 2 0 0 and 1 1 0 peaks representing only amorphous material ⁵⁸. Field emission scanning electron microscopy (FESEM) images were taken using a FEI QUANTA FEG 650 (Oregon, USA) equipped with a Large Field Detector. Samples were coated with a thin layer of carbon or gold (around 20 nm) before the analysis and the micrographs were taken at 10 and 20 kV. The energy-dispersive X-ray spectroscopy (EDX) accessory attached to the microscope was used for the elemental analysis of the samples at 20 kV. Thermogravimetric analyses (TGA) were performed on a Discovery TGA instrument under nitrogen atmosphere, with heating rate of 10 °C/min and temperature range of 35 to 600 °C. Differential scanning calorimetry (DSC)

pp 406–727

⁵⁷ Leavitt SW, Danzer SR (1993) Method for batch processing small wood samples to holocellulose for stable-carbon isotope analysis. *Anal Chem* 65:87–89. doi: 10.1021/ac00049a017

⁵⁸ Segal L, Creely JJ, Martin AE, Conrad CM (1959) An Empirical Method for Estimating the Degree of Crystallinity of Native Cellulose Using the X-Ray Diffractometer. *Text Res J* 29:786–794. doi: 10.1177/004051755902901003

measurements were carried out on a Discovery DSC instrument at a heating rate of 10 °C/min from 35 to 500 °C under nitrogen atmosphere.

1.4 RESULTS AND DISCUSSION

1.4.1 Raw Fique fibers, tow and pulp characterization. Prior to characterization a cleaning step, with ultrasonic radiation, was performed on raw Fique fibers, tow and pulp to remove Fique juice remnants and other contaminants such as calcium carbonates or oxalates, usually found in these materials ^{59 60 61}. After this cleaning step, two solid materials were isolated from the decortication sludge (Figure 1.b): tow and pulp. Fique tow (Figure 1.c) is comprised of short and thin fibers, of vascular origin, ranging from 10 to 30 cm in length and 0.1 mm width, in contrast with Fique long fibers normally spanning up to 1-2 m in length and 0.15-0.25 mm in width. On the other hand, Fique pulp (Figure 1.d) is a heterogeneous material consisting mostly of ground or parenchymal tissue. The final mass of Fique fibers and tow after the drying step in the sample pretreatment stage is in average 4.2% lower than the initial weight.

Table 2. Chemical composition of Fique pulp, tow and fibers (this work) compared to other pulp and fibers sources.

Sample	Composition [%]			References
	Cellulose	Hemicellulose	Lignin	
Fique pulp	30.5 ± 1.1	29.7 ± 1.3	9.6 ± 2.4	This work
Fique tow	52.3 ± 3.0	23.8 ± 6.2	23.9 ± 7.6	This work
Fique fibers	52.9 ± 2.1	23.8 ± 6.2	23.3 ± 3.9	This work

⁵⁹ Castellanos LJ, Blanco-Tirado C, Hinestroza JP, Combariza MY (2012) In situ synthesis of gold nanoparticles using Fique natural fibers as template. *Cellulose* 19:1933–1943. doi: 10.1007/s10570-012-9763-8

⁶⁰ Chacón-Patiño ML, Blanco-Tirado C, Hinestroza JP, Combariza MY (2013) Biocomposite of nanostructured MnO₂ and Fique fibers for efficient dye degradation. *Green Chem* 15:2920. doi: 10.1039/c3gc40911b

⁶¹ Ovalle-Serrano SA, Blanco-Tirado C, Combariza MY (2013) Síntesis in situ de nanopartículas de plata sobre fibras de Fique. *Rev Colomb Química* 42:30–37.

Sample	Composition [%]			References
	Cellulose	Hemicellulose	Lignin	
Fique fibers	63.0-73.0	-	14.5-11.3	(Gañán and Mondragon 2002; Peinado et al. 2006)
Sisal fibers	50-74	14.0	11.0	(Morán et al. 2008)
Wood	46.4	27.1	25.0	(Chen et al. 2011)
Bamboo	41.8	27.2	23.2	
Wheat straw	39.8	34.2	19.8	
Flax	75.4	13.4	3.4	
Jute	45-71.5	15	11	(Abraham et al. 2011; Cao et al. 2012)
Cashew apple pulp	20.6	10.2	35.3	(Correia et al. 2013)
Sugarcane pulp	38.0	32.0	27.0	(Sun et al. 2004; Ramadoss and Muthukumar 2014)
Agave pulp	45.6	19.8	19.9	(Perez-Pimienta et al. 2015)

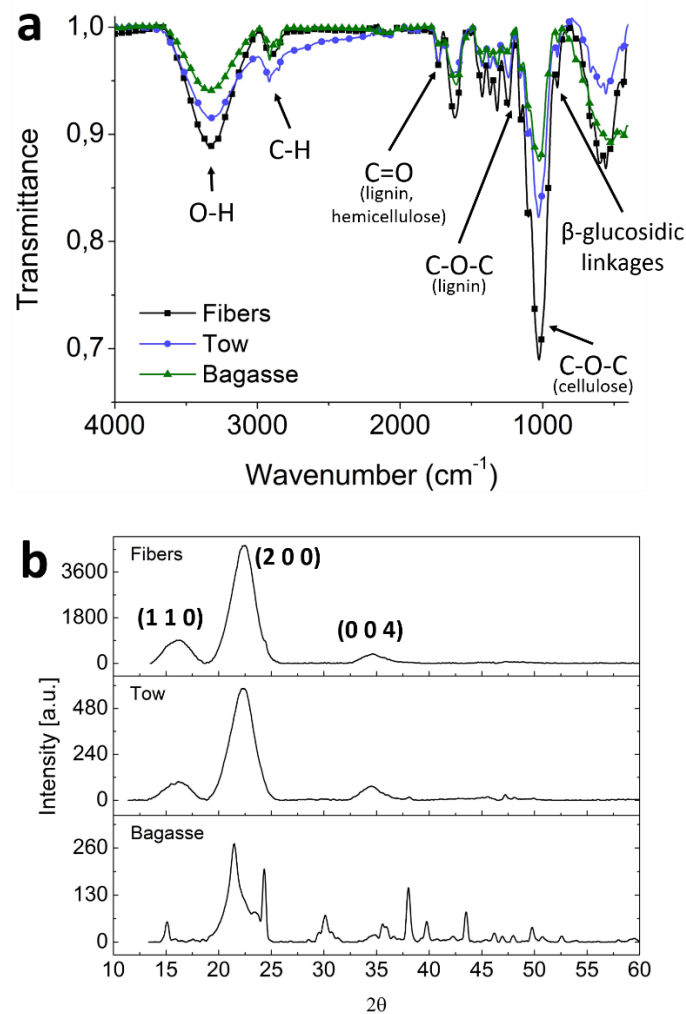
Pretreated raw Fique fibers, tow and pulp compositions are shown in Table 2. Cellulose in fibers and tow represents up to 52%, although some authors report cellulose contents up to 63%⁶² or 73%⁶³ in fibers. It is well known that natural fiber's chemical composition varies according to the plant species. However, cellulose content in Fique fiber and tow is comparable or even higher than other similar fiber sources such as sisal, wood, bamboo, jute, among others (Table 2). On the other hand, cellulose in Fique pulp amounts to 30.5%; this content is higher than the reported content for cashew apple pulp and lower than sugarcane pulp and agave pulp. However, despite the fact that Fique pulp has relatively low cellulose content (30.5%), it is available in larger amounts compared to fibers and tow (17%). Ash, proteins and tannins constitute the remaining components of Fique pulp as occurs

⁶² Gañán P, Mondragon I (2002) Surface modification of Fique fibers. Effect on their physico-mechanical properties. *Polym Compos* 23:383–394. doi: 10.1002/pc.10440

⁶³ Peinado JE, Ospina LF, Rodríguez L, et al. (2006) Guía Ambiental del Subsector Fiquero. Cadena Productiva Nacional del Fique, Bogotá

in pulp from other plant species ^{64 65}. On the other hand, hemicellulose (24%) and lignin (23%) contents in Fique fibers are higher than in sisal and jute fiber but similar to hemicellulose content in wood fibers and bamboo fibers. As for hemicellulose (30%) and lignin (10%) contents in Fique pulp, they are similar to the ones in cashew apple pulp and agave pulp.

Figure 2. (a) IR spectra and (b) XRD patterns of Fique fibers, tow and pulp.



⁶⁴ Prozil SO, Evtuguin D V, Lopes LPC (2012) Chemical composition of grape stalks of *Vitis vinifera* L. from red grape pomaces. *Ind Crops Prod* 35:178–184. doi: 10.1016/j.indcrop.2011.06.035

⁶⁵ Li W, Zhang Y, Li J, et al. (2015) Characterization of cellulose from banana pseudo-stem by heterogeneous liquefaction. *Carbohydr Polym* 132:513–519. doi: 10.1016/j.carbpol.2015.06.066

Figure 2a shows IR analyses of clean Fique pulp, tow and fibers with characteristic bands attributed to the main components of plant tissues: cellulose, hemicellulose, and lignin. The peaks centered at 3327 cm^{-1} and 2911 cm^{-1} are attributed to O-H and C-H stretching vibrations, respectively, present in cellulose, hemicellulose and lignin^{66 67}. Cellulose exhibits two characteristic bands: one at 898 cm^{-1} due to β -glucosidic linkages⁶⁸ and another at 1029 cm^{-1} due to C–O–C pyranose ring skeletal vibrations⁶⁹. In addition, signals at 1731 cm^{-1} and 1240 cm^{-1} correspond to typical vibrations of the C=O linkage of hemicelluloses and C-O-C vibrations of aromatic ether linkages in lignin, respectively^{70 71}. No appreciable differences were observed between the IR signals of Fique fibers, tow and pulp.

XRD analyses of Fique fibers, tow and pulp are shown in Figure 2b. Fique fibers and tow diffraction patterns show diffraction peaks at $2\theta = 16.2^\circ$, 22.5° and 34.8° , corresponding to the (110), (200) and (004) crystallographic planes, characteristic of cellulose I (Joint Committee on Powder Diffraction Standards, JCPDS file, no. 50-2241), space group P21 (No. 4)^{72 73 74}. On the other hand, the pulp XRD pattern

⁶⁶ Chen W, Yu H, Liu Y, et al. (2011) Isolation and characterization of cellulose nanofibers from four plant cellulose fibers using a chemical-ultrasonic process. *Cellulose* 18:433–442. doi: 10.1007/s10570-011-9497-z

⁶⁷ Lu Q, Tang L, Lin F, et al. (2014) Preparation and characterization of cellulose nanocrystals via ultrasonication-assisted FeCl₃-catalyzed hydrolysis. *Cellulose* 21:3497–3506. doi: 10.1007/s10570-014-0376-2

⁶⁸ Rehman N, de Miranda MIG, Rosa SML, et al. (2013) Cellulose and Nanocellulose from Maize Straw: An Insight on the Crystal Properties. *J Polym Environ* 22:252–259. doi: 10.1007/s10924-013-0624-9

⁶⁹ Lu Q, Tang L, Lin F, et al. (2014) Preparation and characterization of cellulose nanocrystals via ultrasonication-assisted FeCl₃-catalyzed hydrolysis. *Cellulose* 21:3497–3506. doi: 10.1007/s10570-014-0376-2

⁷⁰ Rehman N, de Miranda MIG, Rosa SML, et al. (2013) Cellulose and Nanocellulose from Maize Straw: An Insight on the Crystal Properties. *J Polym Environ* 22:252–259. doi: 10.1007/s10924-013-0624-9

⁷¹ Luzi F, Fortunati E, Puglia D, et al. (2014) Optimized extraction of cellulose nanocrystals from pristine and carded hemp fibres. *Ind Crops Prod* 56:175–186. doi: 10.1016/j.indcrop.2014.03.006

⁷² Morán JI, Alvarez VA, Cyras VP, Vázquez A (2008) Extraction of cellulose and preparation of nanocellulose from sisal fibers. *Cellulose* 15:149–159. doi: 10.1007/s10570-007-9145-9

⁷³ Mandal A, Chakrabarty D (2011) Isolation of nanocellulose from waste sugarcane bagasse (SCB) and its characterization. *Carbohydr Polym* 86:1291–1299.

⁷⁴ Sèbe G, Ham-Pichavant F, Ibarboure E, et al. (2012) Supramolecular structure characterization of cellulose II nanowhiskers produced by acid hydrolysis of cellulose I substrates. *Biomacromolecules* 13:570–8. doi: 10.1021/bm201777j

exhibits, apart for some of the cellulose broad peaks, a collection of low-intensity sharp peaks corresponding mostly to calcium oxalate. Pulp comprises a mixture of leaves' epidermis or cuticle and low crystallinity cellulose microfibrils. These materials are initially indistinguishable (Figure 1d) and become differentiated after delignification as will be explained further in this chapter. The crystallinity indexes for Fique fibers, tow and pulp were 63%, 57%, and 35%, respectively. These indexes are similar or even higher to the crystal index of other raw materials such as borer powder of bamboo (35.94%)⁷⁵, Whatman® filter paper number 1 (84.8%)⁷⁶, sisal (75%)⁷⁷, jute (64%)⁷⁸, hemp (83%)⁷⁹, flax (78%)⁸⁰, wood (56%), and rice straw (50.9%)⁸¹. Crystalline indexes in Fique by-products correlate well with each material's function within the plant. For instance, fibers, made mostly of sclerenchymal tissue, exhibit the highest degree of organization (63%) because they serve not only as transport structures but also as mechanical strength components helping the Fique leave maintain an upward position. The same rationale applies to tow (57%). Pulp, however, composed mostly of ground parenchymal (or "filler") tissue exhibits the lowest cellulose crystallinity index (35%). Vascular tissue typically is fibrous and waterproof while parenchymal tissue is spongy and highly hygroscopic. Fique fibers and tow (vascular tissue) showed moisture content up to 35% whereas Fique pulp (parenchymal tissue) had moisture content up to 80%. This

⁷⁵ Hu Y, Tang L, Lu Q, et al. (2014) Preparation of cellulose nanocrystals and carboxylated cellulose nanocrystals from borer powder of bamboo. *Cellulose* 21:1611–1618. doi: 10.1007/s10570-014-0236-0

⁷⁶ Ahmadi M, Madadlou A, Sabouri AA (2015) Isolation of micro- and nano-crystalline cellulose particles and fabrication of crystalline particles-loaded whey protein cold-set gel. *Food Chem* 174:97–103. doi: 10.1016/j.foodchem.2014.11.038

⁷⁷ Morán JI, Alvarez VA, Cyras VP, Vázquez A (2008) Extraction of cellulose and preparation of nanocellulose from sisal fibers. *Cellulose* 15:149–159. doi: 10.1007/s10570-007-9145-9

⁷⁸ Cao X, Ding B, Yu J, Al-Deyab SS (2012) Cellulose nanowhiskers extracted from TEMPO-oxidized jute fibers. *Carbohydr Polym* 90:1075–80. doi: 10.1016/j.carbpol.2012.06.046

⁷⁹ Luzi F, Fortunati E, Puglia D, et al. (2014) Optimized extraction of cellulose nanocrystals from pristine and carded hemp fibres. *Ind Crops Prod* 56:175–186. doi: 10.1016/j.indcrop.2014.03.006

⁸⁰ Chen W, Yu H, Liu Y, et al. (2011) Isolation and characterization of cellulose nanofibers from four plant cellulose fibers using a chemical-ultrasonic process. *Cellulose* 18:433–442. doi: 10.1007/s10570-011-9497-z

⁸¹ Chen W, Yu H, Liu Y, et al. (2011) Isolation and characterization of cellulose nanofibers from four plant cellulose fibers using a chemical-ultrasonic process. *Cellulose* 18:433–442. doi: 10.1007/s10570-011-9497-z

is because water can penetrate easily low-crystallinity cellulose (Fique pulp) but crystalline cellulose (Fique fibers and tow) tends to be impervious to hydration⁸². Parenchymal tissue is composed mainly of water and water-soluble compounds, with low amounts of cellulose and lignin compared to vascular tissue. This also explains why Fique pulp exhibits a lower crystallinity index than Fique fibers or tow⁸³⁸⁴. The elemental analyses of the pretreated Fique fibers, tow and pulp, as determined by X-ray fluorescence (XRF), are shown in Table 3. As expected, organic matter represents the vast majority of the samples, since cellulose, hemicellulose and lignin are the main components. Fique fibers, tow and pulp contain high amounts of calcium (0.24%, 0.31% and 2.19%) and magnesium (0.07%, 0.04% and 0.10%). Calcium, in particular, helps both preserving cell wall integrity and maintaining plant cell function, structure and stability, while magnesium has been reported to play a role in the synthesis of $\beta(1-4)$ glucans^{85 86 87}.

Table 3. Elemental analyses by XRF for Fique fibers, tow and bagasse.

Element	Concentration		
	Fibers	Tow	Bagasse
Organic matter	99.60%	99.50%	97.40%
Ca	0.24%	0.31%	2.19%
Mg	0.07%	0.04%	0.10%
K	62 ppm	0.03%	0.08%
S	0.01%	0.02%	0.05%

⁸² Mazeau K (2015) The hygroscopic power of amorphous cellulose: A modeling study. *Carbohydr Polym* 117:585–591. doi: 10.1016/j.carbpol.2014.09.095

⁸³ Montanari S, Roumani M, Heux L, Vignon MR (2005) Topochemistry of Carboxylated Cellulose Nanocrystals Resulting from TEMPO-Mediated Oxidation. *Macromolecules* 38:1665–1671. doi: 10.1021/ma048396c

⁸⁴ Lamaming J, Hashim R, Leh CP, et al. (2015) Isolation and characterization of cellulose nanocrystals from parenchyma and vascular bundle of oil palm trunk (*Elaeis guineensis*). *Carbohydr Polym* 134:534–540. doi: 10.1016/j.carbpol.2015.08.017

⁸⁵ Brett CT (2000) Cellulose microfibrils in plants: biosynthesis, deposition, and integration into the cell wall. *Int Rev Cytol* 199:161–199. doi: 10.1016/s0074-7696(00)99004-1

⁸⁶ Cybulska J, Zdunek A, Konstankiewicz K (2011) Calcium effect on mechanical properties of model cell walls and apple tissue. *J Food Eng* 102:217–223. doi: 10.1016/j.jfoodeng.2010.08.019

⁸⁷ Silkin PP, Ekimova NV (2012) Relationship of strontium and calcium concentrations with the parameters of cell structure in Siberian spruce and fir tree-rings. *Dendrochronologia* 30:189–194. doi: 10.1016/j.dendro.2011.06.003

Element	Concentration		
	Fibers	Tow	Bagasse
P	79 ppm	0.01%	0.05%

Fique fibers and tow have similar surface structures, with diameters slightly higher than 100 μm in Fique fibers (Figure 3a), and slightly lower than 100 μm in Fique tow (Figure 3b). As in sisal fibers, and other hard fibers, Fique fibers and tow have a hierarchical structure where each fiber is composed of numerous microfibrils of 6 to 30 μm in diameter. These microfibrils, held together by hemicellulose and lignin, are easily distinguishable in the micrographs as channels on the fiber's surface as seen in Figures 3a and 3b^{88 89 90 91}. Fibers and tow, mostly composed of vascular or conductive tissue, provide support and help in nutrients/water transport⁹². This explains why Figure 3b shows a crystal in the center of the fiber, which by means of XRD analysis was later identified as calcium carbonate. On the other hand, Fique pulp (Figure 3c) is mostly composed of parenchymal tissue and Fique leave's upper and lower epidermis (Figure 3c). Similar features are observed for SEM images of sugarcane pulp^{93 94 95}

⁸⁸ Morán JI, Alvarez VA, Cyras VP, Vázquez A (2008) Extraction of cellulose and preparation of nanocellulose from sisal fibers. *Cellulose* 15:149–159. doi: 10.1007/s10570-007-9145-9

⁸⁹ Silva FDA, Chawla N, Filho RDDT (2008) Tensile behavior of high performance natural (sisal) fibers. *Compos Sci Technol* 68:3438–3443. doi: 10.1016/j.compscitech.2008.10.001

⁹⁰ Barreto ACH, Rosa DS, Fachine PBA, Mazzetto SE (2011) Properties of sisal fibers treated by alkali solution and their application into cardanol-based biocomposites. *Compos Part A Appl Sci Manuf* 42:492–500. doi: 10.1016/j.compositesa.2011.01.008

⁹¹ Heidarian P, Behzad T, Karimi K (2016) Isolation and characterization of bagasse cellulose nanofibrils by optimized sulfur-free chemical delignification. *Wood Sci Technol* 1–18. doi: 10.1007/s00226-016-0820-6

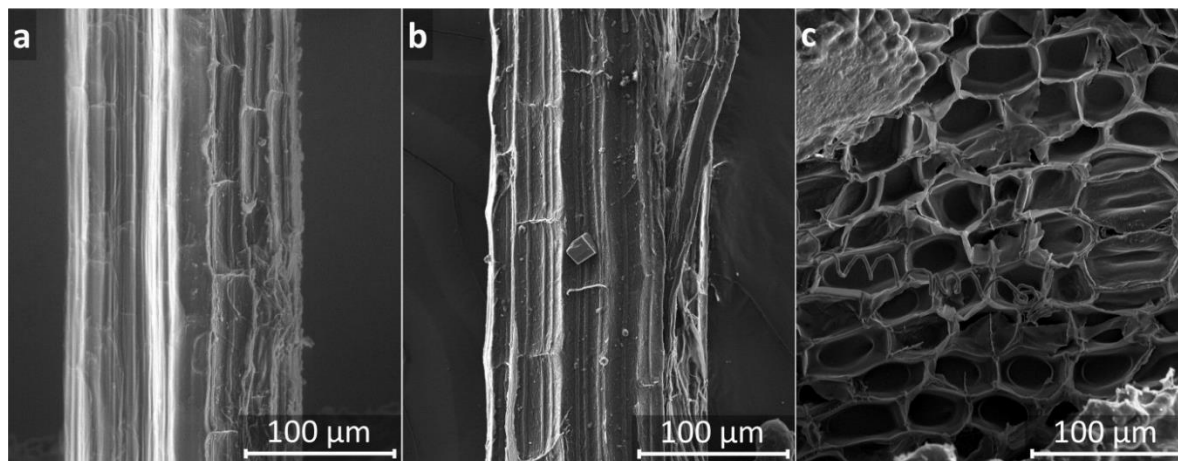
⁹² Lamaming J, Hashim R, Leh CP, et al. (2015) Isolation and characterization of cellulose nanocrystals from parenchyma and vascular bundle of oil palm trunk (*Elaeis guineensis*). *Carbohydr Polym* 134:534–540. doi: 10.1016/j.carbpol.2015.08.017

⁹³ Lataye DH, Mishra IM, Mall ID (2006) Removal of pyridine from aqueous solution by adsorption on bagasse fly ash. *Ind Eng Chem Res* 45:3934–3943. doi: 10.1021/ie051315w

⁹⁴ Mandal A, Chakrabarty D (2011) Isolation of nanocellulose from waste sugarcane bagasse (SCB) and its characterization. *Carbohydr Polym* 86:1291–1299.

⁹⁵ Ramadoss G, Muthukumar K (2014) Ultrasound assisted ammonia pretreatment of sugarcane bagasse for fermentable sugar production. *Biochem Eng J* 83:33–41. doi: 10.1016/j.bej.2013.11.013

Figure 3. SEM images of (a) Fique fibers, (b) Fique tow and (c) Fique pulp.



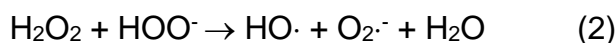
1.4.2 Delignified Fique fibers, tow and pulp characterization. Different methods exist to treat lignocellulosic materials, in order to extract lignin and hemicellulose, and make cellulose accessible. These delignification methods include biological, physical, chemical and physicochemical treatments or their combinations. Common pretreatments involve the use of aggressive chemical agents such as molecular chlorine, which generates toxic chlorinated organic compounds that are further released to the environment ⁹⁶ ⁹⁷. Recently, alkaline hydrogen peroxide (AHP) was reported as an environmentally friendly reagent for delignifying lignocellulosic materials ⁹⁸. An effective delignification process is fundamental for obtaining high-purity cellulose and/or lignin. As shown in equations (1) and (2) the AHP treatment produces highly reactive species, such as hydroxyl radicals ($\text{HO}\cdot$), superoxide anion radicals ($\text{O}_2^{\cdot-}$) and hydroperoxide anions (HOO^-), that will eventually recombine into oxygen and water without leaving toxic residues in the biomass. These active

⁹⁶ Ouchi A (2008) Efficient total halogen-free photochemical bleaching of kraft pulps using alkaline hydrogen peroxide. *J Photochem Photobiol A Chem* 200:388–395. doi: 10.1016/j.jphotochem.2008.09.006

⁹⁷ Correia JADC, Júnior JEM, Gonçalves LRB, Rocha MVP (2013) Alkaline hydrogen peroxide pretreatment of cashew apple bagasse for ethanol production: Study of parameters. *Bioresour Technol* 139:249–256. doi: 10.1016/j.biortech.2013.03.153

⁹⁸ Wójciak A, Kasprzyk H, Sikorska E, et al. (2014) FT-Raman, FT-infrared and NIR spectroscopic characterization of oxygen-delignified kraft pulp treated with hydrogen peroxide under acidic and alkaline conditions. *Vib Spectrosc* 71:62–69. doi: 10.1016/j.vibspec.2014.01.007

species preferentially target ethylenic and carboxylic groups in lignin, transforming them to nonchromophoric species. In addition, they also attack lignin side-chains causing depolymerization and fragmentation of the lignin macrostructure into low-molecular-weight and water-soluble oxidation products ^{99 100 101}. Conversion of chromophoric groups in lignin into nonchromophoric species results in a bleached cellulosic substrate ^{102 103}.



Untreated (raw) Fique fibers/tow usually exhibit cream to light brown shades; after AHP treatment these materials turn white due to lignin elimination. Figures.4a and 4b show the color change from untreated (raw) to delignified Fique fibers/tow, respectively. In Figure 4c comparison of the IR spectra of raw and delignified fibers and tow, show the change in lignin characteristic bands, particularly aromatic skeletal vibrations at 1617, 1507 and 1456 cm^{-1} , as a result of delignification. Also, the main IR bands corresponding to hemicellulose and lignin (1731 and 1240 cm^{-1}) are not discernible after AHP. Lignin content in fibers and tow, by the Klason method, changed from 23.3% to 2.8% after the AHP treatment; this is equivalent to a removal of 88% lignin. This data corroborates our IR observations regarding a significant

⁹⁹ Sun RC, Fang JM, Tomkinson J (2000) Delignification of rye straw using hydrogen peroxide. *Ind Crops Prod* 12:71–83. doi: 10.1016/S0926-6690(00)00039-X

¹⁰⁰ Correia JADC, Júnior JEM, Gonçalves LRB, Rocha MVP (2013) Alkaline hydrogen peroxide pretreatment of cashew apple bagasse for ethanol production: Study of parameters. *Bioresour Technol* 139:249–256. doi: 10.1016/j.biortech.2013.03.153

¹⁰¹ Su Y, Du R, Guo H, et al. (2015) Fractional pretreatment of lignocellulose by alkaline hydrogen peroxide: Characterization of its major components. *Food Bioprod Process* 94:322–330. doi: 10.1016/j.fbp.2014.04.001

¹⁰² Renard CMGC, Rohou Y, Hubert C, et al. (1997) Bleaching of Apple Pomace by Hydrogen Peroxide in Alkaline Conditions: Optimisation and Characterisation of the Products. *LWT - Food Sci Technol* 30:398–405. doi: 10.1006/fstl.1996.0195

¹⁰³ Ouchi A (2008) Efficient total halogen-free photochemical bleaching of kraft pulps using alkaline hydrogen peroxide. *J Photochem Photobiol A Chem* 200:388–395. doi: 10.1016/j.jphotochem.2008.09.006

decrease, or absence, of hemicellulose and lignin characteristic signals after the AHP treatment^{104 105 106}. Likewise, the XRD patterns in Figure 4d show that the crystallinity index for raw and clean Fique fibers/tow, with an average of 63% and 57 %, respectively, increases up to 73% after delignification. High crystallinity index means removal of amorphous materials, such as lignin and hemicellulose, and increase in cellulose content^{107 108}.

Raw Fique fibers/tow are composite structures with average diameters around 100-250 μm . Every macrofiber is a bundle made up of numerous individual microfibrils, or fiber-cells, held together by lignin and hemicellulose. The microfibrils are difficult to identify because they are not only wrapped by hemicellulose and lignin but also have in their surface left over ground tissue in which they are naturally embedded as seen in Figure 4e. However, as the fiber undergoes AHP the lamellar structure is disrupted by the removal of hemicellulose, lignin and ground tissue, and the hierarchical structure is altered releasing the fiber-cells as shown in the FESEM image of Figure 4f^{109 110}.

¹⁰⁴ Wen JL, Sun SL, Yuan TQ, et al. (2013) Structural elucidation of lignin polymers of eucalyptus chips during organosolv pretreatment and extended delignification. *J Agric Food Chem* 61:11067–11075. doi: 10.1021/jf403717q

¹⁰⁵ Bussemaker MJ, Xu F, Zhang D (2013) Manipulation of ultrasonic effects on lignocellulose by varying the frequency, particle size, loading and stirring. *Bioresour Technol* 148:15–23. doi: 10.1016/j.biortech.2013.08.106

¹⁰⁶ Su Y, Du R, Guo H, et al. (2015) Fractional pretreatment of lignocellulose by alkaline hydrogen peroxide: Characterization of its major components. *Food Bioprod Process* 94:322–330. doi: 10.1016/j.fbp.2014.04.001

¹⁰⁷ Chen W, Yu H, Liu Y, et al. (2011) Isolation and characterization of cellulose nanofibers from four plant cellulose fibers using a chemical-ultrasonic process. *Cellulose* 18:433–442. doi: 10.1007/s10570-011-9497-z

¹⁰⁸ Su Y, Du R, Guo H, et al. (2015) Fractional pretreatment of lignocellulose by alkaline hydrogen peroxide: Characterization of its major components. *Food Bioprod Process* 94:322–330. doi: 10.1016/j.fbp.2014.04.001

¹⁰⁹ Wen JL, Sun SL, Yuan TQ, et al. (2013) Structural elucidation of lignin polymers of eucalyptus chips during organosolv pretreatment and extended delignification. *J Agric Food Chem* 61:11067–11075. doi: 10.1021/jf403717q

¹¹⁰ Su Y, Du R, Guo H, et al. (2015) Fractional pretreatment of lignocellulose by alkaline hydrogen peroxide: Characterization of its major components. *Food Bioprod Process* 94:322–330. doi: 10.1016/j.fbp.2014.04.001

Fique pulp, on the other hand, is composed of two kinds of materials: cellulose microfibrils, making up the secondary wall of parenchyma and collenchyma cells; and leaves' epidermis or cuticle. These materials, although hardly indistinguishable (Figure 5a), become easily differentiated after the AHP process (Figure 5b. Green square: epidermis; blue square: cellulose microfibrils). A close up show micrometric (approximately 5 μm in width) cellulose fibrils (Figure 5e) and stomata, bordered by guard cells, on the leaf epidermis (Figure 5f).

Figure 4. Optical images of (a) raw and (b) delignified Fique fibers/tow. (c) IR spectra, (d) XRD patterns and FESEM images of (e) raw and (f) delignified Fique fibers/tow.

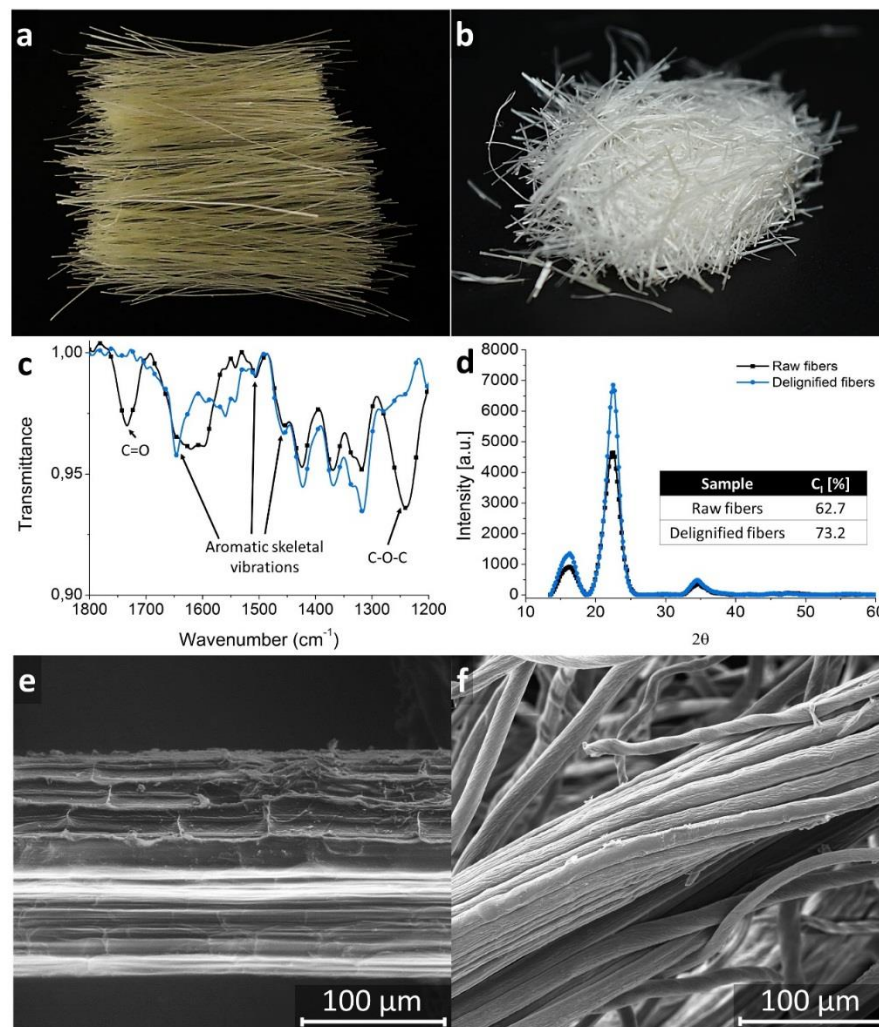
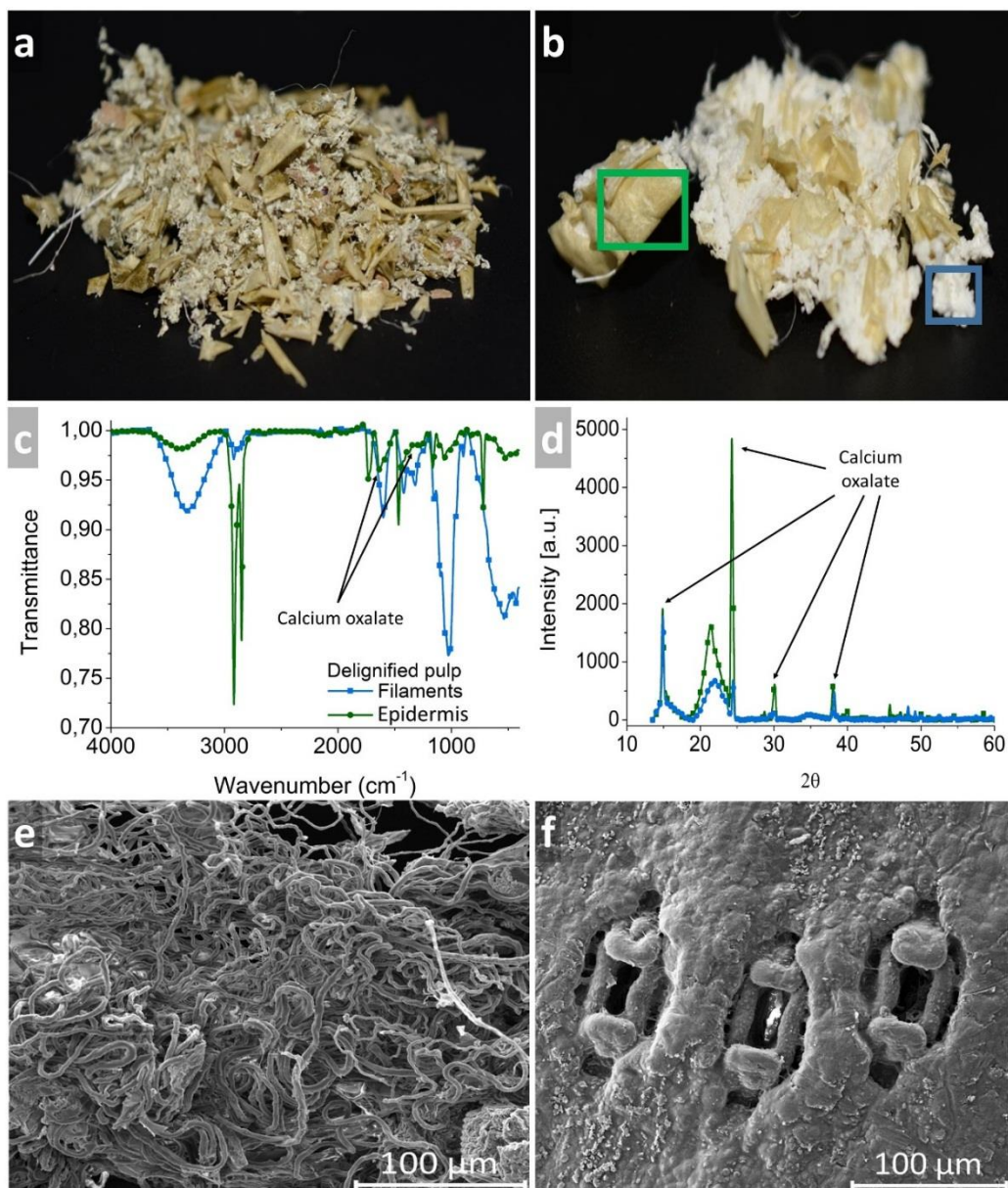


Figure 5. Optical images of (a) raw and (b) delignified Figue pulp. (c) IR spectra and (d) XRD patterns of cellulosic filaments (blue trace) and leaf epidermis (green trace) in delignified Figue pulp. FESEM images of (e) cellulosic filaments and (f) leaf epidermis in delignified Figue pulp.



IR analysis of the filaments (Figure.5c, blue trace) show characteristic bands of cellulose in 3327 and 2911 cm⁻¹ attributed to O-H and C-H stretching vibrations; additionally, signals at 898 and 1029 cm⁻¹ are due to β-glucosidic linkages and C-

O–C pyranose ring skeletal vibrations, respectively ¹¹¹. Also, as in the case of fibers/tow, the main IR bands corresponding to hemicellulose and lignin (1731 and 1240 cm⁻¹) are significantly reduced after the AHP treatment. On the other hand, the IR spectrum of the epidermis (Figure 5e, green trace) shows a band around 3300 cm⁻¹, related to stretching vibrations of hydroxyl groups, attributed to the polysaccharide fraction and the non-esterified hydroxyl groups of cutin. Bands at 2916 and 2849 cm⁻¹ (stretching vibrations of CH₂ groups) and 1466 cm⁻¹ (bending vibration of CH₂ groups) are associated to materials present in the epidermis' cuticle, such as waxes, cutin and cutan, which are mixtures of hydrophobic aliphatic compounds, with chain lengths between C16 and C36, used to confer hydrophobicity and to prevent water loss. Signals at 1731 cm⁻¹ (C=O stretching ester vibration) and 1164 and 1104 cm⁻¹ (C-O-C stretching ester vibration) are attributed to the cutin matrix ¹¹². For Fique pulp the lignin content changed from 9.6% to 2.1% after the AHP treatment, equivalent to a removal of 79% lignin. Finally, signals related to the presence of calcium oxalate are shown at 1622 cm⁻¹ (antisymmetric carbonyl stretching band) and 1322 cm⁻¹ (the metal-carboxylate stretch). XRD patterns also show the presence of calcium oxalate in the leaf epidermis (Figure .5d green trace) as well as characteristic bands of cellulose in the fibrils (Figure .5e blue trace) with a crystallinity index of 47% ^{113 114}.

¹¹¹ Lu Q, Tang L, Lin F, et al. (2014) Preparation and characterization of cellulose nanocrystals via ultrasonication-assisted FeCl₃-catalyzed hydrolysis. *Cellulose* 21:3497–3506. doi: 10.1007/s10570-014-0376-2

¹¹² Heredia-Guerrero JA, Benítez JJ, Domínguez E, et al. (2014) Infrared and Raman spectroscopic features of plant cuticles: a review. *Front Plant Sci* 5:1–14. doi: 10.3389/fpls.2014.00305

¹¹³ Satyanarayana KG, Flores-Sahagun THS, Dos Santos LP, et al. (2013) Characterization of blue agave bagasse fibers of Mexico. *Compos Part A Appl Sci Manuf* 45:153–161. doi: 10.1016/j.compositesa.2012.09.001

¹¹⁴ Perez-Pimienta J a., Lopez-Ortega MG, Chavez-Carvayar J a., et al. (2015) Characterization of agave bagasse as a function of ionic liquid pretreatment. *Biomass and Bioenergy* 75:180–188. doi: 10.1016/j.biombioe.2015.02.026

Figure 6. TGA and DTG thermograms of (a) raw and (b) delignified fibers/tow and DSC thermograms (c) for raw and delignified fibers/tow.

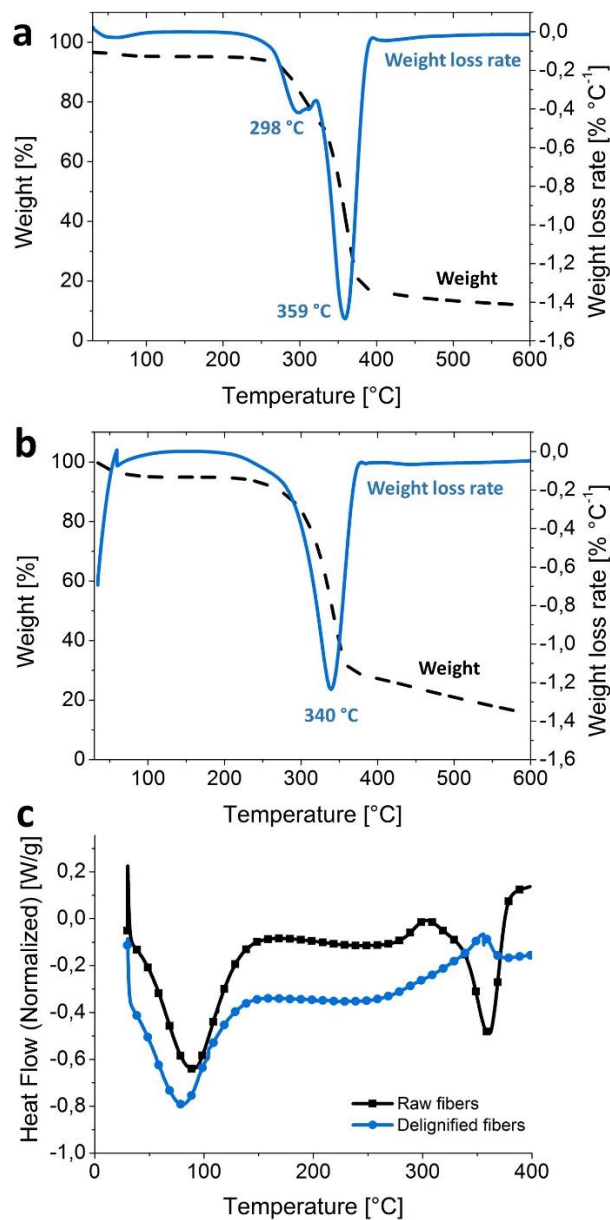


Figure .6 shows thermal analyses for raw and delignified Fique fibers/tow. Pyrolysis of lignocellulosic materials occurs usually in four stages: loss of humidity, hemicellulose, cellulose and lignin decomposition ¹¹⁵. In all the samples analyzed is

¹¹⁵ Yang H, Yan R, Chen H, et al. (2007) Characteristics of hemicellulose, cellulose and lignin

first observed a small weight change, between 30-140 °C, of 2% for raw and 6% for delignified fibers/tow attributed to loss of humidity in the former and a combination of humidity and low molecular weight compounds remaining from the AHP process in the later. Also in raw fibers (Figure 6a) is registered an additional weight loss (18%) at 298 °C consequence, as several authors report, of hemicellulose decomposition; the onset of hemicellulose decomposition (T_d) is approximately 250°C¹¹⁶. Unlike hemicellulose, cellulose is a lineal polymer with no branches and a higher order, which gives it a higher thermal stability¹¹⁷. The maximum weight loss rate for the raw fiber/tow sample was observed in the 320 to 410 °C range, with 359 °C as the point for maximum cellulose decomposition. This is similar to the point for maximum cellulose decomposition of other lignocellulosic materials such as raw cotton linter (340 °C)¹¹⁸, maize straw (320 °C)¹¹⁹, sweet potato residue (336 °C)¹²⁰, jute fibers (338 °C)¹²¹, sisal fibers (355 °C) and commercial cellulose (348 °C)¹²². DTG curves show that degradation temperatures for delignified fiber/tow samples were lower (340 °C) than of raw fibers (359 °C). Lowered degradation temperatures in delignified materials may be due to smaller fiber dimensions compared to raw fibers, leading to high surface areas exposure to heat¹²³.

pyrolysis. *Fuel* 86:1781–1788. doi: 10.1016/j.fuel.2006.12.013

¹¹⁶ Morán JI, Alvarez VA, Cyras VP, Vázquez A (2008) Extraction of cellulose and preparation of nanocellulose from sisal fibers. *Cellulose* 15:149–159. doi: 10.1007/s10570-007-9145-9

¹¹⁷ Yang H, Yan R, Chen H, et al. (2007) Characteristics of hemicellulose, cellulose and lignin pyrolysis. *Fuel* 86:1781–1788. doi: 10.1016/j.fuel.2006.12.013

¹¹⁸ Morais JPS, Rosa M de F, Filho M de S, et al. (2013) Extraction and characterization of nanocellulose structures from raw cotton linter. *Carbohydr Polym* 91:229–235.

¹¹⁹ Rehman N, de Miranda MIG, Rosa SML, et al. (2013) Cellulose and Nanocellulose from Maize Straw: An Insight on the Crystal Properties. *J Polym Environ* 22:252–259. doi: 10.1007/s10924-013-0624-9

¹²⁰ Lu H, Gui Y, Zheng L, Liu X (2013) Morphological, crystalline, thermal and physicochemical properties of cellulose nanocrystals obtained from sweet potato residue. *Food Res Int* 50:121–128. doi: 10.1016/j.foodres.2012.10.013

¹²¹ Cao X, Ding B, Yu J, Al-Deyab SS (2012) Cellulose nanowhiskers extracted from TEMPO-oxidized jute fibers. *Carbohydr Polym* 90:1075–80. doi: 10.1016/j.carbpol.2012.06.046

¹²² Morán JI, Alvarez VA, Cyras VP, Vázquez A (2008) Extraction of cellulose and preparation of nanocellulose from sisal fibers. *Cellulose* 15:149–159. doi: 10.1007/s10570-007-9145-9

¹²³ Jiang F, Hsieh Y-L (2013) Chemically and mechanically isolated nanocellulose and their self-assembled structures. *Carbohydr Polym* 95:32–40. doi: 10.1016/j.carbpol.2013.02.022

On the other hand, the region of maximum weight loss for AHP-treated Fique fibers/tow is broader than for the raw sample starting at 260 °C and ending at 380 °C. The presence of only one weight loss for the AHP-treated samples indicates the removal of most of amorphous structures (hemicellulose and lignin) in the fibers. Raw fibers had residual mass of 12% while treated fibers had residual masses of at least 20%. High amounts of residual char are explained by favored dehydration reactions. For instance, in an ideal pyrolytic process hydrogen and oxygen are released through a dehydration reaction as H₂O while carbon will yield a theoretical residual mass of 44.4%. However, during this process additional reactions, such as decarboxylation, may occur releasing CO and CO₂ as gases and lowering the carbonaceous residue yields. Thus, as dehydrations reaction are favored the yields of carbonaceous residue increases; this fact explains the high residual mass registered for the treated fibers ¹²⁴.

DSC curves (Figure 6b) of all samples show an endothermic peak due to water evaporation from 30 to 130 °C, also corroborated by TGA data. However, raw fibers showed a higher final temperature (90 °C) for this process perhaps due to the presence of amorphous components (hemicellulose and lignin) that help to retain moisture by chemi- and physisorption processes. Delignified samples contain lower amounts of hemicellulose and lignin, leaving cellulose to adsorb moisture with more uniform sorptive forces, causing water evaporation at lower temperature (79 °C)¹²⁵. From 165 °C to 260 °C hemicellulose degradation occurs in raw fibers followed by an exothermic peak, related to α -cellulose depolymerization and formation of 1,6-anidrogucose, from 270 °C to 320 °C ^{126 127}. Raw fibers showed also an endothermic

¹²⁴ Jiang F, Hsieh Y-L (2013) Chemically and mechanically isolated nanocellulose and their self-assembled structures. *Carbohydr Polym* 95:32–40. doi: 10.1016/j.carbpol.2013.02.022

¹²⁵ Mandal A, Chakrabarty D (2011) Isolation of nanocellulose from waste sugarcane bagasse (SCB) and its characterization. *Carbohydr Polym* 86:1291–1299.

¹²⁶ Belaadi A, Bezazi A, Bourchak M, et al. (2014) Thermochemical and statistical mechanical properties of natural sisal fibres. *Compos Part B Eng* 67:481–489. doi: 10.1016/j.compositesb.2014.07.029

¹²⁷ Li W, Zhang Y, Li J, et al. (2015) Characterization of cellulose from banana pseudo-stem by heterogeneous liquefaction. *Carbohydr Polym* 132:513–519. doi: 10.1016/j.carbpol.2015.06.066

peak at 360 °C, corresponding to the fusion of crystalline cellulose ¹²⁸. Delignified Fique/tow samples showed a second exothermic process between 325 and 365 °C due to the thermal transition involving decomposition and degradation of fibers/tow cellulose ^{129 130}.

1.4.3 Experimental designs: optimal conditions. Table 4 shows the effects of H₂O₂ concentration, reaction time and loading on crystallinity index after the AHP process for the experimental design in Fique fibers delignification. Reaction time was the only significant parameter (P value < 0.05) with a positive effect on the crystallinity index. Parameters such as H₂O₂ concentration and loading and their interactions were not significant at least for the conditions tested in the experimental design. However, the interaction between H₂O₂ concentration and reaction time had a p-value close to 0.05 indicating that this interaction might be slightly significant on the crystallinity index after the AHP process. The response surfaces for crystallinity index are shown in Figure 1.7. Both graphics depict crystallinity index versus H₂O₂ concentration and reaction time with loadings of 1% w/v and 8% w/v. It can be inferred that regardless of loading, higher crystallinity indexes can be obtained with high H₂O₂ concentration (10% w/w) and long reaction times (120 min) (Rabelo et al. 2008). In both cases, shorter reaction times resulted in lower crystallinity indexes, which agrees with literature reports ¹³¹(Rabelo et al. 2014).

¹²⁸ Morán JI, Alvarez VA, Cyras VP, Vázquez A (2008) Extraction of cellulose and preparation of nanocellulose from sisal fibers. *Cellulose* 15:149–159. doi: 10.1007/s10570-007-9145-9

¹²⁹ Barreto ACH, Rosa DS, Fachine PBA, Mazzetto SE (2011) Properties of sisal fibers treated by alkali solution and their application into cardanol-based biocomposites. *Compos Part A Appl Sci Manuf* 42:492–500. doi: 10.1016/j.compositesa.2011.01.008

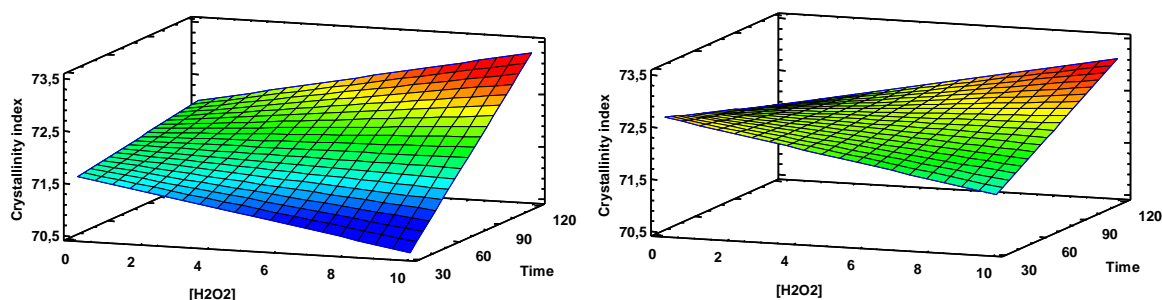
¹³⁰ Miranda MIG, Bica CID, Nachtigall SMB, et al. (2013) Kinetic thermal degradation study of maize straw and soybean hull celluloses by simultaneous DSC–TGA and MDSC techniques. *Thermochim Acta* 565:65–71. doi: 10.1016/j.tca.2013.04.012

¹³¹ Lu H, Gui Y, Zheng L, Liu X (2013) Morphological, crystalline, thermal and physicochemical properties of cellulose nanocrystals obtained from sweet potato residue. *Food Res Int* 50:121–128. doi: 10.1016/j.foodres.2012.10.013

Table 4. Effects on crystallinity index after AHP process.

Factor	F ratio	p value
A: H₂O₂ concentration [% w/w]	0.09	0.7916
B: Time [min]	19.22	0.0483
C: Load [% w/v]	2.89	0.2310
AB	17.07	0.0539
AC	0.00	0.9519
BC	5.40	0.1458

Figure 7. Crystallinity index as a function of H₂O₂ concentration and reaction time using (a) 1% w/v and (b) 8% w/v loadings.



A long reaction time, for ultrasound-assisted processes, may seem counterintuitive since ultrasonic treatments are energy intensive and short reaction times are always recommended. However, the media where sonication is applied influences the mechanoacoustic effects, which are the most likely to occur at low frequencies, such as 40 kHz¹³². The density of the AHP solution might attenuate the effect of ultrasound so longer reaction times are required for effective delignification processes¹³³. On the other hand, it must be noted that biomass load was not significant since crystallinity indexes for 1% or 8% w/v are really close (around 73%).

¹³² Bussemaker MJ, Xu F, Zhang D (2013) Manipulation of ultrasonic effects on lignocellulose by varying the frequency, particle size, loading and stirring. *Bioresour Technol* 148:15–23. doi: 10.1016/j.biortech.2013.08.106

¹³³ García A, Gandini A, Labidi J, et al. (2016) Industrial and crop wastes: A new source for nanocellulose biorefinery. *Ind Crops Prod* 93:26–38. doi: 10.1016/j.indcrop.2016.06.004

Thus, despite longer reaction times are required for a more effective delignification process, high biomass load can be used, which would be an important factor to consider when escalating the process.

1.5 CONCLUSIONS

Fique decortication by-products (tow and pulp), have cellulose contents of 52.3% and 30.5%, respectively. The cellulose in tow has the same physicochemical and spectroscopic characteristics than that of long Fique fibers. On the other hand, Fique pulp is composed of two distinctive materials: cellulose filaments from secondary cell walls and leaf epidermis. Cellulose filaments in Fique pulp are highly amorphous exhibiting low crystallinity; while the epidermis shows the presence of oxalates and waxes, common to the leaf cuticle. The pretreatment of Fique decortication by-products with AHP was effective in the removal of non-cellulosic compounds such as hemicellulose and lignin. Optimal conditions for the delignification of Fique fibers and tow were reached when the samples were subjected to 120 min treatment at 70 °C with a H₂O₂ concentration of 10% w/w at pH 11.5 in the presence of ultrasound. The maximum lignin removal in Fique fibers and tow achieved with this procedure was around 88%, while for Fique pulp the lignin removal was of about 79%. After AHP, IR spectra showed the decrease, or absence, of signals attributed to hemicellulose and lignin, while XRD patterns showed increased crystallinity indexes. Thermal analyses corroborated the removal of components other than cellulose and FESEM pictures showed how the lamellar structure in the macro fiber is disrupted by the removal of hemicellulose, lignin and ground tissue, leaving cellulose microfibrils exposed. As the first in-depth report on Fique by-products characterization, our analyses indicate that alternative uses for Fique by-products such as pulp and tow are highly feasible due to the physicochemical characteristics of these residues and their significant content of crystalline and amorphous cellulose. Furthermore, Fique pulp and tow are produced in greater excess (five times more)

than Figue fibers, which make them an alternative source for extracting cellulose because of their wide availability and low cost.

2. ISOLATION AND CHARACTERIZATION OF CELLULOSE NANOFIBRILS FROM COLOMBIAN FIQUE DECORTICATION BY-PRODUCTS

2.1 ABSTRACT

Fique fibers are extracted from *Furcraea spp* leaves, with 5% average mass yield, using mechanical decortication. Juice, pulp and tow, the by-products of this process, amount 95% of the leaf weight and are considered waste. Cellulose nanofibrils (CNF) were extracted from Fique tow, via ultrasound-assisted TEMPO followed by mechanical disintegration with sonication. Fique CNF exhibit diameters around 100 nm, degree of oxidation (DO) of 0.27 and surface charge density (σ) of 1.6 mmol/g. Fique CNF aqueous suspensions show optical birefringence and high colloidal stability due to a high ζ potential (-53 mV). The morphology, chemical structure, crystallinity and phase transitions of Fique CNF were studied using FESEM, IR-ATR, XRD and TGA. The delignification pretreatment and the TEMPO reaction assisted by ultrasound significantly increase Fique CNF σ and ζ potential, in contrast with the oxidation carried out without ultrasound or with raw (lignified) tow.

2.2 INTRODUCTION

Socio-economic and climate change issues are compelling governments and companies to promote sustainable growth based on transformation of low-cost and renewable resources¹³⁴. Agro-industrial residues, widely distributed, abundant and biodegradable may play an important role in a sustainable future economy worldwide^{135 136}. Many agro-industrial biomass residues are cellulose-rich, which makes them

¹³⁴ García, A., Gandini, A., Labidi, J., Belgacem, N., & Bras, J. (2016). Industrial and crop wastes: A new source for nanocellulose biorefinery. *Industrial Crops and Products*, 93, 26–38. <https://doi.org/10.1016/j.indcrop.2016.06.004>

¹³⁵ Moriana, R., Vilaplana, F., & Ek, M. (2015). Forest residues as renewable resources for bio-based polymeric materials and bioenergy: chemical composition, structure and thermal properties. *Cellulose*, 22(5), 3409–3423. <https://doi.org/10.1007/s10570-015-0738-4>

¹³⁶ Wang, B., Sain, M., & Oksman, K. (2007). Study of Structural Morphology of Hemp Fiber from the

an attractive alternative for the production of biomaterials. Compared to wood by-products, these residues have lower contents of lignin and hemicelluloses which make them a convenient feedstock for biomaterials production ¹³⁷ ¹³⁸. For instance, several researchers have been studying the extraction of nanocellulose from agro-industrial residues such as banana by-products, jute and pineapple leaves ¹³⁹, oil palm empty fruit bunch¹⁴⁰, hemp fibers ¹⁴¹, cotton, sisal and flax fibers, corn stover and rice husk ¹⁴² and *eucalyptus globulus* and rice straw ¹⁴³, among others.

Nanocellulose (NC), dubbed as “super-material”, is an attractive natural resource with outstanding mechanical, rheological, chemical and structural properties and a myriad of potential applications. NC can be extracted as cellulose nanocrystals (CNC) or cellulose nanofibers (CNF) through chemical and mechanical processes from lignocellulosic materials (e.g. wood pulp, cotton, tunicates, bacterial cellulose,

Micro to the Nanoscale. *Applied Composite Materials*, 14(2), 89–103. <https://doi.org/10.1007/s10443-006-9032-9>

¹³⁷ García, A., Gandini, A., Labidi, J., Belgacem, N., & Bras, J. (2016). Industrial and crop wastes: A new source for nanocellulose biorefinery. *Industrial Crops and Products*, 93, 26–38. <https://doi.org/10.1016/j.indcrop.2016.06.004>

¹³⁸ Wang, B., Sain, M., & Oksman, K. (2007). Study of Structural Morphology of Hemp Fiber from the Micro to the Nanoscale. *Applied Composite Materials*, 14(2), 89–103. <https://doi.org/10.1007/s10443-006-9032-9>

¹³⁹ Abraham, E., Deepa, B., Pothan, L. A., Jacob, M., Thomas, S., Cvelbar, U., et al. (2011). Extraction of nanocellulose fibrils from lignocellulosic fibres: A novel approach. *Carbohydrate Polymers*, 86, 1468–1475.

¹⁴⁰ Haafiz, M. K. M., Hassan, A., Zakaria, Z., & Inuwa, I. M. (2014). Isolation and characterization of cellulose nanowhiskers from oil palm biomass microcrystalline cellulose. *Carbohydrate Polymers*, 103(1), 119–125. <https://doi.org/10.1016/j.carbpol.2013.11.055>

¹⁴¹ Wang, B., Sain, M., & Oksman, K. (2007). Study of Structural Morphology of Hemp Fiber from the Micro to the Nanoscale. *Applied Composite Materials*, 14(2), 89–103. <https://doi.org/10.1007/s10443-006-9032-9>

¹⁴² Ludueña, L. N., Vecchio, A., Stefani, P. M., & Alvarez, V. A. (2013). Extraction of cellulose nanowhiskers from natural fibers and agricultural byproducts. *Fibers and Polymers*, 14(7), 1118–1127. <https://doi.org/10.1007/s12221-013-1118-z>

¹⁴³ Lee, B.-M., Jeun, J.-P., Kang, P.-H., Choi, J.-H., & Hong, S.-K. (2017). Isolation and characterization of nanocrystalline cellulose from different precursor materials. *Fibers and Polymers*, 18(2), 272–277. <https://doi.org/10.1007/s12221-017-6548-6>

etc.)^{144 145 146}. Industrially CNC are usually obtained by acid hydrolysis of cellulose, while CNF are frequently produced by high-shear mechanical treatment or catalyzed oxidation reactions. Structurally CNF show both amorphous and crystalline regions whereas in CNC the amorphous part of cellulose is removed during the hydrolysis¹⁴⁷. In CNF production, the TEMPO (2,2,6,6-tetramethylpiperidine-1-oxyl)-mediated oxidation of native cellulose stands out amongst the most used chemical methods. The material derived from this process is commonly called TOCN (Tempo-Oxidized Cellulose Nanofibrils). TEMPO converts primary –OH bound to the C6 in the glucose units of cellulose, into their carboxyl derivatives –COOH, using sodium hypochlorite and sodium bromide as oxidant and co-oxidant agents, respectively¹⁴⁸. TEMPO-oxidation occurs only superficially in both crystalline and amorphous regions of cellulose, usually without significant alteration of the biopolymer's crystallinity index^{149 150}. TOCN characterization is given in terms of aspect ratio (nanometric width and micrometric length), crystallinity, and thermal and suspension stability in aqueous solution (ζ potential). The TEMPO reaction occurs generally under conditions such as pH around 10.5 and room temperature and sonicating after the

¹⁴⁴ Isogai, A., Saito, T., & Fukuzumi, H. (2011). TEMPO-oxidized cellulose nanofibers. *Nanoscale*, 3(1), 71–85. <https://doi.org/10.1039/C0NR00583E>

¹⁴⁵ Lavoine, N., Desloges, I., Dufresne, A., & Bras, J. (2012). Microfibrillated cellulose – Its barrier properties and applications in cellulosic materials: A review. *Carbohydrate Polymers*, 90(2), 735–764. <https://doi.org/10.1016/j.carbpol.2012.05.026>

¹⁴⁶ Saito, T., Nishiyama, Y., Putaux, J.-L., Vignon, M., & Isogai, A. (2006). Homogeneous Suspensions of Individualized Microfibrils from TEMPO-Catalyzed Oxidation of Native Cellulose. *Biomacromolecules*, 7(6), 1687–1691. <https://doi.org/10.1021/bm060154s>

¹⁴⁷ Lichtenstein, K., & Lavoine, N. (2017). Toward a deeper understanding of the thermal degradation mechanism of nanocellulose. *Polymer Degradation and Stability*, 146, 53–60. <https://doi.org/10.1016/j.polymdegradstab.2017.09.018>

¹⁴⁸ Habibi, Y., Lucia, L. A., & Rojas, O. J. (2010). Cellulose nanocrystals: chemistry, self-assembly, and applications. *Chemical Reviews*, 110(6), 3479–3500.

¹⁴⁹ Kuramae, R., Saito, T., & Isogai, A. (2014). TEMPO-oxidized cellulose nanofibrils prepared from various plant holocelluloses. *Reactive and Functional Polymers*, 85, 126–133. <https://doi.org/10.1016/j.reactfunctpolym.2014.06.011>

¹⁵⁰ Puangsin, B., Yang, Q., Saito, T., & Isogai, A. (2013). Comparative characterization of TEMPO-oxidized cellulose nanofibril films prepared from non-wood resources. *International Journal of Biological Macromolecules*, 59, 208–213. <https://doi.org/10.1016/j.ijbiomac.2013.04.016>

oxidation reaction is done to promote the mechanical disintegration¹⁵¹ ¹⁵² ¹⁵³. Interestingly, recent reports also propose the use of ultrasonic radiation during the actual oxidation reaction to facilitate the oxidation of native cellulose¹⁵⁴ ¹⁵⁵ ¹⁵⁶. Ultrasound produces mechanoacoustic and sonochemical effects capable of altering the surface of the lignocellulosic materials and increasing reaction rates through a process called cavitation (formation, growth and violent collapse of bubbles)¹⁵⁷. The high energy generated by this process (10–100 kJ/mol)¹⁵⁸ is enough to disrupt interfibrillar hydrogen bonds between cellulose molecules (19–21 kJ mol)¹⁵⁹. In this way, ultrasound-assisted reactions provide an alternative way to achieve high oxidation yields (increasing the amount of carboxylate functional groups up to 100%) and homogeneous cellulosic nanostructures under mild reaction conditions (25 °C)¹⁶⁰ ¹⁶¹.

¹⁵¹ Cao, X., Ding, B., Yu, J., & Al-Deyab, S. S. (2012). Cellulose nanowhiskers extracted from TEMPO-oxidized jute fibers. *Carbohydrate Polymers*, *90*(2), 1075–1080. <https://doi.org/10.1016/j.carbpol.2012.06.046>

¹⁵² Liu, C., Li, B., Du, H., Lv, D., Zhang, Y., Yu, G., et al. (2016). Properties of nanocellulose isolated from corncob residue using sulfuric acid, formic acid, oxidative and mechanical methods. *Carbohydrate Polymers*, *151*, 716–724. <https://doi.org/10.1016/j.carbpol.2016.06.025>

¹⁵³ Saito, T., Kimura, S., Nishiyama, Y., & Isogai, A. (2007). Cellulose Nanofibers Prepared by TEMPO-Mediated Oxidation of Native Cellulose. *Biomacromolecules*, *8*(8), 2485–2491. <https://doi.org/10.1021/bm0703970>

¹⁵⁴ Mishra, S. P., Thirree, J., Manent, A., & Chabot, B. (2011). Ultrasound-catalyzed tempo-mediated oxidation of native cellulose for the production of nanocellulose: effect of process variables, *6*(Brown 2010), 121–143.

¹⁵⁵ Rattaz, A., Mishra, S. P., Chabot, B., & Daneault, C. (2011). Cellulose nanofibres by sonocatalysed-TEMPO-oxidation. *Cellulose*, *18*(3), 585–593. <https://doi.org/10.1007/s10570-011-9529-8>

¹⁵⁶ Rohaizu, R., & Wanrosli, W. D. (2017). Sono-assisted TEMPO oxidation of oil palm lignocellulosic biomass for isolation of nanocrystalline cellulose. *Ultrasonics Sonochemistry*, *34*, 631–639. <https://doi.org/10.1016/j.ultsonch.2016.06.040>

¹⁵⁷ Ramadoss, G., & Muthukumar, K. (2015). Influence of dual salt on the pretreatment of sugarcane bagasse with hydrogen peroxide for bioethanol production. *Chemical Engineering Journal*, *260*, 178–187. <https://doi.org/10.1016/j.cej.2014.08.006>

¹⁵⁸ Chen, W., Yu, H., Liu, Y., Chen, P., Zhang, M., & Hai, Y. (2011). Individualization of cellulose nanofibers from wood using high-intensity ultrasonication combined with chemical pretreatments. *Carbohydrate Polymers*, *83*(4), 1804–1811. <https://doi.org/10.1016/j.carbpol.2010.10.040>

¹⁵⁹ Rohaizu, R., & Wanrosli, W. D. (2017). Sono-assisted TEMPO oxidation of oil palm lignocellulosic biomass for isolation of nanocrystalline cellulose. *Ultrasonics Sonochemistry*, *34*, 631–639. <https://doi.org/10.1016/j.ultsonch.2016.06.040>

¹⁶⁰ Mishra, S. P., Manent, A.-S., Chabot, B., & Daneault, C. (2012). Production of nanocellulose from native cellulose - various options utilizing ultrasound. *Bioresources*, *7*(1), 422–436.

¹⁶¹ Rohaizu, R., & Wanrosli, W. D. (2017). Sono-assisted TEMPO oxidation of oil palm lignocellulosic biomass for isolation of nanocrystalline cellulose. *Ultrasonics Sonochemistry*, *34*, 631–639.

Colombia is the largest producer of Fique fibers in the world, with a net production of 30,000 tons per year. However, the fibers only represent 5% of the Fique leaves weight while the remaining by-products, 95 wt%, lack commercial applications and are typically disposed of in surface waters polluting and causing serious environmental damage^{162 163}. These by-products include tow (8%), pulp (17%) and juice (70%). Fique pulp and tow are mainly composed of cellulose, hemicellulose and lignin¹⁶⁴. The cellulose content in these two Fique by-products ranges from 30 to 70 wt% depending on the species, season and age of the plant¹⁶⁵. Fique tow has physicochemical properties similar to those of Fique fibers; the only difference between these two materials is essentially their length and width. While Fique fibers are typically 1-2 m long and 0.15-0.25 mm thick, Fique tow has an average length of 30 cm and 0.1-0.2 mm thickness. On the other hand, Fique pulp is mostly composed of cellulose with low crystallinity (30.5 wt%)¹⁶⁶.

In Fique tow, as in fibers, cellulose, hemicelluloses and lignin self-assemble to form a natural composite tied up by strong interactions, such as covalent and hydrogen bonds, and weak forces of the van der Waals type^{167 168}. The hierarchical structure of these materials is responsible for their well-known mechanical strength and high

<https://doi.org/10.1016/j.ultsonch.2016.06.040>

¹⁶² Peinado, J. E., Ospina, L. F., Rodríguez, L., Miller, J., Carvajal, C., & Negrete, R. (2006). *Guía Ambiental del Subsector Fiquero*. Bogotá: Cadena Productiva Nacional del Fique.

¹⁶³ Quintero, M., Castro, L., Ortiz, C., Guzmán, C., & Escalante, H. (2012). Enhancement of starting up anaerobic digestion of lignocellulosic substrate: Fique's bagasse as an example. *Bioresource Technology*, *108*, 8–13. <https://doi.org/10.1016/j.biortech.2011.12.052>

¹⁶⁴ Ovalle-Serrano, S. A., Blanco-Tirado, C., & Combariza, M. Y. (2018). Exploring the composition of raw and delignified Colombian Fique fibers, tow and pulp. *Cellulose*, *25*(1), 151–165. <https://doi.org/10.1007/s10570-017-1599-9>

¹⁶⁵ Cao, Y., Jiang, Y., Song, Y., Cao, S., Miao, M., Feng, X., et al. (2015). Combined bleaching and hydrolysis for isolation of cellulose nanofibrils from waste sackcloth. *Carbohydrate Polymers*, *131*, 152–158. <https://doi.org/10.1016/j.carbpol.2015.05.063>

¹⁶⁶ Ovalle-Serrano, S. A., Blanco-Tirado, C., & Combariza, M. Y. (2018). Exploring the composition of raw and delignified Colombian Fique fibers, tow and pulp. *Cellulose*, *25*(1), 151–165. <https://doi.org/10.1007/s10570-017-1599-9>

¹⁶⁷ Habibi, Y., Lucia, L. A., & Rojas, O. J. (2010). Cellulose nanocrystals: chemistry, self-assembly, and applications. *Chemical Reviews*, *110*(6), 3479–3500.

¹⁶⁸ Oudiani, a. El, Chaabouni, Y., Msahli, S., & Sakli, F. (2011). Crystal transition from cellulose I to cellulose II in NaOH treated Agave americana L. fibre. *Carbohydrate Polymers*, *86*(3), 1221–1229. <https://doi.org/10.1016/j.carbpol.2011.06.037>

performance. However, disassembling strategies involving chemical or mechanical processes are needed to disrupt this highly-ordered structure in order to access the cellulose ¹⁶⁹. The use of acid/alkaline processes, steam explosion, organosolv and ionic liquids rank amongst the most common chemical treatments for cellulose delignification, being the acid-chlorite delignification procedure the most used in the paper industry. These processes usually need special corrosion resistant reactors and have intensive energy requirements. An interesting alternative for cellulose delignification (of non-wooded materials) is the alkaline hydrogen peroxide treatment, that requires mild conditions without toxic by-product formation ^{170 171}. Last chapter showed that the use of the alkaline hydrogen peroxide treatment for the delignification of Fique fibers, tow and pulp allows significant removal of non-cellulosic compounds, up to 80% ¹⁷². A logical step towards biomass valorization, in the case of the Fique crops in Colombia, would involve the isolation of added-value materials from by-products such as tow. Since Fique tow amounts to 8 wt% of the total Fique leaf weight, it is an interesting raw source for isolating nanocellulose (nanofibers and nanocrystals).

As reviewed above, nowadays the use of residual biomass is quickly becoming a mainstream industrial approach for the production of advanced biodegradable materials, such as nanocellulose. The use of residual biomass promotes alternative uses for these sustainable feedstock which in some cases, particularly in developing countries such as Colombia, would become wastes with negative environmental impact. In this chapter is demonstrated that cellulose nanofibrils (CNF) can be

¹⁶⁹ Dufresne, A. (2013a). Nanocellulose: a new ageless bionanomaterial. *Materials Today*, 16(6), 220–227. <https://doi.org/10.1016/j.mattod.2013.06.004>

¹⁷⁰ Argun, H., & Onaran, G. (2015). Delignification of vineyard pruning residues by alkaline peroxide treatment. *Industrial Crops and Products*, 74, 697–702. <https://doi.org/10.1016/j.indcrop.2015.05.031>

¹⁷¹ Sun, R. C., Fang, J. M., & Tomkinson, J. (2000). Delignification of rye straw using hydrogen peroxide. *Industrial Crops and Products*, 12(2), 71–83. [https://doi.org/10.1016/S0926-6690\(00\)00039-X](https://doi.org/10.1016/S0926-6690(00)00039-X)

¹⁷² Ovalle-Serrano, S. A., Blanco-Tirado, C., & Combariza, M. Y. (2018). Exploring the composition of raw and delignified Colombian Fique fibers, tow and pulp. *Cellulose*, 25(1), 151–165. <https://doi.org/10.1007/s10570-017-1599-9>

extracted from Fique by-products using a standard chemical oxidation process (TEMPO) aided by ultrasound energy. The chemical properties of these materials vary depending on the oxidation reaction conditions. CNF from Fique exhibit similar physicochemical, thermal, and microscopic properties than CNF from different biomasses. To the best of our knowledge, extraction of nanocellulose from lignocellulosic biomass from Colombian Fique crops has not been reported. Fique CNF were characterized by means of field emission scanning electron microscopy (FESEM), attenuated total reflectance infrared spectroscopy (ATR-IR), X-ray diffraction (XRD), thermogravimetric analyses (TGA), optical birefringence, carboxylate content and ζ potential.

2.3 EXPERIMENTAL

2.3.1 Materials. Residues from Fique leaves decortication (containing pulp, juice and tow) were collected from Fique crops of the species “uña de águila” (*Furcraea macrophylla*) in the rural area of San Joaquín, Santander, Colombia. Hydrogen peroxide (H_2O_2), sodium bromide (NaBr), sodium hydroxide (NaOH), hydrochloric acid (HCl, 37 %) and ethanol (analytical grade) were purchased from Merck (Darmstadt, Germany). 2,2,6,6-Tetramethyl-piperidin-1-oxyl (TEMPO, 98 %) was purchased from Sigma Aldrich (Saint Louis, MO, USA). Sodium hypochlorite (NaClO, 5 % Cl) was purchased from Carlo Erba Reagents (Milan, Italy). All chemical reagents were used with no further purification. Aqueous solutions and suspensions were prepared with ultrapure water (18 M Ω ·cm @ 25 °C).

2.3.2 Tow pretreatment. Fique tow was isolated by sieving from juice, and manually from bagasse. The collected material was filtered and washed thoroughly with distilled water and sonicated at 40 °C for 60 minutes in an ultrasonic bath (Bransonic CPX3800, 40 kHz, 130 Watt) to remove Fique juice remnants and other water-soluble materials as well as calcium carbonates and oxalates commonly found in these hard cellulosic fibers. Samples were finally dried at 60 °C for 24 h. Fique tow

contains 52.3% cellulose, 23.8% hemicellulose and 23.9% lignin in average. Fique tow was delignified following the procedure reported in the last chapter¹⁷³. In brief, pretreated Fique tow was cut into lengths of about 1 cm and immersed in a 10% w/w H₂O₂ solution brought to pH 11.5 by dropwise addition of NaOH 4 N, keeping a biomass load of 8% w/v. This mixture was allowed to react for 120 min, at 70 °C under ultrasonic irradiation. Finally, the product was filtrated, washed thoroughly with distilled water and dried at 60 °C for 24 h.

2.3.4 TEMPO-mediated oxidation of Fique tow. A slightly modified procedure than the one reported by Saito & Isogai¹⁷⁴ was followed. 1 g of delignified Fique tow was suspended in 100 mL of water (1% wt.). 16 mg of TEMPO and 100 mg of NaBr were added to the suspension under magnetic stirring at room temperature. Immediately, the primary oxidant (NaClO, 0.037 mol) was added dropwise and the reaction was carried out on an ultrasonic bath (Bransonic CPX3800, 40 kHz, 130 Watt), while pH was kept at 10.5 with NaOH 0.5 N during the course of the reaction. When no consumption of NaOH was registered (around 120 min) ethanol was added to neutralize residual NaClO and to quench the reaction. Finally, to remove unreacted chemical species and separate the Fique tow TOCN (a white precipitate), the mixture was centrifuged (4700 rpm for 15 min) and washed with deionized water until neutral pH. As control tests the same procedure was repeated using 1 g of raw Fique tow. Additionally, to highlight the effect of ultrasound in the reaction the procedure was also performed using 1 g of delignified Fique tow without ultrasound during the reaction.

2.3.5 Mechanical disintegration. To obtain uniform dispersions of individual nanofibrils after TEMPO, 0.5 % wt of aqueous suspension of the Fique tow TOCN

¹⁷³ Ovalle-Serrano, S. A., Blanco-Tirado, C., & Combariza, M. Y. (2018). Exploring the composition of raw and delignified Colombian Fique fibers, tow and pulp. *Cellulose*, 25(1), 151–165. <https://doi.org/10.1007/s10570-017-1599-9>

¹⁷⁴ Saito, T., & Isogai, A. (2004). TEMPO-Mediated Oxidation of Native Cellulose. The Effect of Oxidation Conditions on Chemical and Crystal Structures of the Water-Insoluble Fractions. *Biomacromolecules*, 5(5), 1983–1989. <https://doi.org/10.1021/bm0497769>

were subjected to ten-minute cycles of sonication using an Ultrasonic Processor (Sonics vibra-cell VC750, 20 kHz, 750 Watt) operated at 40% amplitude. To prevent localized heating, a double wall glass beaker attached to a recirculating cooling system was used so that the solution temperature was always kept at 20 °C. Finally, the suspension was centrifuged at 4700 rpm for 20 min to remove non-fibrillated cellulose and the supernatant, a translucent suspension of Fique tow TOCN, was collected and stored for characterization.

2.3.6 Conversion to free carboxyl groups. After TEMPO-mediated regioselective oxidation of Fique tow, the superficial carboxyl groups in the resulting nanofibrils are in the form of sodium carboxylate salt (-COONa). To convert the sodium carboxylates into the free acid form (-COOH) a HCl solution (0.5 N) was added to an aqueous dispersion of Fique tow TOCN (0.5% wt.) until pH 2 under magnetic stirring during 0.5 h, according to the procedure reported by Fujisawa ¹⁷⁵. After ion exchange the solution of Fique tow TOCN became a translucent gel by the conversion of the -COONa groups to -COOH. To remove the excess acid, the gel was washed until pH 4 with distilled water, using vacuum filtration, and then it was re-dispersed in water. The aqueous suspensions of TOCN were collected and dried for further characterization.

2.3.7 Characterization. The colloidal stability of Fique tow TOCN in aqueous suspension 0.5% wt. was determined according to the zeta potential value, ζ , measured with a Malvern Zetasizer Nano ZS90 instrument (Worcestershire, UK), equipped with a capillary cell 1070. The optical phenomenon of birefringence was observed when a 0.5% wt. Fique tow TOCN suspension was placed between two crossed polarizers and irradiated with visible light¹⁷⁶. Field emission scanning electron microscopy (FESEM) images were taken on a FEI QUANTA FEG 650

¹⁷⁵ Fujisawa, S., Okita, Y., Fukuzumi, H., Saito, T., & Isogai, A. (2011). Preparation and characterization of TEMPO-oxidized cellulose nanofibril films with free carboxyl groups. *Carbohydrate Polymers*, 84(1), 579–583. <https://doi.org/10.1016/j.carbpol.2010.12.029>

¹⁷⁶ Ibit.

(Oregon, USA) instrument equipped with a large field detector. Samples were coated with a thin layer of carbon or gold (around 20 nm) before imaging and the micrographs were taken at 10 kV. For attenuated total reflectance (ATR-IR) measurements a Bruker Tensor 27 (Billerica, MA) FTIR instrument equipped with a Platinum Diamond ATR unit A225/Q (Billerica, MA) was used at a resolution of 2 cm⁻¹ and 32 scans were accumulated for each spectrum. X-Ray diffraction (XRD) analyses were performed on a Bruker D8 DISCOVER X-ray diffractometer (Billerica, MA) with a DaVinci geometry, using a CuK α 1 radiation source (40 kV and 30 mA), an area detector VANTEC-500, and a poly(methyl methacrylate) sample holder. Thermogravimetric (TGA) analyses were performed with a TA Instruments analyzer Discovery TGA (Newcastle, England), using nitrogen at 50 mL/min and a heating rate 10 °C/min starting from room temperature up to 500 °C.

2.3.8 Conductimetry. The carboxyl content of Fique tow TOCN was measured by conductimetric titration according to the procedure reported by Habibi¹⁷⁷ and Jiang and Hsieh¹⁷⁸. 50 mg of Fique tow TOCN were suspended in 0.01 M HCl until pH 2 to ensure protonation of carboxylate groups. Conductimetric titrations were performed on the suspensions using 0.01 M NaOH. The titration curves typically show three stages: (1) a sharp decrease in conductivity due to the HCl/NaOH reaction, (2) slow decrease due to the reaction between a weak acid (carboxyl groups) and NaOH and (3) an increase in conductivity due to the excess of NaOH added since all acids (strong and weak) had been neutralized. This allows the calculation of the degree of oxidation (DO) and the surface charge density (σ), also known as carboxyl content, by the following equations:

¹⁷⁷ Habibi, Y., Chanzy, H., & Vignon, M. R. (2006). TEMPO-mediated surface oxidation of cellulose whiskers. *Cellulose*, 13(6), 679–687. <https://doi.org/10.1007/s10570-006-9075-y>

¹⁷⁸ Jiang, F., & Hsieh, Y.-L. (2013). Chemically and mechanically isolated nanocellulose and their self-assembled structures. *Carbohydrate Polymers*, 95(1), 32–40. <https://doi.org/10.1016/j.carbpol.2013.02.022>

$$DO = \frac{162 \times c \times (V_2 - V_1)}{m - 36 \times c \times (V_2 - V_1)} \quad (1)$$

$$\sigma = \frac{c \times (V_2 - V_1)}{m} \quad (2)$$

Where c is the NaOH concentration (in mol/L), V_1 and V_2 are the amount of NaOH (in L), m is the mass of TOCN (in g) and the value of 36 corresponds to the difference between the molecular weight of an anhydroglucose unit (162 g/mol) and that of the sodium salt of a glucuronic acid moiety (198 g/mol). Triplicate measurements were performed for each sample.

2.4 RESULTS AND DISCUSSION

The mechanical decortication of the Fique leaves results in the extraction of Fique fibers and by-products namely: tow, pulp and juice. Fique fibers and tow have similar chemical composition, with cellulose contents ranging from 50-70%¹⁷⁹. The main difference between these materials lies in the length and width of the fibers; while tow is comprised of short and thin fibers, from 10 to 30 cm in length and 0.1-0.2 mm in width, Fique fibers are up to 1-2 m long and 0.15 to 0.25 mm wide. The short length of Fique tow is the reason why it ends up with the decortication by-products¹⁸⁰¹⁸¹¹⁸². However, its high cellulose content and percentage weight in the Fique leave (up to 8%) makes it a suitable raw material for nanocellulose isolation.

¹⁷⁹ Ovalle-Serrano, S. A., Blanco-Tirado, C., & Combariza, M. Y. (2018). Exploring the composition of raw and delignified Colombian Fique fibers, tow and pulp. *Cellulose*, 25(1), 151–165. <https://doi.org/10.1007/s10570-017-1599-9>

¹⁸⁰ Gañán, P., & Mondragon, I. (2002). Surface modification of Fique fibers. Effect on their physico-mechanical properties. *Polymer Composites*, 23(3), 383–394. <https://doi.org/10.1002/pc.10440>

¹⁸¹ Ovalle-Serrano, S. A., Blanco-Tirado, C., & Combariza, M. Y. (2018). Exploring the composition of raw and delignified Colombian Fique fibers, tow and pulp. *Cellulose*, 25(1), 151–165. <https://doi.org/10.1007/s10570-017-1599-9>

¹⁸² Peinado, J. E., Ospina, L. F., Rodríguez, L., Miller, J., Carvajal, C., & Negrete, R. (2006). *Guía Ambiental del Subsector Fiquero*. Bogotá: Cadena Productiva Nacional del Fique.

Figures 8a and 8b show Fique tow before and after the delignification process, respectively. Untreated Fique tow usually exhibits cream to light brown shades due to the presence of lignin (~23%). For Fique tow delignification we followed an alkaline hydrogen peroxide procedure previously reported by Sun et al ¹⁸³. This procedure allowed us to remove lignin via formation of a strong nucleophile (hydroperoxide ion, HOO⁻) able to transform chromophoric groups in lignin into nonchromophoric species. Hydroxyl (HO[·]) and superoxide anion (O₂^{·-}) radicals, also produced during the treatment, bleach the material attacking lignin side-chains and producing low-molecular-weight and water-soluble oxidation products ^{184 185}. This process converts Fique tow into a clear material easily discerned from the light brown original material. FESEM images of untreated (Figure 8c) and delignified Fique tow (Figure 8d) show the structural change in the fiber after the delignification process. The removal of hemicellulose and lignin reduces the Fique tow width to less than 0.1 mm and also alters the hierarchical structure of the macrofibers allowing separation of the individual microfibrils ^{186 187}. After tow delignification lignin content went down from 23.3% to 2.8% while cellulose content increased from 52.3% to 83.6%. Additionally, micrographs of the delignified material show an “unraveling” of the fiber macrostructure as consequence of the chemical treatment. This preliminary deconstruction of the fiber impacts positively the yield of nanocellulose in later steps.

¹⁸³ Sun, R. C., Fang, J. M., & Tomkinson, J. (2000). Delignification of rye straw using hydrogen peroxide. *Industrial Crops and Products*, 12(2), 71–83. [https://doi.org/10.1016/S0926-6690\(00\)00039-X](https://doi.org/10.1016/S0926-6690(00)00039-X)

¹⁸⁴ Ouchi, A. (2008). Efficient total halogen-free photochemical bleaching of kraft pulps using alkaline hydrogen peroxide. *Journal of Photochemistry and Photobiology A: Chemistry*, 200(2–3), 388–395. <https://doi.org/10.1016/j.jphotochem.2008.09.006>

¹⁸⁵ Sun, R. C., Fang, J. M., & Tomkinson, J. (2000). Delignification of rye straw using hydrogen peroxide. *Industrial Crops and Products*, 12(2), 71–83. [https://doi.org/10.1016/S0926-6690\(00\)00039-X](https://doi.org/10.1016/S0926-6690(00)00039-X)

¹⁸⁶ Ouchi, A. (2008). Efficient total halogen-free photochemical bleaching of kraft pulps using alkaline hydrogen peroxide. *Journal of Photochemistry and Photobiology A: Chemistry*, 200(2–3), 388–395. <https://doi.org/10.1016/j.jphotochem.2008.09.006>

¹⁸⁷ Su, Y., Du, R., Guo, H., Cao, M., Wu, Q., Su, R., et al. (2015). Fractional pretreatment of lignocellulose by alkaline hydrogen peroxide: Characterization of its major components. *Food and Bioproducts Processing*, 94(April), 322–330. <https://doi.org/10.1016/j.fbp.2014.04.001>

We employed TEMPO regioselective oxidation of the C6 primary alcohol of the monomeric D-anhydroglucose unit of cellulose to induce cellulose nanofibers disaggregation and surface modification. During the first stage of the reaction we obtained a homogeneous and translucent aqueous suspension of TOCN (TEMPO-oxidized cellulose nanofibrils), which are in the form of the sodium salt ($-\text{COO}^- \text{Na}^+$) (Figure 9a). In this form Fique tow TOCNs form a stable dispersion in water due to the presence of ionic species, e.g. $-\text{COO}^-$ units on the surface of cellulose and Na^+ ions in solution. The $-\text{COO}^-$ groups on the cellulose inhibit hydrogen bond formation between the nanofibrils because of Coulombic repulsion, keeping the Fique-TOCNs dispersed in water. This effect, known as 'hydrogen bond lock', was suggested by Missoum¹⁸⁸ who found that addition of NaCl to an aqueous suspension of TOCN prevents the formation of hydrogen bonds, and allows redispersion of the material in water after lyophilization. To transform the $-\text{COO}^- \text{Na}^+$ groups in Fique tow TOCN into the free acid form we performed ion exchange using HCl. After this exchange, the TOCN suspension became a homogeneous, non-flowable and translucent gel (Figure 9b), due to an increase in specific surface area of the TOCN in comparison with the original Fique tow sample. These new features are probably due to the difference in the hydrogen bonding patterns between TOCN- $\text{COO}^- \text{Na}^+$ and TOCN-COOH. Since $\text{COO}^- \text{Na}^+$ groups cannot form intra- and inter-nanofibril hydrogen bonds, these bonds in TOCN- $\text{COO}^- \text{Na}^+$ are only formed between hydroxyl groups. On the other hand, -COOH groups are able to form intra- and inter-nanofibril hydrogen bonds, making TOCN-COOH less hydrophilic than TOCN- $\text{COO}^- \text{Na}^+$ ¹⁸⁹.

¹⁸⁸ Missoum, K., Bras, J., & Belgacem, M. N. (2012). Water Redispersible Dried Nanofibrillated Cellulose by Adding Sodium Chloride. *Biomacromolecules*, 13(12), 4118–4125. <https://doi.org/10.1021/bm301378n>

¹⁸⁹ Fujisawa, S., Okita, Y., Fukuzumi, H., Saito, T., & Isogai, A. (2011). Preparation and characterization of TEMPO-oxidized cellulose nanofibril films with free carboxyl groups. *Carbohydrate Polymers*, 84(1), 579–583. <https://doi.org/10.1016/j.carbpol.2010.12.029>

Figure 8. Images of (a) untreated and (b) delignified Figue tow. FESEM images of (c) untreated and (d) delignified Figue tow.

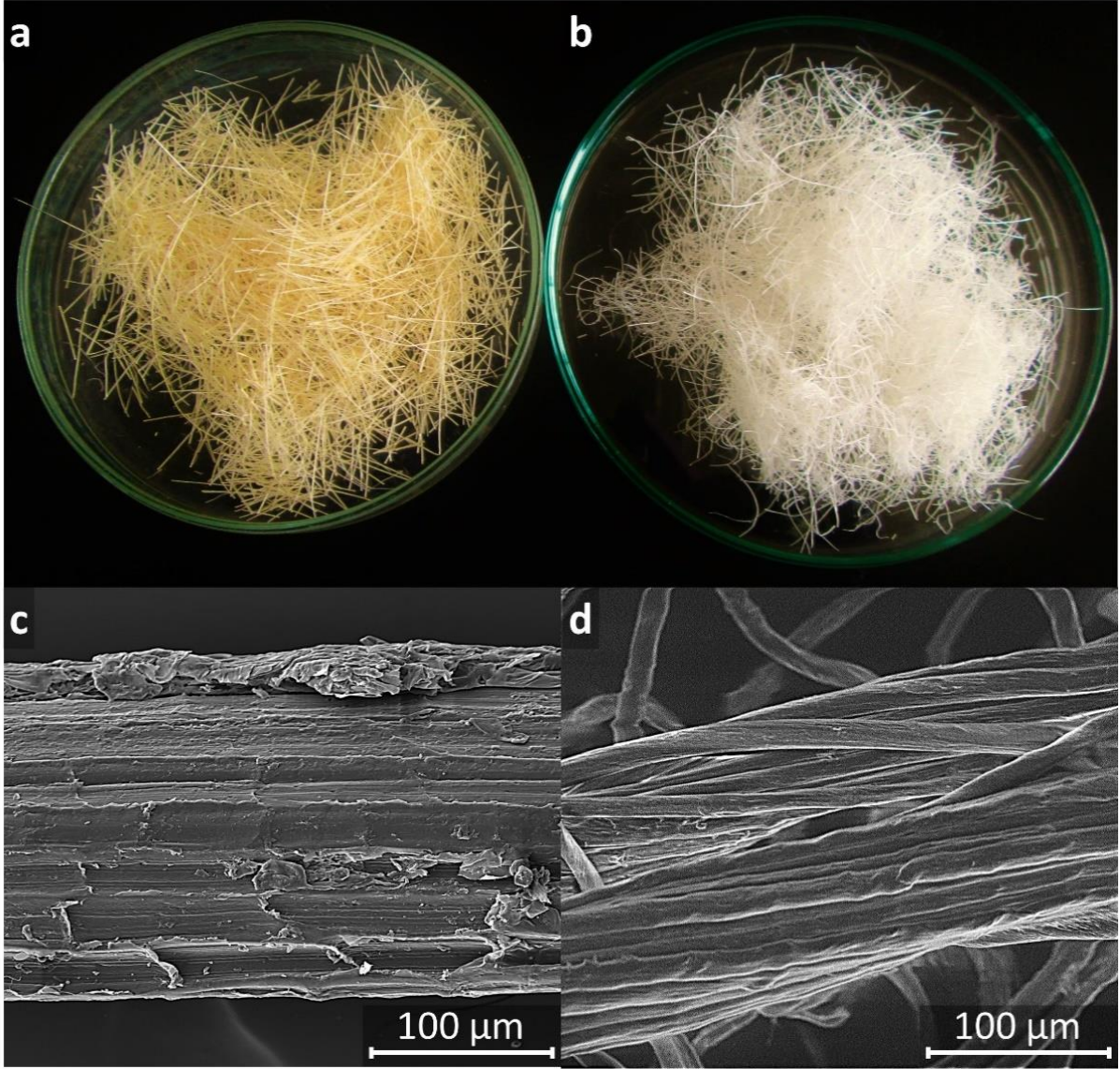
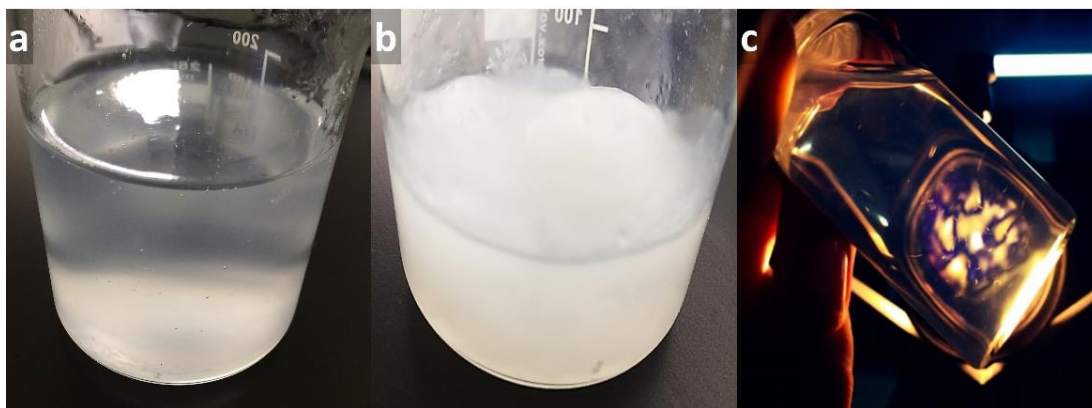


Figure 9. (a) Delignified Figue tow TOCN aqueous suspension (0.5 %wt.), (b) gel-like appearance of TOCN in free acid form and (c) Optical phenomena of birefringence.



TOCN usually exhibit anisotropic behavior in aqueous suspensions. At dilute concentrations, nanocellulose appears as spheroids or ovaloids with ordered domains similar to tactoids¹⁹⁰. However, when increasing the concentration above a critical value ($\sim 30\%$)¹⁹¹ TOCN suspensions separate into isotropic (top layer with smaller particles) and anisotropic (bottom layer, larger particles) phases¹⁹². In the isotropic phase, particles arrange with equal probability in every direction while in the anisotropic phase they cluster around a preferred direction¹⁹³. These arrangements correspond to liquid crystalline phases (known as lyotropic mesophases) with a chiral nematic long-range order characterized by the self-orientation of the particles in the same direction along a vector director, also called

¹⁹⁰ Habibi, Y., Lucia, L. A., & Rojas, O. J. (2010). Cellulose nanocrystals: chemistry, self-assembly, and applications. *Chemical Reviews*, 110(6), 3479–3500.

¹⁹¹ Wertz, J. L., Bédué, O., & Mercier, J. P. (2010). Structure and Properties of Cellulose. In *Cellulose Science and Technology* (pp. 87–140). EPFL Press. Retrieved from <http://books.google.pt/books?id=XI4nfkRyfGQC>

¹⁹² de Souza Lima, M. M., & Borsali, R. (2004). Rodlike Cellulose Microcrystals: Structure, Properties, and Applications. *Macromolecular Rapid Communications*, 25(7), 771–787. <https://doi.org/10.1002/marc.200300268>

¹⁹³ Azizi Samir, M. A. S., Alloin, F., & Dufresne, A. (2005). Review of recent research into cellulosic whiskers, their properties and their application in nanocomposite field. *Biomacromolecules*, 6(2), 612–626. <https://doi.org/10.1021/bm0493685>

the cholesteric state^{194 195}. The cholesteric state minimize electrostatic interactions in the suspension¹⁹⁶ by favorably excluding volume interactions, leading to higher packing entropy compared with the disordered phase¹⁹⁷. In this state the structural alignment gives the transparent suspension an iridescent/pearlescent appearance that becomes apparent when the suspension is placed between crossed polarizers, due to the birefringence of individual domains. We observed this feature in the aqueous suspensions of Fique tow TOCN when the sample was placed between crossed polarizers (Figure 9c). This optical phenomenon supports the colloidal nature of the Fique tow TOCNs.

After TEMPO oxidation, the stability of aqueous TOCN dispersions depends on the degree of cellulose surface modification in terms of number of carboxylic units. To measure the oxidation degree (OD) or carboxylate content of Fique tow TOCNs we performed conductimetric titrations using a standard NaOH solution. Using the equations 1 and 2 it was calculated a DO of 0.27 and a carboxylate content of 1.6 mmol/g for delignified Fique tow oxidized in the presence of ultrasonic waves. On the other hand, when raw Fique tow was used in the TEMPO-oxidation reaction, the DO was 0.17 and the carboxylate content was 1.0 mmol/g. TEMPO-oxidation of delignified Fique tow without ultrasonic irradiation during the reaction resulted on a DO of 0.21 and a carboxylate content of 1.2 mmol/g. Clearly, delignification and use of ultrasound increase DO in TOCN up to 37% and 22%, respectively. These results are shown in Figure 10.

¹⁹⁴ de Souza Lima, M. M., & Borsali, R. (2004). Rodlike Cellulose Microcrystals: Structure, Properties, and Applications. *Macromolecular Rapid Communications*, 25(7), 771–787. <https://doi.org/10.1002/marc.200300268>

¹⁹⁵ Wertz, J. L., Bédué, O., & Mercier, J. P. (2010). Structure and Properties of Cellulose. In *Cellulose Science and Technology* (pp. 87–140). EPFL Press. Retrieved from <http://books.google.pt/books?id=XI4nfkRyfGQC>

¹⁹⁶ Ten, E., Jiang, L., & Wolcott, M. P. (2012). Strategies for Preparation of Oriented Cellulose Nanowhiskers Composites. In *ACS Symposium Series* (Vol. 1107, pp. 17–36). <https://doi.org/10.1021/bk-2012-1107.ch002>

¹⁹⁷ Habibi, Y., Lucia, L. A., & Rojas, O. J. (2010). Cellulose nanocrystals: chemistry, self-assembly, and applications. *Chemical Reviews*, 110(6), 3479–3500.

Fique tow TOCN (using delignified material and ultrasound for the TEMPO reaction) has similar or higher carboxylate content (1.6 mmol/g cellulose) to TOCN extracted from other lignocellulosic materials. For instance, when hemp bast, commercial bamboo pulp and bagasse bleached kraft pulp were subjected to TEMPO oxidation, they exhibited carboxylate contents ranging from 1.5 to 1.7 mmol/g¹⁹⁸. TOCN obtained from eucalyptus, ginkgo and rice straw showed carboxylate contents of 0.8-1.4 mmol/g and 1.3-1.6 mmol/g when low (5 mmol) and high (10 mmol) NaClO concentrations were used for the TEMPO reaction, respectively¹⁹⁹. On the other hand, ultrasound is also reported to have a significant effect in the carboxylate content of TOCN. For instance, Rohaizu and Wanrosli²⁰⁰ reported how carboxylate contents went up by more than 100% (from 0.58 to 1.31 mmol/g) in TOCN from oil palm empty fruit bunch cellulose when ultrasound irradiation was used during the TEMPO oxidation reaction. Sonochemical effects increase localized temperatures (5000 K) and pressures (1000 atm) in solution affecting the TEMPO oxidation reaction by promoting alteration of the raw material's morphology and structure, and enhancing mass transfer processes. Combination of these effects lead to improved TEMPO reaction efficiency which is translated into an increased carboxylate content in the TOCN^{201 202}. Our results also support the reported findings since we went from a carboxylate content of 1.2 mmol/g without using ultrasonic irradiation to 1.6 mmol/g when we applied ultrasound during the TEMPO-oxidation reaction. Interestingly, when using raw Fique tow as starting material it was evident that the presence of

¹⁹⁸ Puangsin, B., Yang, Q., Saito, T., & Isogai, A. (2013). Comparative characterization of TEMPO-oxidized cellulose nanofibril films prepared from non-wood resources. *International Journal of Biological Macromolecules*, 59, 208–213. <https://doi.org/10.1016/j.ijbiomac.2013.04.016>

¹⁹⁹ Kuramae, R., Saito, T., & Isogai, A. (2014). TEMPO-oxidized cellulose nanofibrils prepared from various plant holocelluloses. *Reactive and Functional Polymers*, 85, 126–133. <https://doi.org/10.1016/j.reactfunctpolym.2014.06.011>

²⁰⁰ Rohaizu, R., & Wanrosli, W. D. (2017). Sono-assisted TEMPO oxidation of oil palm lignocellulosic biomass for isolation of nanocrystalline cellulose. *Ultrasonics Sonochemistry*, 34, 631–639. <https://doi.org/10.1016/j.ultsonch.2016.06.040>

²⁰¹ Ramadoss, G., & Muthukumar, K. (2015). Influence of dual salt on the pretreatment of sugarcane bagasse with hydrogen peroxide for bioethanol production. *Chemical Engineering Journal*, 260, 178–187. <https://doi.org/10.1016/j.cej.2014.08.006>

²⁰² Rohaizu, R., & Wanrosli, W. D. (2017). Sono-assisted TEMPO oxidation of oil palm lignocellulosic biomass for isolation of nanocrystalline cellulose. *Ultrasonics Sonochemistry*, 34, 631–639. <https://doi.org/10.1016/j.ultsonch.2016.06.040>

hemicellulose and lignin make less effective the TEMPO-oxidation reaction since a carboxylate content of 1.0 mmol/g was obtained with this material, when compared to the 1.6 mmol/g with delignified Fique tow. This decrease in carboxylate content is due to usage of NaClO to degrade and remove hemicellulose and lignin as water-soluble fractions, which consequently decrease the amount of oxidant left to react with the TEMPO system^{203 204}. Stability of TOCN aqueous suspensions mostly depends on electrostatic repulsion between surface ionic groups, this effect is quantitatively represented by the measurement of the Z (ζ) potential. The value of this potential can be used to determine the stability (reluctance to aggregate) of a colloidal dispersion²⁰⁵. For instance, a low ζ potential (from 0 to ± 30 mV) indicates rapid coagulation or flocculation processes as a result of attractive forces overcoming electrostatic repulsion. On the other hand, suspensions with high ζ potential ($> \pm 40$ mV) are stable over time²⁰⁶. We followed the ζ potential values of Fique TOCN dispersions when using delignified and raw Fique tow as starting materials with and without ultrasound (Figure 10a). The electrostatic repulsion directly depends on carboxylate content, which in turn depends not only on the oxidation conditions but also on the starting material. ζ values varied from -53 mV when delignified Fique tow under ultrasonic conditions was used to extract TOCN, to -41 mV when the reaction was under the same conditions but with raw Fique tow as the starting material. Additionally, when we did not apply ultrasonic radiation during the TEMPO-oxidation reaction, ζ also decreased (-45 mV) despite the fact the starting material was delignified Fique tow. This change in ζ indicates an increase in

²⁰³ Kuramae, R., Saito, T., & Isogai, A. (2014). TEMPO-oxidized cellulose nanofibrils prepared from various plant holocelluloses. *Reactive and Functional Polymers*, 85, 126–133. <https://doi.org/10.1016/j.reactfunctpolym.2014.06.011>

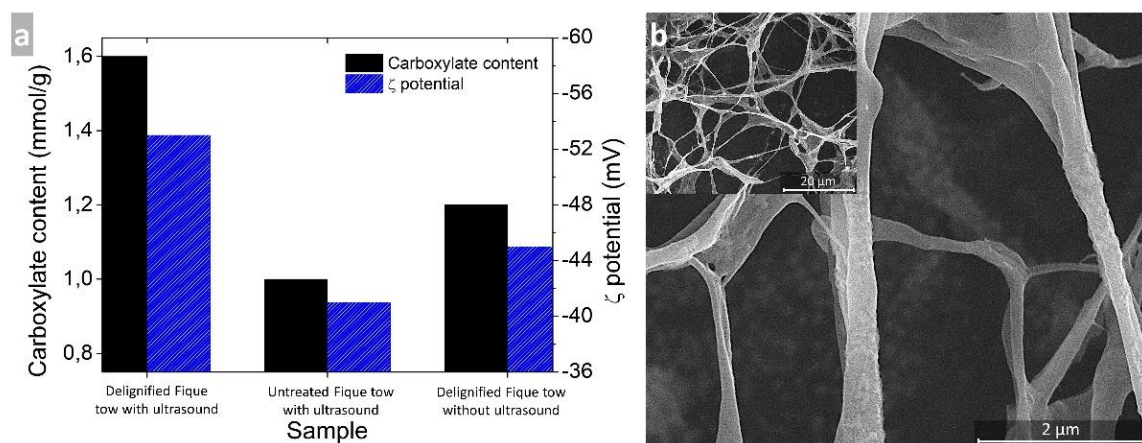
²⁰⁴ Puangsin, B., Yang, Q., Saito, T., & Isogai, A. (2013). Comparative characterization of TEMPO-oxidized cellulose nanofibril films prepared from non-wood resources. *International Journal of Biological Macromolecules*, 59, 208–213. <https://doi.org/10.1016/j.ijbiomac.2013.04.016>

²⁰⁵ Liu, C., Li, B., Du, H., Lv, D., Zhang, Y., Yu, G., et al. (2016). Properties of nanocellulose isolated from corncob residue using sulfuric acid, formic acid, oxidative and mechanical methods. *Carbohydrate Polymers*, 151, 716–724. <https://doi.org/10.1016/j.carbpol.2016.06.025>

²⁰⁶ Wicaksono, R., Syamsu, K., Yuliasih, I., & Nasir, M. (2013). Cellulose Nanofibers from Cassava Bagasse: Characterization and Application on Tapioca-Film. *Chemistry and Materials Research*, 3(13), 79–87

carboxylate groups on the surface of cellulose as the reaction is ultrasound-assisted and as the starting material has been treated to remove non-cellulosic components, as previously reported.^{207 208}. The ζ values obtained for Fique tow TOCN are similar or even higher than the reported values for TEMPO-oxidized corncob (-23 mV)²⁰⁹, TEMPO-oxidized softwood bleached Kraft pulp (-58 mV)²¹⁰ and hydrolyzed cassava bagasse (-52 mV)²¹¹

Figure 10. Fique tow TOCN: (a) ζ potential and carboxylate contents, (b) FESEM image.



The ultrasound-assisted TEMPO-mediated oxidation reaction not only promotes cellulose surface oxidation, but also allows cellulose nanofibrils further release from

²⁰⁷ Kuramae, R., Saito, T., & Isogai, A. (2014). TEMPO-oxidized cellulose nanofibrils prepared from various plant holocelluloses. *Reactive and Functional Polymers*, 85, 126–133. <https://doi.org/10.1016/j.reactfunctpolym.2014.06.011>

²⁰⁸ Puangsin, B., Yang, Q., Saito, T., & Isogai, A. (2013). Comparative characterization of TEMPO-oxidized cellulose nanofibril films prepared from non-wood resources. *International Journal of Biological Macromolecules*, 59, 208–213. <https://doi.org/10.1016/j.ijbiomac.2013.04.016>

²⁰⁹ Liu, C., Li, B., Du, H., Lv, D., Zhang, Y., Yu, G., et al. (2016). Properties of nanocellulose isolated from corncob residue using sulfuric acid, formic acid, oxidative and mechanical methods. *Carbohydrate Polymers*, 151, 716–724. <https://doi.org/10.1016/j.carbpol.2016.06.025>

²¹⁰ Fujisawa, S., Okita, Y., Fukuzumi, H., Saito, T., & Isogai, A. (2011). Preparation and characterization of TEMPO-oxidized cellulose nanofibril films with free carboxyl groups. *Carbohydrate Polymers*, 84(1), 579–583. <https://doi.org/10.1016/j.carbpol.2010.12.029>

²¹¹ Wicaksono, R., Syamsu, K., Yuliasih, I., & Nasir, M. (2013). Cellulose Nanofibers from Cassava Bagasse: Characterization and Application on Tapioca-Film. *Chemistry and Materials Research*, 3(13), 79–87

the Figue tow macrofiber bundles. Figure 10b shows a FESEM image of Figue tow TOCNs characteristic networks formed by elongated and highly entangled structures, with diameters around 100 nm and lengths of several micrometers. However, this is not likely to be the state of these materials in solution since FESEM has two main drawbacks preventing observation of the native TOCNs structure: the use of coatings, which increase the size of the nanomaterial, and self-aggregation processes driven by solvent removal as result of TOCN drying²¹². For instance, SEM analysis of corncob-derived TOCN show widths ranging from 200-1500 nm and lengths of several micrometers; however, TEM and AFM measurements of the same material showed average widths and lengths of 2 nm and 438 nm, respectively²¹³. Another study reported the production of microfibrillated cellulose from flax, jute, hemp, sisal and abaca by TEMPO-oxidation reaction, with 20-50 nm in width and several microns in length²¹⁴. They also found that microfibrillated cellulose extracted from fibers obtained from leaves (such as sisal and abaca) are less inclined to form entangled networks. Comparing the TOCN dimensions obtained by SEM of corncob-derived TOCN²¹⁵ to the Figue tow TOCN dimensions it can be seen that their nanomaterial had higher width and length. This might be because we used ultrasonic irradiation during the TEMPO oxidation reaction while they did not. The use of ultrasound induces shock waves, micro-jets and high-speed collisions within the reaction mixture, promoting a 'delamination effect' of elementary cellulose fibrils. This increases the specific contact area and allows production of high aspect ratio nanofibrils²¹⁶. Increasing the nanofibrils aspect ratio produces webs stronger than

²¹² Liu, C., Li, B., Du, H., Lv, D., Zhang, Y., Yu, G., et al. (2016). Properties of nanocellulose isolated from corncob residue using sulfuric acid, formic acid, oxidative and mechanical methods. *Carbohydrate Polymers*, 151, 716–724. <https://doi.org/10.1016/j.carbpol.2016.06.025>

²¹³ Ibid.

²¹⁴ Alila, S., Besbes, I., Vilar, M. R., Mutjé, P., & Boufi, S. (2013). Non-woody plants as raw materials for production of microfibrillated cellulose (MFC): A comparative study. *Industrial Crops and Products*, 41, 250–259. <https://doi.org/10.1016/j.indcrop.2012.04.028>

²¹⁵ Liu, C., Li, B., Du, H., Lv, D., Zhang, Y., Yu, G., et al. (2016). Properties of nanocellulose isolated from corncob residue using sulfuric acid, formic acid, oxidative and mechanical methods. *Carbohydrate Polymers*, 151, 716–724. <https://doi.org/10.1016/j.carbpol.2016.06.025>

²¹⁶ Mishra, S. P., Thirree, J., Manent, A., & Chabot, B. (2011). Ultrasound-catalyzed tempo-mediated oxidation of native cellulose for the production of nanocellulose: effect of process variables, 6(*Brown* 2010), 121–143.

the initial lignocellulosic material because of the creation of more and stronger bonds²¹⁷, which also might be the reason why our Fique tow TOCN produced entangled networks, in a similar behavior as reported by Alila *et al.*²¹⁸. In combination with the TEMPO oxidation reaction of Fique tow, ultrasound energy also induces interfibrillar hydrogen bond decoupling by superficial electrostatic repulsion effects, upon introduction of carboxylic units; this effect increases nanofibrils reactivity leading to stable aqueous suspensions of TOCN²¹⁹.

Figure 11a shows infrared spectra of untreated and delignified Fique tow and TOCN-COO-Na⁺ and TOCN-COOH. From untreated and delignified Fique tow spectra significant differences can be drawn for signals typical of hemicelluloses and lignin. For instance, the bands at 1731 and 1240 cm⁻¹ due to the stretching vibration of carbonyl units (C=O) characteristic of lignin and hemicellulose and C-O-C vibrations of aromatic ether linkages in lignin^{220 221}, respectively, are significantly decreased or not present at all in the delignified Fique tow sample. This observation suggests the removal of lignin and hemicellulose after the alkaline hydrogen peroxide treatment²²². On the other hand, cellulose characteristic signals are prevalent and common to all spectra. Typical cellulose signals include the wide band between 3650 and 3000 cm⁻¹ corresponding to O-H stretching vibrations; the stretching vibration of

²¹⁷ Ferrer, A., Quintana, E., Filpponen, I., Solala, I., Vidal, T., Rodríguez, A., ... Rojas, O. J. (2012). Effect of residual lignin and heteropolysaccharides in nanofibrillar cellulose and nanopaper from wood fibers. *Cellulose*, 19(6), 2179–2193. <https://doi.org/10.1007/s10570-012-9788-z>

²¹⁸ Alila, S., Besbes, I., Vilar, M. R., Mutjé, P., & Boufi, S. (2013). Non-woody plants as raw materials for production of microfibrillated cellulose (MFC): A comparative study. *Industrial Crops and Products*, 41, 250–259. <https://doi.org/10.1016/j.indcrop.2012.04.028>

²¹⁹ Saito, T., Kimura, S., Nishiyama, Y., & Isogai, A. (2007). Cellulose Nanofibers Prepared by TEMPO-Mediated Oxidation of Native Cellulose. *Biomacromolecules*, 8(8), 2485–2491. <https://doi.org/10.1021/bm0703970>

²²⁰ Abraham, E., Deepa, B., Pothan, L. A., Jacob, M., Thomas, S., Cvelbar, U., et al. (2011). Extraction of nanocellulose fibrils from lignocellulosic fibres: A novel approach. *Carbohydrate Polymers*, 86, 1468–1475.

²²¹ Ramadoss, G., & Muthukumar, K. (2016). Mechanistic study on ultrasound assisted pretreatment of sugarcane bagasse using metal salt with hydrogen peroxide for bioethanol production. *Ultrasonics Sonochemistry*, 28, 207–217. <https://doi.org/10.1016/j.ultsonch.2015.07.006>

²²² Ovalle-Serrano, S. A., Blanco-Tirado, C., & Combariza, M. Y. (2018). Exploring the composition of raw and delignified Colombian Fique fibers, tow and pulp. *Cellulose*, 25(1), 151–165. <https://doi.org/10.1007/s10570-017-1599-9>

the aliphatic saturated C-H unit at 2901 cm^{-1} ; the C6-H2 flexion between 1424 and 1315 cm^{-1} ; the C-O-C stretching vibration of pyranose ring skeletal at 1160 cm^{-1} ; the characteristic C-O vibration (from C2, C3 and C6) at 1055-1032 cm^{-1} ; and the vibration signal of the anomeric carbon C1-H around 900 cm^{-1} ²²³. TOCN-COO-Na⁺ spectrum exhibits characteristic signals at 1600 cm^{-1} of the C=O carbonyl stretching vibrations. After HCl treatment to obtain TOCN in free acid form (TOCN-COOH spectrum), this signal shifted to 1722 cm^{-1} attributed to the C=O stretching vibration of the free carboxylic acids as result of the exchange of Na⁺ by H⁺ ions. The presence of this characteristic signals confirms the surface oxidation of the delignified Fique tow²²⁴.

Native cellulose (type I), the most common polymorph found in nature, is composed of two phases: I α and I β , arranged in triclinic and monoclinic crystalline systems, respectively^{225 226 227}. X-ray patterns of untreated Fique tow, delignified Fique tow d TOCN are similar, as seen in Figure 11.b, which indicate no changes in the internal crystalline structure of the biopolymer. The diffraction patterns in Figure 11b coincide with characteristic signals of cellulose I crystallographic planes as reported by the Joint Committee on Powder Diffraction Standards (JCPDS file, No. 50-2241), space

²²³ Pretsch, E., Bühlmann, P., & Badertscher, M. (2009). *Structure Determination of Organic Compounds. Structure Determination of Organic Compounds: Tables of Spectral Data*. Berlin, Heidelberg: Springer Berlin Heidelberg. <https://doi.org/10.1007/978-3-540-93810-1>

²²⁴ Fujisawa, S., Okita, Y., Fukuzumi, H., Saito, T., & Isogai, A. (2011). Preparation and characterization of TEMPO-oxidized cellulose nanofibril films with free carboxyl groups. *Carbohydrate Polymers*, 84(1), 579–583. <https://doi.org/10.1016/j.carbpol.2010.12.029>

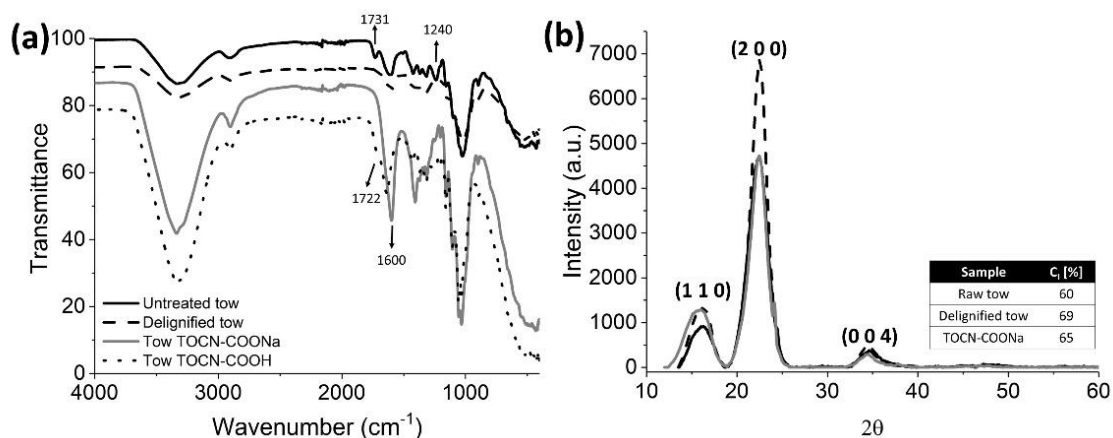
²²⁵ French, A. D. (2013). Idealized powder diffraction patterns for cellulose polymorphs. *Cellulose*, 21(2), 885–896. <https://doi.org/10.1007/s10570-013-0030-4>

²²⁶ Habibi, Y., Lucia, L. A., & Rojas, O. J. (2010). Cellulose nanocrystals: chemistry, self-assembly, and applications. *Chemical Reviews*, 110(6), 3479–3500.

²²⁷ Moon, R. J., Martini, A., Nairn, J., Simonsen, J., & Youngblood, J. (2011). Cellulose nanomaterials review: structure, properties and nanocomposites. *Chemical Society Reviews*, 40(7), 3941–3994. <https://doi.org/10.1039/c0cs00108b>

group P21 (No 4)^{228 229 230}, where the broad band at 15.1° is due to overlapping of signals at $2\theta = 14.8^\circ$ and 16.8° characteristic of crystallographic planes (1 -1 0) and (1 1 0), respectively. The signals in 22.7° and 34.6° correspond to the crystallographic planes (2 0 0) and (0 0 4)^{231 232 233}.

Figure 11. (a) IR-ATR spectra and (b) XRD patterns of untreated, delignified, TOCN-COO-Na⁺ and TOCN-COOH Figue tow.



Crystallinity indexes (CI) were determined using the Segal method²³⁴. For untreated Figue tow, bleached Figue tow and TOCN-COONa, CI were 60%, 69% and 65%,

²²⁸ Mandal, A., & Chakrabarty, D. (2011). Isolation of nanocellulose from waste sugarcane bagasse (SCB) and its characterization. *Carbohydrate Polymers*, 86, 1291–1299.

²²⁹ Morán, J. I., Alvarez, V. A., Cyras, V. P., & Vázquez, A. (2008). Extraction of cellulose and preparation of nanocellulose from sisal fibers. *Cellulose*, 15(1), 149–159. <https://doi.org/10.1007/s10570-007-9145-9>

²³⁰ Sèbe, G., Ham-Pichavant, F., Ibarboure, E., Koffi, A. L. C., & Tingaut, P. (2012). Supramolecular structure characterization of cellulose II nanowhiskers produced by acid hydrolysis of cellulose I substrates. *Biomacromolecules*, 13(2), 570–8. <https://doi.org/10.1021/bm201777j>

²³¹ French, A. D. (2013). Idealized powder diffraction patterns for cellulose polymorphs. *Cellulose*, 21(2), 885–896. <https://doi.org/10.1007/s10570-013-0030-4>

²³² Morán, J. I., Alvarez, V. A., Cyras, V. P., & Vázquez, A. (2008). Extraction of cellulose and preparation of nanocellulose from sisal fibers. *Cellulose*, 15(1), 149–159. <https://doi.org/10.1007/s10570-007-9145-9>

²³³ Okita, Y., Saito, T., & Isogai, A. (2010). Entire Surface Oxidation of Various Cellulose Microfibrils by TEMPO-Mediated Oxidation. *Biomacromolecules*, 11(6), 1696–1700. <https://doi.org/10.1021/bm100214b>

²³⁴ Segal, L., Creely, J. J., Martin, A. E., & Conrad, C. M. (1959). An Empirical Method for Estimating the Degree of Crystallinity of Native Cellulose Using the X-Ray Diffractometer. *Textile Research Journal*, 29(10), 786–794. <https://doi.org/10.1177/004051755902901003>

respectively. The lower CI in TOCN-COONa might be due to alteration of the crystalline cellulosic tridimensional network, because of the mechanical stress induced by ultrasound radiation, and also because of the actual oxidation reaction²³⁵. On this regard, Puangsin²³⁶) reported that a slight decrease (< 10%) in CI from raw cellulose to TOCN is likely due to oxidation of –OH groups on the surface of crystalline cellulose and does not affect significantly the mechanical properties of the biopolymer. Reduced CI for various lignocellulosic materials after TEMPO oxidation have been reported: corncob (61.5% before and 49.9% after)²³⁷, jute (63.7% before and 69.9% after)²³⁸, commercial bamboo pulp (42% before and 38% after)²³⁹ and oil palm empty fruit bunch (75% before and 72% after)²⁴⁰.

Thermal degradation of cellulose comprises a group of endothermic reactions related to dehydration, hydrolysis, oxidation, decarboxylation and trans glycosylation processes. These reactions occur into two stages: at low temperatures, below 200 °C, and at temperatures above 300 °C. For untreated Fique tow, bleached Fique tow and Fique TOCNs the first thermal event occurs from 25 to 100 °C corresponding to sample dehydration with a weight reduction of 2%, 6% and 5%, respectively (Figure 12a)²⁴¹. The next event corresponds to cellulose thermal decomposition (Td) with

²³⁵ Abdul Khalil, H. P. S., Davoudpour, Y., Islam, M. N., Mustapha, A., Sudesh, K., Dungani, R., et al. (2014). Production and modification of nanofibrillated cellulose using various mechanical processes: a review. *Carbohydrate Polymers*, 99, 649–65. <https://doi.org/10.1016/j.carbpol.2013.08.069>

²³⁶ Puangsin, B., Yang, Q., Saito, T., & Isogai, A. (2013). Comparative characterization of TEMPO-oxidized cellulose nanofibril films prepared from non-wood resources. *International Journal of Biological Macromolecules*, 59, 208–213. <https://doi.org/10.1016/j.ijbiomac.2013.04.016>

²³⁷ Liu, C., Li, B., Du, H., Lv, D., Zhang, Y., Yu, G., et al. (2016). Properties of nanocellulose isolated from corncob residue using sulfuric acid, formic acid, oxidative and mechanical methods. *Carbohydrate Polymers*, 151, 716–724. <https://doi.org/10.1016/j.carbpol.2016.06.025>

²³⁸ Cao, X., Ding, B., Yu, J., & Al-Deyab, S. S. (2012). Cellulose nanowhiskers extracted from TEMPO-oxidized jute fibers. *Carbohydrate Polymers*, 90(2), 1075–1080. <https://doi.org/10.1016/j.carbpol.2012.06.046>

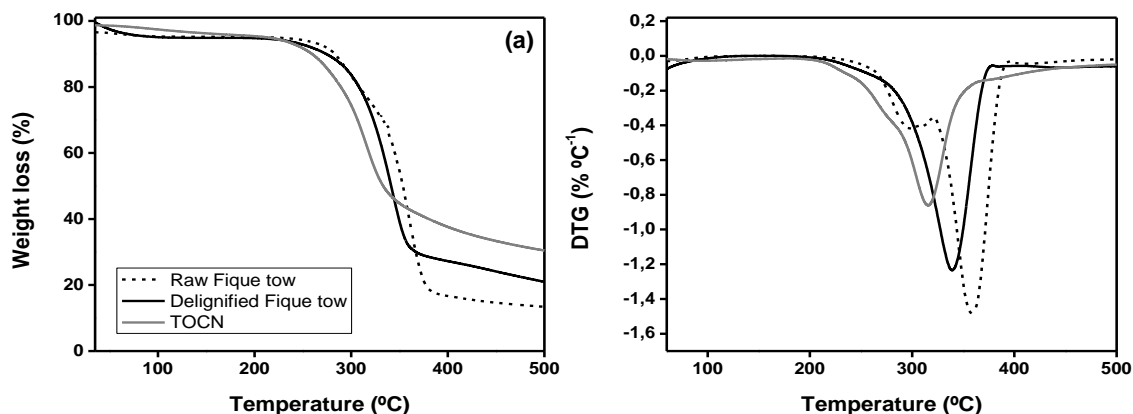
²³⁹ Puangsin, B., Yang, Q., Saito, T., & Isogai, A. (2013). Comparative characterization of TEMPO-oxidized cellulose nanofibril films prepared from non-wood resources. *International Journal of Biological Macromolecules*, 59, 208–213. <https://doi.org/10.1016/j.ijbiomac.2013.04.016>

²⁴⁰ Rohaizu, R., & Wanrosli, W. D. (2017). Sono-assisted TEMPO oxidation of oil palm lignocellulosic biomass for isolation of nanocrystalline cellulose. *Ultrasonics Sonochemistry*, 34, 631–639. <https://doi.org/10.1016/j.ultsonch.2016.06.040>

²⁴¹ Cao, X., Ding, B., Yu, J., & Al-Deyab, S. S. (2012). Cellulose nanowhiskers extracted from TEMPO-oxidized jute fibers. *Carbohydrate Polymers*, 90(2), 1075–1080.

onset around 250 °C for all samples; at this stage, the weight loss reaches up to 10% because the decomposition of cellulose glycosidic units to water, carbon dioxide (CO₂), carbon monoxide (CO) and carbon.

Figure 12. (a) TGA curves and (b) DTG curves for raw Fique tow, delignified Fique tow and TOCN.



At temperatures above the T_d, the degree of depolymerization increases for all cellulosic materials and the thermogravimetric curves decrease to 20% wt. From 300 °C onwards a different reaction occurs (known as tar route) resulting in cellulose depolymerization by cleavage of the glycosidic linkages to produce mainly tar fractions. Over 450 °C the production of volatiles is completed and the continuous weight loss is due to oxidation of remnant carbon to CO₂, CO and water²⁴². In Figure 12b, the derivative thermogravimetric curves (DTG) show a lower decomposition temperature for Fique TOCN (310 °C) when compared to untreated and delignified Fique tow (360 °C and 322 °C, respectively). The TOCN DTG curve presents a slight shoulder at 275 °C followed by a well-defined band at 310 °C. The first event is attributed to decomposition of Fique TOCN surface carboxylic units while the second and more pronounced signal corresponds to decomposition of the cellulose

<https://doi.org/10.1016/j.carbpol.2012.06.046>

²⁴² Dufresne, A. (2013b). *Nanocellulose: From Nature to High Performance Tailored Materials*. Grenoble: Walter de Gruyter. Retrieved from https://books.google.com.co/books/about/Nanocellulose.html?id=6Mfuk_b7gncC&redir_esc=y

backbone structure²⁴³. In comparison TOCN extracted from jute fibers show lower thermal stability (290 °C) than Fique TOCN (310 °C)²⁴⁴, as well as TOCN from rice straw (265 °C)²⁴⁵ and corncob (305 °C)²⁴⁶.

The low degradation temperature of Fique TOCN, when compared with raw and delignified Fique tow, can be rationalized in terms of the high surface area exposed to the heat in the case of TOCN. In addition, carboxylate groups on the TOCN surface facilitate direct solid-to-gas phase transitions from decarboxylation, since CO₂ is produced primarily by decarboxylation reactions²⁴⁷. Also, CNF with different carboxylate contents and degree of oxidation, as a consequence of variations in the length of the TEMPO reaction, significantly affect thermal and mechanical behaviors in reinforced CNF-polymer nanocomposites as reported by Ben Hamou *et al.*²⁴⁸. Regarding reaction residuals, above 380 °C, it is remarkable that char from TOCN (35%) is almost 1.6 times higher than in delignified Fique tow (22%) and doubles that of untreated Fique tow (17%). When pure cellulose is subjected to pyrolysis its char residue should be theoretically of 44% since H₂O would be liberated by dehydration but other reactions such as CO and CO₂ decarboxylation and the production of H₂ and CH₄ prevent this from happening. Since increased char

²⁴³ Fukuzumi, H., Saito, T., Okita, Y., & Isogai, A. (2010). Thermal stabilization of TEMPO-oxidized cellulose. *Polymer Degradation and Stability*, 95(9), 1502–1508. <https://doi.org/10.1016/j.polymdegradstab.2010.06.015>

²⁴⁴ Cao, X., Ding, B., Yu, J., & Al-Deyab, S. S. (2012). Cellulose nanowhiskers extracted from TEMPO-oxidized jute fibers. *Carbohydrate Polymers*, 90(2), 1075–1080. <https://doi.org/10.1016/j.carbpol.2012.06.046>

²⁴⁵ Jiang, F., & Hsieh, Y.-L. (2013). Chemically and mechanically isolated nanocellulose and their self-assembled structures. *Carbohydrate Polymers*, 95(1), 32–40. <https://doi.org/10.1016/j.carbpol.2013.02.022>

²⁴⁶ Liu, C., Li, B., Du, H., Lv, D., Zhang, Y., Yu, G., et al. (2016). Properties of nanocellulose isolated from corncob residue using sulfuric acid, formic acid, oxidative and mechanical methods. *Carbohydrate Polymers*, 151, 716–724. <https://doi.org/10.1016/j.carbpol.2016.06.025>

²⁴⁷ Jiang, F., & Hsieh, Y.-L. (2013). Chemically and mechanically isolated nanocellulose and their self-assembled structures. *Carbohydrate Polymers*, 95(1), 32–40. <https://doi.org/10.1016/j.carbpol.2013.02.022>

²⁴⁸ Hamou, K. Ben, Kaddami, H., Dufresne, A., Boufi, S., Magnin, A., & Erchiqui, F. (2018). Impact of TEMPO-oxidization strength on the properties of cellulose nanofibril reinforced polyvinyl acetate nanocomposites. *Carbohydrate Polymers*, 181(November), 1061–1070. <https://doi.org/10.1016/j.carbpol.2017.11.043>

residues for nanocelluloses has been widely reported^{249 250 251}, it is presumed that surface groups favor the dehydration reaction, so that char residues would be closer to the theoretically expected value²⁵².

2.5 CONCLUSIONS

Cellulose nanofibrils (CNF) were successfully extracted from delignified Fique tow through TEMPO oxidation assisted with ultrasonic radiation. We observed TOCN with 'rod-like' structures and diameters around 100 nm and lengths of several micrometers. These CNF, with a carboxylate content of 1.6 mmol -COOH/g cellulose, corresponding to 35% -COOH functional groups, formed stable aqueous suspensions with ζ potential of -53 mV as a result of electrostatic repulsion. Such stability was also confirmed by optical birefringence phenomenon of aqueous suspensions of TOCN. Crystallinity index of these CNF was higher than 60% and thermal degradation temperatures did not vary significantly upon oxidation when compared to the raw Fique tow and delignified Fique tow. We also show the significant effect of the delignification pretreatment and the use of ultrasound in the TEMPO oxidation reaction. A degree of oxidation of 0.27 and a carboxylate content of 1.6 mmol/g were measured for CNF from delignified Fique tow when the TEMPO reaction was carried out in the presence of ultrasonic energy. In absence of sonication, we registered a degree of oxidation of 0.21 and a carboxylate content of 1.2 mmol/g. In addition, when raw Fique tow was used in the TEMPO-oxidation

²⁴⁹ Cao, X., Ding, B., Yu, J., & Al-Deyab, S. S. (2012). Cellulose nanowhiskers extracted from TEMPO-oxidized jute fibers. *Carbohydrate Polymers*, 90(2), 1075–1080. <https://doi.org/10.1016/j.carbpol.2012.06.046>

²⁵⁰ Liu, C., Li, B., Du, H., Lv, D., Zhang, Y., Yu, G., et al. (2016). Properties of nanocellulose isolated from corn cob residue using sulfuric acid, formic acid, oxidative and mechanical methods. *Carbohydrate Polymers*, 151, 716–724. <https://doi.org/10.1016/j.carbpol.2016.06.025>

²⁵¹ Rohaizu, R., & Wanrosli, W. D. (2017). Sono-assisted TEMPO oxidation of oil palm lignocellulosic biomass for isolation of nanocrystalline cellulose. *Ultrasonics Sonochemistry*, 34, 631–639. <https://doi.org/10.1016/j.ultsonch.2016.06.040>

²⁵² Jiang, F., & Hsieh, Y.-L. (2013). Chemically and mechanically isolated nanocellulose and their self-assembled structures. *Carbohydrate Polymers*, 95(1), 32–40. <https://doi.org/10.1016/j.carbpol.2013.02.022>

reaction, the degree of oxidation was 0.17 and the carboxylate content was 1.0 mmol/g. Clearly, delignification and use of ultrasound increase degree of oxidation in TOCN up to 37 and 22%, respectively. Finally, Fique CNF exhibit similar physicochemical, thermal and microscopic behaviors than CNF from different sources such as hemp bast, commercial bamboo pulp, bagasse bleached Kraft pulp, palm oil empty bunches, rice straw, jute, sisal and abaca, among others. These properties make them suitable materials for applications as surface-active additives for the oil industry (particularly for emulsion inhibition and breakage in up-and down-stream processes); raw materials for synthesizing super hydrophobic compounds; or production of new nano and micro fibers in spinning processes, among others. To the best of our knowledge, this contribution reported for the first time the extraction and characterization of nanocellulose from Colombian Fique lignocellulosic biomass.

3. POST-OXIDATION AND HIDROFOBIZATION OF CELLULOSE NANOFIBRILS FROM COLOMBIAN FIQUE TOW

3.1 ABSTRACT

This chapter shows the advances in the development of functionalized materials through a post-oxidation followed by a 'one-pot' amidation reaction of TEMPO oxidized cellulose nanofibrils (TOCN) extracted from Fique tow. The TOCN and TOCN-P (TOCN post-oxidized) obtained had an elongated morphology in a network structure, with diameters around 60 and 40 nm, respectively, and lengths of several micrometers. Carboxyl content in TOCN was 1.57 mmol/g cellulose which was raised up to 2.20 mmol/g cellulose after the post-oxidation process. The amidation was achieved using TBTU as coupling agent and octadecylamine (ODA) to greatly increase the hydrophobicity of both TOCN and TOCN-P. FT-IR results confirmed the covalent coupling of TOCN and TOCN-R with ODA, and FESEM images showed the morphology of the final products. The transition hydrophilic/hydrophobic behavior of cellulose nanofibrils was discussed based on solubility tests, thermogravimetric analysis (TGA) and contact angle measurement (CAM).

3.2 INTRODUCTION

In recent years, the use of agricultural bio-waste has attracted great interest as a new source of cellulose due to its wide availability and low cost to develop cellulose bio-inspired products considered as the materials of the future²⁵³. The use of secondary and tertiary cellulose sources (i.e., lignocellulosic residual biomass derived from agricultural activities) has become the best choice for the production of nanocellulose in terms of costs, energy consumption and economic development²⁵⁴

²⁵³ García A, Gandini A, Labidi J, et al (2016) Industrial and crop wastes: A new source for nanocellulose biorefinery. *Ind Crops Prod* 93:26–38 . doi: 10.1016/j.indcrop.2016.06.004

²⁵⁴ Faruk O, Bledzki AK, Fink H-P, Sain M (2012) Biocomposites reinforced with natural fibers: 2000–2010. *Prog Polym Sci* 37:1552–1596 . doi: 10.1016/j.progpolymsci.2012.04.003

²⁵⁵. This is why the research community has increased its interest in the valorization of agro-industrial biomass to produce new nanotechnological products²⁵⁶.

In Colombia, Fique (*Furcraea spp.*) is a national plant used mainly as a source of hard cellulose fibers²⁵⁷. From the mechanical decortication of Fique sheets for fiber extraction, juice, tow and bagasse are generated as by-products of this process in 70%, 17% and 8% in weight, respectively. These by-products, considered as secondary/tertiary cellulosic sources, represent approximately 95% of the Fique leaf weight and only 5% corresponds to Fique fibers. Although Fique tow is a by-product considered as waste, it is a profitable material due to its chemical composition with a high cellulose content (52% cellulose, 24% hemicellulose and 23% lignin)²⁵⁸. However, it is commonly found deposited in the fields where the mechanical decortication took place or thrown into water sources generating environmental pollution²⁵⁹. Therefore, the development of new high value-added products, such as nanocellulosic materials, becomes an alternative to strengthen the agro-industrial cycle of the Fique industry, providing great socio-economic and environmental benefits for the implementation of agricultural biomass transformation processes.

Native cellulose, also known as cellulose I, is a structural and linear homopolysaccharide made up of D-glucopyranose units linked by glycosidic bonds β -D(1 \rightarrow 4)²⁶⁰. The cellulose microfibrillated structure has multiple scales formed by

²⁵⁵ Keijsers ERP, Yılmaz G, van Dam JEG (2013) The cellulose resource matrix. *Carbohydr Polym* 93:9–21 . doi: 10.1016/j.carbpol.2012.08.110

²⁵⁶ Kallel F, Bettaieb F, Khiari R, et al (2016) Isolation and structural characterization of cellulose nanocrystals extracted from garlic straw residues. *Ind Crops Prod* 87:287–296 . doi: 10.1016/j.indcrop.2016.04.060

²⁵⁷ Peinado JE, Ospina LF, Rodríguez L, et al (2006) Guía Ambiental del Subsector Fiquero. Cadena Productiva Nacional del Fique, Bogotá

²⁵⁸ Ovalle-Serrano SA, Blanco-Tirado C, Combariza MY (2018a) Exploring the composition of raw and delignified Colombian fique fibers, tow and pulp. *Cellulose* 25:151–165 . doi: 10.1007/s10570-017-1599-9

²⁵⁹ Peinado JE, Ospina LF, Rodríguez L, et al (2006) Guía Ambiental del Subsector Fiquero. Cadena Productiva Nacional del Fique, Bogotá

²⁶⁰ Habibi Y, Lucia LA, Rojas OJ (2010) Cellulose nanocrystals: chemistry, self-assembly, and applications. *Chem Rev* 110:3479–3500

microfibrils (CMF), with diameters between 15-50 nm depending on their biological origin. The CMF in turn are conformed by cellulose nanofibrils (CNF) of smaller diameter and crystalline and amorphous regions in their structure²⁶¹. Thus, cellulose is assembled by hydrogen bonds, covalent bonds and weak van der Waals forces with hemicellulose and lignin in the secondary cell wall of plants protecting the CMF²⁶². CNF can be isolated from the cell wall of plants by (i) mechanic (ii) biological and (iii) chemical treatments. Although several methods have been developed to obtain CNF, most of them involve treatments with a high energy consumption and environmental impact. However, TEMPO-mediated oxidation, a chemical treatment, shows a high efficiency, selectivity and low energy consumption.²⁶³.

The production of CNF usually requires a previous processing of the raw material known as delignification. This treatment removes non-cellulosic amorphous compounds such as hemicellulose and lignin and improves the efficiency of the TEMPO-mediated oxidation²⁶⁴. The most common methods are steam explosion (Li et al. 2009), ammonia fiber expansion²⁶⁵ and acid/alkaline/organosolv pretreatments²⁶⁶. However, most of these treatments need catalysts, high temperatures, pressures and energy consumption. However, delignification of untreated Figue tow also may be accomplished by the use of hydrogen peroxide in alkaline medium to make the cellulose more accessible to the TEMPO-mediated

²⁶¹ Keijsers ERP, Yılmaz G, van Dam JEG (2013) The cellulose resource matrix. *Carbohydr Polym* 93:9–21 . doi: 10.1016/j.carbpol.2012.08.110

²⁶² Habibi Y, Lucia LA, Rojas OJ (2010) Cellulose nanocrystals: chemistry, self-assembly, and applications. *Chem Rev* 110:3479–3500

²⁶³ Osong SH, Norgren S, Engstrand P (2016) Processing of wood-based microfibrillated cellulose and nanofibrillated cellulose , and applications relating to papermaking : a review. *Cellulose* 23:93–123 . doi: 10.1007/s10570-015-0798-5

²⁶⁴ Dutra ED, Santos FA, Alencar BRA, et al (2017) Alkaline hydrogen peroxide pretreatment of lignocellulosic biomass: status and perspectives. *Biomass Convers Biorefinery*. doi: 10.1007/s13399-017-0277-3

²⁶⁵ Sundaram V, Muthukumarappan K, Kamireddy SR (2015) Effect of ammonia fiber expansion (AFEX™) pretreatment on compression behavior of corn stover, prairie cord grass and switchgrass. *Ind Crops Prod* 74:45–54 . doi: 10.1016/j.indcrop.2015.04.027

²⁶⁶ Chaudhary G, Singh LK, Ghosh S (2012) Alkaline pretreatment methods followed by acid hydrolysis of *Saccharum spontaneum* for bioethanol production. *Bioresour Technol* 124:111–118 . doi: 10.1016/j.biortech.2012.08.067

oxidation²⁶⁷. H₂O₂ can be dissociated in water at high pH values to generate the hydroperoxide anion (HOO⁻). This anion can react with remaking hydrogen peroxide to form more active radicals such as the hydroxyl radical (OH[·]) and the superoxide radical anion (O₂^{·-}) which are the most important species in oxidation reactions²⁶⁸. This treatment has advantages over other alternative methods because it has low environmental impact, provides high efficiency of delignification and has low-energy consumption²⁶⁹. In addition, the reaction can be mechanically assisted or improved with the use of ultrasound, since sonication can break interfaces between the polymers linked mainly by Van der Waals forces ^{270 271 272}.

After delignification, the OH groups available on the surface of cellulose fibers serve as active sites for chemical modifications to produce functional materials, with most reactions being focused on the primary alcohol, the most reactive of three hydroxyl groups²⁷³. This is the mechanism for the TEMPO-mediated oxidation, where OH groups of C6 (primary alcohol) from cellulose are selectively oxidized to carboxylates through aldehyde groups by the addition of NaClO, which acts as the primary oxidant, to aqueous suspensions of cellulose containing the radical TEMPO and NaBr (co-oxidant) under basic conditions²⁷⁴. TEMPO-mediated oxidation occurs

²⁶⁷ Mittal A, Katahira R, Donohoe BS, et al (2017) Alkaline Peroxide Delignification of Corn Stover. *ACS Sustain Chem Eng* 5:6310–6321 . doi: 10.1021/acssuschemeng.7b01424

²⁶⁸ Xiang Q, Lee YY (2000) Oxidative Cracking of Precipitated Hardwood Lignin by Hydrogen Peroxide. *Appl Biochem Biotechnol* 84–86:153–162 . doi: 10.1385/ABAB:84-86:1-9:153

²⁶⁹ Mittal A, Katahira R, Donohoe BS, et al (2017) Alkaline Peroxide Delignification of Corn Stover. *ACS Sustain Chem Eng* 5:6310–6321 . doi: 10.1021/acssuschemeng.7b01424

²⁷⁰ Li W, Zhao X, Liu S (2013) Preparation of entangled nanocellulose fibers from APMP and its magnetic functional property as matrix. *Carbohydr Polym* 94:278–285 . doi: 10.1016/j.carbpol.2013.01.052

²⁷¹ García A, Gandini A, Labidi J, et al (2016) Industrial and crop wastes: A new source for nanocellulose biorefinery. *Ind Crops Prod* 93:26–38 . doi: 10.1016/j.indcrop.2016.06.004

²⁷² Ovalle-Serrano SA, Blanco-Tirado C, Combariza MY (2018a) Exploring the composition of raw and delignified Colombian fique fibers, tow and pulp. *Cellulose* 25:151–165 . doi: 10.1007/s10570-017-1599-9

²⁷³ Gómez FN, Combariza MY, Blanco-Tirado C (2017) Facile cellulose nanofibrils amidation using a “one-pot” approach. *Cellulose* 24:717–730 . doi: 10.1007/s10570-016-1174-9

²⁷⁴ Saito T, Okita Y, Nge TT, et al (2006) TEMPO-mediated oxidation of native cellulose: Microscopic analysis of fibrous fractions in the oxidized products. *Carbohydr Polym* 65:435–440 . doi: 10.1016/j.carbpol.2006.01.034

superficially in crystalline and amorphous regions of cellulose. After the regioselective oxidation, the resulting TEMPO-oxidized cellulose nanofibers (TOCN) have carboxylic units in the form of sodium salt (COONa)^{275 276}. The carboxylic groups have anionic charges in water that generate electrostatic repulsions between the CMF facilitating the defibrillation²⁷⁷. The resulting TOCN-COONa are transparent gels highly hydrophilic and insoluble in polar aprotic organic solvents²⁷⁸. TOCN are featured by large surface areas, large modulus of elasticity and great capacity for the formation of films²⁷⁹. Additionally, remaining aldehydes in TOCN can be selectively oxidized to carboxylate groups using NaClO₂, resulting in highly oxidized TOCN with a wide range of applications in science as superhydrophilic materials²⁸⁰.

Several reports have discussed the application of CNF in the reinforcement of non-polar polymer matrices to improve their tensile strength and toughness²⁸¹. However, this has been a challenge for researchers since the integration of hydrophilic CNF and hydrophobic materials leads to low adhesion and therefore a weak interfacial bond in the resulting material. One alternative to increase cellulose fiber-polymer interactions is the surface modification of cellulose by the attachment of specific functional groups to the carboxylate groups created on the surface of the CNF to change its chemical properties²⁸².

²⁷⁵ Saito T, Isogai A (2004) TEMPO-Mediated Oxidation of Native Cellulose. The Effect of Oxidation Conditions on Chemical and Crystal Structures of the Water-Insoluble Fractions. *Biomacromolecules* 5:1983–1989 . doi: 10.1021/bm0497769

²⁷⁶ Gert E V., Torgashov VI, Zubets O V., Kaputskii FN (2005) Preparation and properties of enterosorbents based on carboxylated microcrystalline cellulose. *Cellulose* 12:517–526 . doi: 10.1007/s10570-005-7134-4

²⁷⁷ Benkaddour A, Journoux-Lapp C, Jradi K, et al (2014) Study of the hydrophobization of TEMPO-oxidized cellulose gel through two routes: amidation and esterification process. *J Mater Sci* 49:2832–2843 . doi: 10.1007/s10853-013-7989-y

²⁷⁸ Okita Y, Fujisawa S, Saito T, Isogai A (2011) TEMPO-Oxidized Cellulose Nanofibrils Dispersed in Organic Solvents. *Biomacromolecules* 12:518–522 . doi: 10.1021/bm101255x

²⁷⁹ Abe K, Yano H (2011) Formation of hydrogels from cellulose nanofibers. *Carbohydr Polym* 85:733–737 . doi: 10.1016/j.carbpol.2011.03.028

²⁸⁰ Isogai T, Saito T, Isogai A (2010) TEMPO electromediated oxidation of some polysaccharides including regenerated cellulose fiber. *Biomacromolecules* 11:1593–1599 . doi: 10.1021/bm1002575

²⁸¹ Bhatnagar A (2005) Processing of Cellulose Nanofiber-reinforced Composites. *J Reinf Plast Compos* 24:1259–1268 . doi: 10.1177/0731684405049864

²⁸² Salas C, Nypelö T, Rodriguez-Abreu C, et al (2014) Nanocellulose properties and applications in

There are numerous reports about surface modifications of CNF to increase its hydrophobicity without affecting its internal structure^{283 284 285}. CNF surfaces have been hydrophobized by the formation of ionic and covalent bonds using silanes or alkylamines, via chemical reactions such as esterification, silylation and amidation. Cellulose amidation reactions (which may or may not involve TOCN) are commonly carried out by the use of coupling agents such as water-soluble carbodiimides like EDC [1-ethyl-3-(3-dimethylaminopropyl) carbodiimide] or its analogs (EDAC, DCC) and NHS (N-hydroxysuccinimide) which promote the formation of a stable carboxylamine conjugated system. However, these processes involve slow reactions requiring high temperature, specific pH values and multiple stages, making them tedious; therefore, it is of great interest to develop more efficient and faster procedures such as the so-called 'one-pot' amidation reactions to produce functional materials with great potential for various applications such as active-surface agents²⁸⁶. Previously, our group reported a 'one-pot' synthetic approach to TOCN (from commercial microcrystalline cellulose) surface amidation by coupling up to 70% of superficial carboxylic units (1.25 mmol COOH/g cellulose) with long alkyl chain primary amines (dodecylamine and octadecylamine) using TBTU uronium salt as amidating agent²⁸⁷.

In this chapter, TOCN extracted from Fique tow and TOCN-P were used to obtain functional hydrophobic materials with improved thermal properties through a 'one-pot' amidation reaction. The high degree of oxidation in TOCN and TOCN-P

colloids and interfaces. *Curr Opin Colloid Interface Sci* 19:383–396 . doi: 10.1016/j.cocis.2014.10.003

²⁸³ Bledzki AK, Mamun AA, Lucka-Gabor M, Gutowski VS (2008) The effects of acetylation on properties of flax fibre and its polypropylene composites. *Express Polym Lett* 2:413–422 . doi: 10.3144/expresspolymlett.2008.50

²⁸⁴ Xu Y, Kawata S, Hosoi K, et al (2009) Thermomechanical properties of the silanized-kenaf/polystyrene composites. *Express Polym Lett* 3:657–664 . doi: 10.3144/expresspolymlett.2009.82

²⁸⁵ Benkaddour A, Journoux-Lapp C, Jradi K, et al (2014) Study of the hydrophobization of TEMPO-oxidized cellulose gel through two routes: amidation and esterification process. *J Mater Sci* 49:2832–2843 . doi: 10.1007/s10853-013-7989-y

²⁸⁶ Gómez FN, Combariza MY, Blanco-Tirado C (2017) Facile cellulose nanofibrils amidation using a "one-pot" approach. *Cellulose* 24:717–730 . doi: 10.1007/s10570-016-1174-9

²⁸⁷ Ibid.

extracted from Figue tow, compared to the TOCN from commercial microcrystalline cellulose, increased the coupling degree between ODA and the carboxyl groups. This resulted in higher contact angle values and higher stability in apolar solvents such as toluene. To our knowledge, no similar carboxylate content has been reported elsewhere after a post-oxidation process for TOCN and no one has used an experimental scheme similar to ours.

3.3 EXPERIMENTAL

3.3.1 Materials. Figue tow (*Furcraea macrophylla*) was collected from Figue leaves decortication in the rural area of San Joaquín, Santander, Colombia. 2,2,6,6-Tetramethyl-piperidin-1-oxyl (TEMPO) was purchased from Sigma Aldrich (Saint Louis, MO, USA) and sodium hypochlorite (NaClO, 15%) from Carlo Erba Reagents (Milan, Italy). Sodium bromide (NaBr), hydrogen peroxide (H₂O₂), sodium hydroxide (NaOH), sodium chlorite (NaClO₂, 25%), ethanol (EtOH), methanol (MeOH), N,N-dimethyl-formamide (DMF), 3,7-bis(Dimethylamino)-phenothiazin-5-ium chloride (methylene blue (MB)), acetic acid (glacial) and hydrochloric acid (HCl, 37%) were purchased from Merck (Darmstadt, Germany). [O-(1Hbenzotriazol-1-yl)-N,N,N',N'-tetramethyluronium tetrafluoroborate] (TBTU) 97% was purchased from Chempep (Wellington, FL, USA). All chemical reagents were used with no further purification. Aqueous solutions and suspensions were prepared with ultrapure water (18 MΩ·cm @ 25 °C).

3.3.2 Figue tow treatment, delignification and TOCN extraction. Figue tow was immersed in an ultrasound bath (Branson CPX3800, 40 kHz, 130 Watt) with distilled water for 60 min at 40 °C to remove Figue juice remnants and minerals such as carbonates and oxalates usually found in it. Figue tow was then dried in an oven at 60 °C for 24 h²⁸⁸ and labelled as “untreated Figue tow”.

²⁸⁸ Ovalle-Serrano SA, Blanco-Tirado C, Combariza MY (2018a) Exploring the composition of raw and delignified Colombian figue fibers, tow and pulp. *Cellulose* 25:151–165 . doi: 10.1007/s10570-

To remove non-cellulosic compounds such as hemicellulose and lignin, we used the procedure described in Chapter 1²⁸⁹. In brief, untreated Fique tow was cut into short lengths (1 cm) and 8 g were immersed in 100 mL of a H₂O₂ solution (10% w/w), which was basified to pH 11.5 by dropwise addition of NaOH (4 N). The mixture was kept in an ultrasonic bath for 2 h at 70 °C. Then, delignified tow was washed by filtration with distilled water and dried at 60 °C for 24 h.

We followed the procedure shown in Chapter 2 to obtain TEMPO-oxidized cellulose nanofibers (TOCN) from delignified Fique tow²⁹⁰. Initially, 1 g of delignified Fique tow was suspended in 100 mL of water. TEMPO (16 mg) and sodium bromide (100 mg) were dissolved in distilled water and added slowly to the suspension. Then, NaClO (0.037 mol) was added dropwise to start the oxidation reaction which was carried out in an ultrasonic bath (Bransonic CPX3800, 40 kHz, 130 Watt), keeping the pH at 10.5 with a 0.5 N NaOH solution at room temperature. When the oxidation process ended (no more NaOH was needed) the reaction was stopped by the addition of ethanol. The oxidized cellulose was centrifuged several times at 4700 rpm for 15 min with ultrapure water until neutral pH to remove unreacted chemicals and separate the TOCN. Fique tow TOCN aqueous suspensions of 0.5% wt were mechanically disintegrated by sonication in an Ultrasonic Processor (Sonics vibra-cell VC750, 20 kHz, 750 Watt) for 10 min (1:1 pulses) at 40% amplitude. Finally, the product was centrifuged again under the aforementioned conditions and the soluble fraction in water (supernatant) was stored for characterization.

3.3.3 Post-oxidation with NaClO₂. Aldehydes in Fique tow TOCN were oxidized to carboxylic acids according to the procedure reported by Mishra et al. (Mishra et al.

017-1599-9

²⁸⁹ Ovalle-Serrano SA, Blanco-Tirado C, Combariza MY (2018a) Exploring the composition of raw and delignified Colombian fique fibers, tow and pulp. *Cellulose* 25:151–165 . doi: 10.1007/s10570-017-1599-9

²⁹⁰ Ovalle-Serrano SA, Gómez FN, Blanco-Tirado C, Combariza MY (2018b) Isolation and characterization of cellulose nanofibrils from Colombian Fique decortication by-products. *Carbohydr Polym* 189:169–177 . doi: 10.1016/j.carbpol.2018.02.031

2012). 2 g of Fique tow TOCN were oxidized with 20 mL of a 25% w/w NaClO₂ solution and acetic acid at pH 3-4. The mixture was taken to a cellulose concentration of 1% w/v by adding water and was allowed to react for 2 h at 50 °C. Finally, Fique tow TOCN post-oxidized (TOCN-P) was cooled at room temperature and washed thoroughly with ultrapure water by filtration. After post-oxidation, the increase in the carboxyl content was taken as the aldehyde content in the Fique tow TOCN.

3.3.4 Conversion to free carboxyl groups. The regioselective TEMPO-mediated oxidation of delignified Fique tow, results in Fique tow TOCN with carboxylic units in the form of sodium salt (-COONa). These units were converted to their free forms of carboxylic acids (-COOH) by ion exchange using excess acid following the procedure reported by Fujisawa²⁹¹. HCl 1 M was added to aqueous dispersions of Fique tow TOCN and TOCN-P (0.5 wt%) until pH 2 under stirring for 30 min. The product was washed by filtration until pH 4 with a 0.01 M HCl solution and water to remove the excess acid. Finally, Fique tow TOCN-COOH and TOCN-P-COOH were re-dispersed in water and stored for further characterization.

3.3.5 Hydrofobization. Fique tow TOCN and TOCN-P suspensions were coupled to octadecylamine (ODA) using the procedure previously reported by Gómez et al.²⁹². TOCN and TOCN-P suspensions (100 mL, 1% wt.) were mixed with TBTU salt (2:1 molar ratio TBTU:TOCN) previously dissolved in DMF under stirring for 30 min at room temperature. Then, an octadecylamine solution in excess (4:1 molar ratio amine:COOH group) was added to the mixture and it was allowed to react for 2 h with constant stirring at room temperature. Once the reaction was done, the product turned light yellow and migrated to the surface of the reaction medium. The final products, labeled as TOCN-ODA and TOCN-P-ODA, were washed under vacuum

²⁹¹ Fujisawa S, Okita Y, Fukuzumi H, et al (2011) Preparation and characterization of TEMPO-oxidized cellulose nanofibril films with free carboxyl groups. *Carbohydr Polym* 84:579–583 . doi: 10.1016/j.carbpol.2010.12.029

²⁹² Gómez FN, Combariza MY, Blanco-Tirado C (2017) Facile cellulose nanofibrils amidation using a “one-pot” approach. *Cellulose* 24:717–730 . doi: 10.1007/s10570-016-1174-9

filtration with methanol, HCl (0.01 M) and water to remove the by-products of the reaction and residual amines.

3.3.6 Conductimetry. The degree of oxidation (DO), the surface charge density or carboxylate content (σ) and the degree of coupling after amidation process (DC) of the cellulose samples (untreated Fique tow, delignified Fique tow, TOCN, TOCN-P, TOCN-ODA and TOCN-P-ODA) were measured by a conductometric titration method according to the procedure reported by Habibi et al.²⁹³. 50 mg of cellulose samples were suspended in a 0.01 M HCl solution until pH 2 and stirred for 15 min. The suspensions were then titrated with a 0.01 M NaOH solution. All the experiments were carried out in triplicate. Generally, conductimetric titration curves show two flexion or equivalent points: the first one shows the neutralization of the strong acid, HCl, where the conductance value decreases rapidly due to the displacement of the H^+ by Na^+ cations, and the second one represents the neutralization of the weak acid, -COOH, where the conductance remains constant. When both acids have been completely neutralized, the conductivity increases due to the excess of OH^- ions from the base²⁹⁴. The volume of NaOH used to neutralize the carboxylic groups in the cellulose samples allows us to calculate the DO, σ and DC as shown in the following equations:

$$DO = 162 (V_2 - V_1)c [m - 36 (V_2 - V_1)c]^{-1} \quad (1)$$

$$\sigma = [c (V_2 - V_1)]m^{-1} \quad (2)$$

$$DC = DO_{(TOCN(P)-ODA)} - DO_{(TOCN(P))} \quad (3)$$

²⁹³ Habibi Y, Chanzy H, Vignon MR (2006) TEMPO-mediated surface oxidation of cellulose whiskers. *Cellulose* 13:679–687 . doi: 10.1007/s10570-006-9075-y

²⁹⁴ Smith KC, Edionwe E, Michel B (2010) Conductimetric titrations: A predict-observe-explain activity for general chemistry. *J Chem Educ* 87:1217–1221 . doi: 10.1021/ed100538q

Where c is the concentration (mol/L) of the titrant solution, V_1 and V_2 is the volume (L) of NaOH needed to neutralize the strong and weak acid, respectively, and m is the mass of the sample (g). In equation 3, the subscripts TOCN (P) and TOCN (P) - ODA refer to TOCN and TOCN-P before and after the amidation reaction, respectively.

3.3.7 Solubility Tests. 0.01 g of cellulose samples (TOCN, TOCN-P, TOCN-ODA and TOCN-P-ODA) were added to a glass recipient and different solvents were added to obtain concentrations of 0.2 % w/v. The mixtures were stirred at room temperature for 2 h (1500 rpm). Transmittance measurements from 285 to 750 nm using a Shimadzu UV-Vis spectrophotometer (UV-2401PC), were used as the criterion for a satisfactory solubility in each solvent²⁹⁵.

3.3.8 Characterization. FT-IR spectra were collected using a Bruker Tensor 27 Fourier transform infrared (FT-IR) spectrometer equipped with a Platinum Diamond ATR unit A225/Q (Billerica, MA). A total of 32 scans were taken for each spectrum at a resolution of 2 cm^{-1} (4000-500 cm^{-1}). Crystalline properties were analyzed by X-ray diffraction (XRD) spectroscopy on a Bruker D8 DISCOVER X-ray diffractometer (Billerica, MA) with a DaVinci geometry (CuK α 1 radiation ($k = 1.54 \text{ \AA}$), 40 kv/40 mA) using an area detector VANTEC-500 and a poly(methyl methacrylate) sample holder. Contact angle measurements were carried out on an OCA 15EC contact angle system (Data Physics, Filderstadt, Germany) equipped with a dosing syringe using the sessile drop technique (1 μL of deionized water) on film samples²⁹⁶. Films of TOCN, TOCN-P, TOCN-ODA and TOCN-P-ODA were prepared according to the reported by Gómez et al.²⁹⁷ as follows: microscopy glass slides were coated with a

²⁹⁵ Saito T, Kimura S, Nishiyama Y, Isogai A (2007) Cellulose Nanofibers Prepared by TEMPO-Mediated Oxidation of Native Cellulose. *Biomacromolecules* 8:2485–2491 . doi: 10.1021/bm0703970

²⁹⁶ Lif A, Stenstad P, Syverud K, et al (2010) Fischer-Tropsch diesel emulsions stabilised by microfibrillated cellulose and nonionic surfactants. *J Colloid Interface Sci* 352:585–592 . doi: 10.1016/j.jcis.2010.08.052

²⁹⁷ Gómez FN, Combariza MY, Blanco-Tirado C (2017) Facile cellulose nanofibrils amidation using a “one-pot” approach. *Cellulose* 24:717–730 . doi: 10.1007/s10570-016-1174-9

1% w/w suspension of each sample (TOCN derivatives in water and TOCN-amidated derivatives in toluene) and dried at room temperature for 24 h. All measurements were performed in triplicated with an accuracy of 0° – $180^{\circ} \pm 0.1$ for angle measurement. Thermal decomposition behaviors (TGA) of freeze-dried samples (10 mg) were investigated using a STA 449 F5 Jupiter instrument (São Paulo, Brazil) under nitrogen flow (50 mL/min). The samples were scanned from room temperature up to 500 °C at a heating rate of 10 °C/min. Surface morphology was characterized by field emission scanning electron microscopy (FESEM) with a FEI QUANTA FEG 650 (Oregon, USA) instrument operating at 20 kV and equipped with a large field detector. Samples were coated with gold using a Quorum 150T ES system (Oregon, USA). ζ potential measurements were made using a Malvern Zetasizer Nano ZS90 instrument (Worcestershire, UK) equipped with a capillary cell 1070. Experiments were performed with nanocellulose suspensions at 0.1% (w/v).

3.4 RESULTS AND DISCUSSION

Untreated Fique tow (Figure 13a) is a hard fiber with a rigid texture and due to its lignin content is characterized as a light yellow material. In addition to its high cellulose content, it also contains some minerals such as calcium oxalate ²⁹⁸. After AHP treatment, Fique tow becomes a white material (Figure 13b) with less rigidity. The physical-chemical changes during the alkaline hydrogen peroxide (AHP) treatment get started when H₂O₂ reacts with lignin through the anion hydroperoxide (HOO⁻), a strong nucleophile that, particularly attacks chromophores species which are the most prone to chemical attacks. However, decomposition of hydrogen peroxide in molecular oxygen and other radical species (e.g., OH[·]), may also degrade lignin and hemicellulose, making the oxidation reaction mechanism

²⁹⁸ Ovalle-Serrano SA, Blanco-Tirado C, Combariza MY (2018a) Exploring the composition of raw and delignified Colombian fique fibers, tow and pulp. *Cellulose* 25:151–165 . doi: 10.1007/s10570-017-1599-9

extremely complicated²⁹⁹. The oxidative reaction with H₂O₂ involves cleavage of the lignin ring, aryl ether bond and other linkages³⁰⁰.

Figure 13. Images of (a) untreated and (b) delignified Figue tow, (c) TOCN in water and (d) TOCN-ODA in toluene.

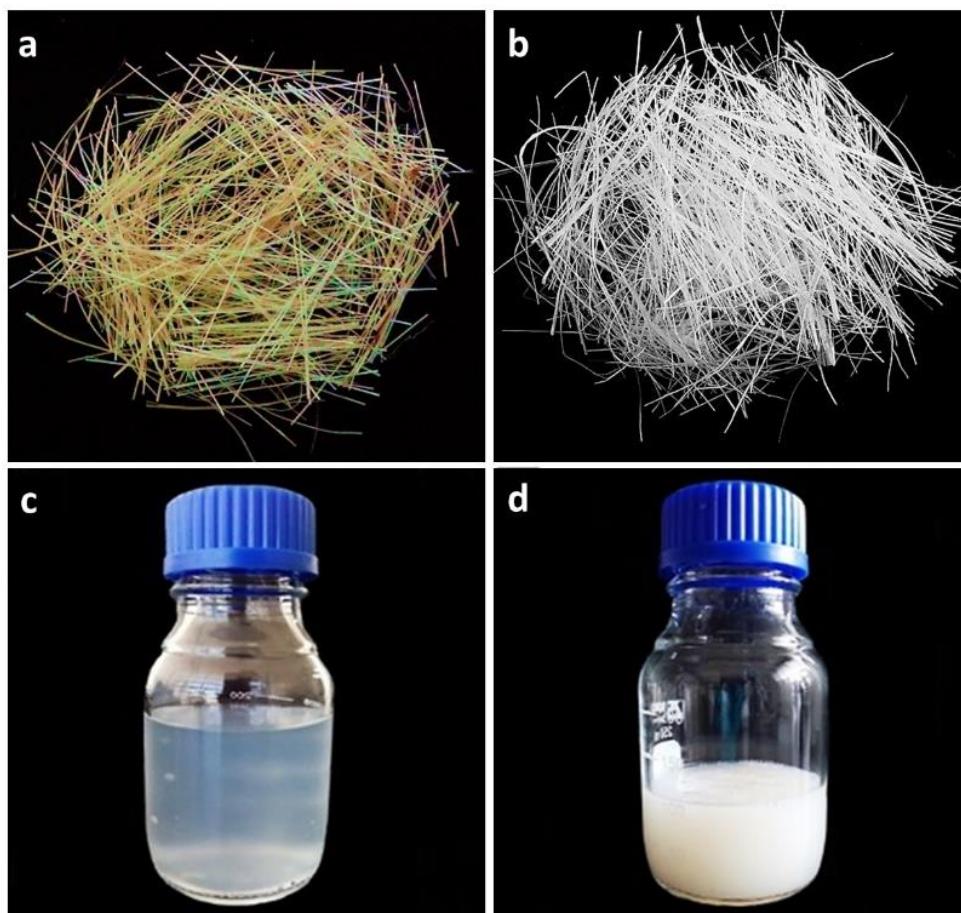


Figure 13c shows the stable aqueous suspension of TOCN. After mild oxidation of the remaining surface aldehydes of TOCN, a hydrophilic material (TOCN-P) was obtained, which also formed a homogeneous and translucent suspension as TOCN. Figure 13d shows an image of TOCN-ODA in toluene. It can be seen that the

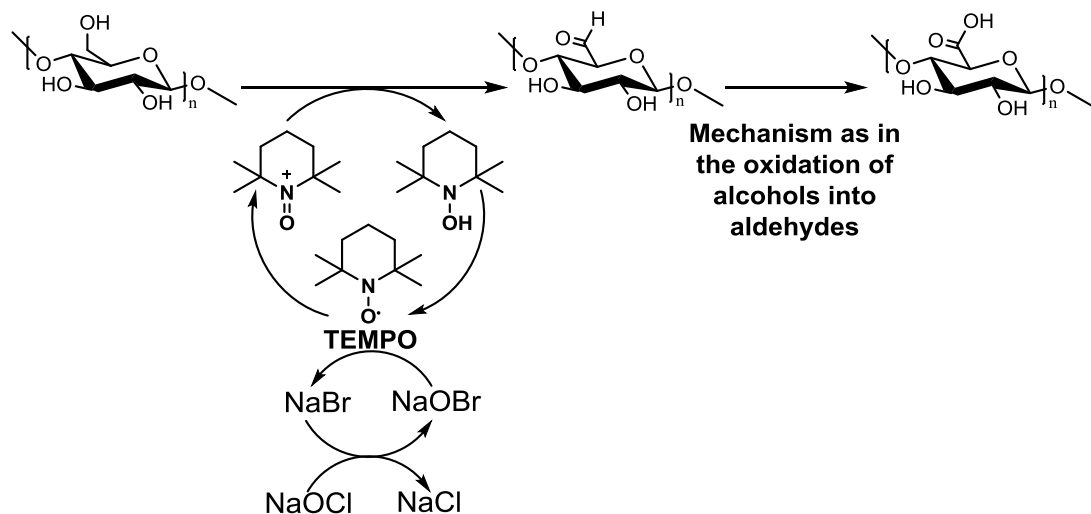
²⁹⁹ Sun RC, Fang JM, Tomkinson J (2000) Delignification of rye straw using hydrogen peroxide. *Ind Crops Prod* 12:71–83 . doi: 10.1016/S0926-6690(00)00039-X

³⁰⁰ Xiang Q, Lee YY (2000) Oxidative Cracking of Precipitated Hardwood Lignin by Hydrogen Peroxide. *Appl Biochem Biotechnol* 84–86:153–162 . doi: 10.1385/ABAB:84-86:1-9:153

suspension was transformed into a light yellow product, with lower density than water and hydrophobic, soluble in toluene.

The TEMPO-mediated oxidation of delignified tow consists in oxidation-reduction reactions where NaClO starts by oxidizing the NaBr to sodium hypobromite (NaOBr) and it transforms TEMPO, or a related stable radical, in a nitrosonium ion which selectively oxidizes the primary hydroxyl from cellulose to aldehyde by reducing itself into hydroxylamine³⁰¹. Finally, the aldehyde group is oxidized to carboxylic acid by the same process because the nitrosonium ion can be regenerated again from the hydroxylamine completing the catalytic cycle (Bragd et al. 2000). It has been shown that two molar equivalents of NaClO oxidize one molar primary -OH to -COOH³⁰². The reaction is shown in Figure 14.

Figure 14. TEMPO-mediated oxidation of primary hydroxyls to carboxyl groups.



The process continues with a mechanical treatment such as mechanical waves (ultrasound), since it has a significant impact on the TEMPO-mediated oxidation

³⁰¹ Isogai A, Saito T, Fukuzumi H (2011) TEMPO-oxidized cellulose nanofibers. *Nanoscale* 3:71–85 . doi: 10.1039/C0NR00583E

³⁰² Yang H (2011) Investigation and characterization of oxidized cellulose and cellulose nanofiber films

reaction^{303 304}. The ultrasonic energy is transferred to the cellulose chains through a process called cavitation. Cavitation consists in the formation, growth and violent collapse of steam cavities of a liquid when it reaches its vapor pressure, generating waves that travel at speeds close to those of sound with enough energy to break hydrogen bonds. Therefore, the ultrasonic impact can gradually disintegrate the micrometric cellulose fibers into nanofibers depending on the treatment conditions³⁰⁵.

As shown in Figure 14, oxidation of the primary hydroxyl to carboxylates in the surface of CNF goes through an “intermediate aldehyde” by a combination of TEMPO and mechanical treatment. However, there have been reports that not all aldehydes are completely oxidized to carboxyls and remained in the final product³⁰⁶ despite long reaction times. Aldehyde content in TOCN is mainly due to the incomplete oxidation of the primary alcohols and to secondary reactions, such as the oxidation by NaClO that generates C2-C3 cleavage of anhydroglucose units generating aldehydes and dicarboxylic structures during TEMPO oxidation^{307 308}. In addition, as reported by Tojo and Fernandez³⁰⁹, remaining aldehydes are common due to non-competitive inhibition by TEMPO when the oxidation of the aldehydes proceeded through a radical mechanism. This is why the oxidation can be carried

³⁰³ Dai L, Wang B, Long Z, et al (2015) Properties of hydroxypropyl guar/TEMPO-oxidized cellulose nanofibrils composite films. *Cellulose* 22:3117–3126 . doi: 10.1007/s10570-015-0691-2

³⁰⁴ Ovalle-Serrano SA, Gómez FN, Blanco-Tirado C, Combariza MY (2018b) Isolation and characterization of cellulose nanofibrils from Colombian Fique decortication by-products. *Carbohydr Polym* 189:169–177 . doi: 10.1016/j.carbpol.2018.02.031

³⁰⁵ Chen W, Yu H, Liu Y, et al (2011) Individualization of cellulose nanofibers from wood using high-intensity ultrasonication combined with chemical pretreatments. *Carbohydr Polym* 83:1804–1811 . doi: 10.1016/j.carbpol.2010.10.040

³⁰⁶ Mishra SP, Manent A-S, Chabot B, Daneault C (2012) The Use of Sodium Chlorite in Post-Oxidation of TEMPO-Oxidized Pulp: Effect on Pulp Characteristics and Nanocellulose Yield. *J Wood Chem Technol* 32:137–148 . doi: 10.1080/02773813.2011.624666

³⁰⁷ Besemer A (1993) The bromide catalyzed hypochlorite oxidation of starch and inulin. Delft University of Technology

³⁰⁸ Bragd PL, Besemer AC, Van Bekkum H (2000) Bromide-free TEMPO-mediated oxidation of primary alcohol groups in starch and methyl α -D-glucopyranoside. *Carbohydr Res* 328:355–363 . doi: 10.1016/S0008-6215(00)00109-9

³⁰⁹ Tojo G, Fernández M (2007) Oxidation of primary alcohols to carboxylic acids: a guide to current common practice

out in the presence of oxygen and stopped easily in the aldehyde stage. Therefore, the carboxyl groups in TOCN come exclusively from the TEMPO-mediated oxidation and not from an over-oxidation due to side reactions. In addition, formation of intra and intermolecular hemiacetals with hydroxyls groups of other cellulose chains also prevents the complete oxidation of the aldehydes by steric hindrance³¹⁰.

To increase the carboxyl content of TEMPO-oxidized nanocellulose, we additionally converted the remaining aldehydes to carboxyl groups using NaClO₂ and acetic acid at pH 3-4. NaClO₂ has been widely used to oxidize aldoses to aldonic acids since other species, such as alditols and ketoses, are inert to it in an acidic medium³¹¹. In aqueous solution, NaClO₂ is in equilibrium with the chlorous acid (HClO₂), which is responsible for the oxidation of the aldehydes. It is necessary to keep the pH of the reaction between 2 and 4 to favor its formation³¹². Hence, NaClO₂ is an effective choice for the selective oxidation of “intermediate aldehydes” in TOCN and to decrease interference of amine coupling to form covalent bonds, as will be demonstrated later.

Figures 15a and 15b show the morphological changes after delignification of raw Fique tow. It can be observed that the diameter of the tow was reduced from 233 μm to 155 μm, due to the removal and solubilization of amorphous compounds (lignin and hemicellulose)³¹³. The formation of elongated cellulose networks after oxidation reaction for TOCN and TOCN-P is shown in Figures 15c and 15d, respectively. The diameters of TOCN went from 60 nm to 40 nm in TOCN-P. The increase in the

³¹⁰ Saito T, Isogai A (2004) TEMPO-Mediated Oxidation of Native Cellulose. The Effect of Oxidation Conditions on Chemical and Crystal Structures of the Water-Insoluble Fractions. *Biomacromolecules* 5:1983–1989 . doi: 10.1021/bm0497769

³¹¹ Mishra SP, Manent A-S, Chabot B, Daneault C (2012) The Use of Sodium Chlorite in Post-Oxidation of TEMPO-Oxidized Pulp: Effect on Pulp Characteristics and Nanocellulose Yield. *J Wood Chem Technol* 32:137–148 . doi: 10.1080/02773813.2011.624666

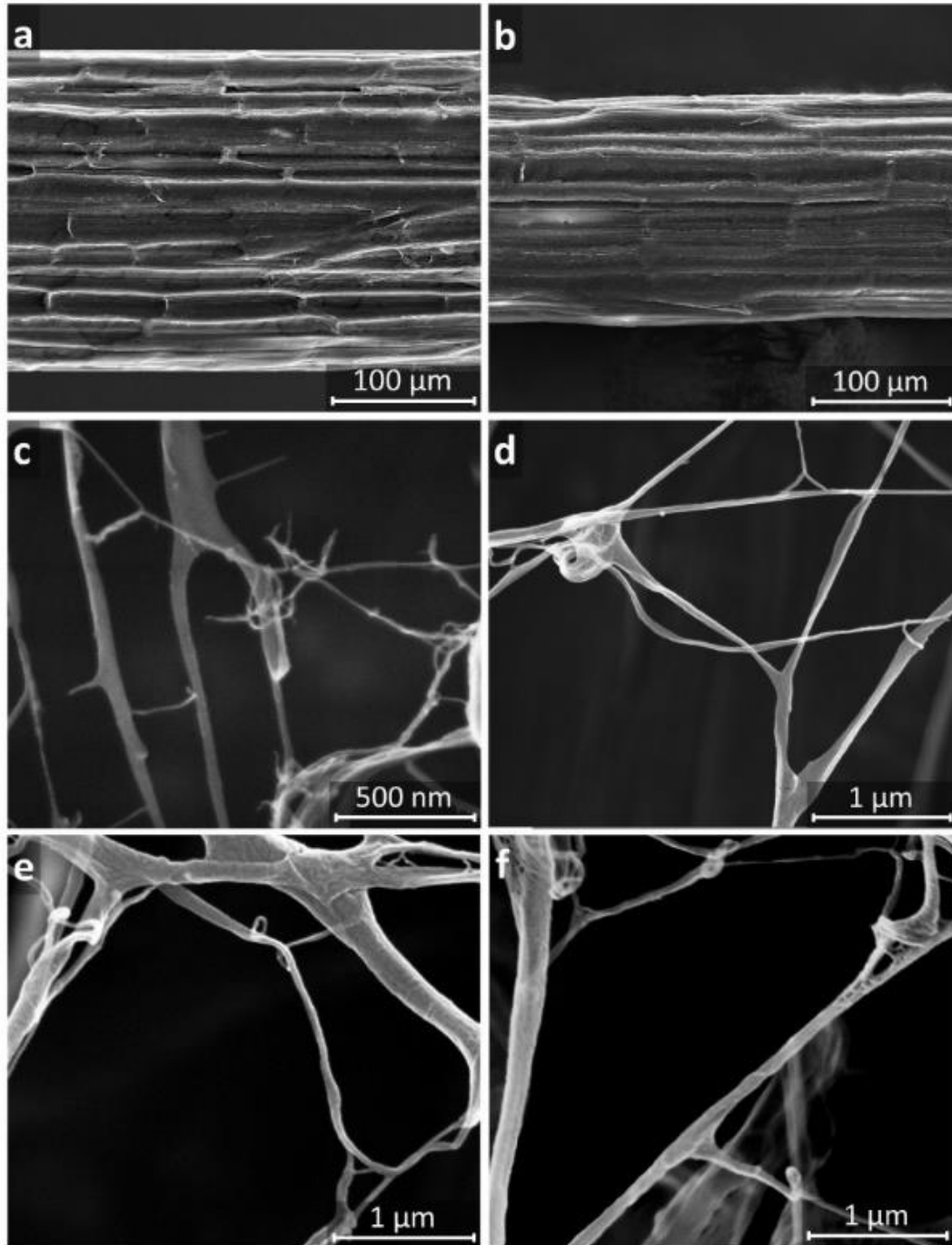
³¹² Williams DR, Nishitani K (1980) A mild oxidation of aldehydes to α,β-unsaturated aldehydes. *Tetrahedron Lett* 21:4417–4420 . doi: 10.1016/S0040-4039(00)92188-9

³¹³ Ovalle-Serrano SA, Blanco-Tirado C, Combariza MY (2018a) Exploring the composition of raw and delignified Colombian fique fibers, tow and pulp. *Cellulose* 25:151–165 . doi: 10.1007/s10570-017-1599-9

carboxylate content in TOCN-P probably caused more electrostatic repulsions among the nanofibrils contributing to the defibrillation process. On the other hand, Figures 15e and 15f show FESEM images of TOCN-ODA and TOCN-P-ODA, respectively. These images reveal that after coupling with long octadecylamine chains on the surface of TOCN and TOCN-P, no significant change was observed on its morphology, thus keeping nanofibril-like structure with an increment of approximately 10 nm in diameter. A similar increase in the diameter of CNF was found in the work of Missoum et al.³¹⁴ after coupling the nanofibrils with long aliphatic isocyanate chains.

³¹⁴ Missoum K, Bras J, Belgacem MN (2012) Organization of aliphatic chains grafted on nanofibrillated cellulose and influence on final properties. *Cellulose* 19:1957–1973 . doi: 10.1007/s10570-012-9780-7

Figure 15. FESEM images of (a) untreated and (b) delignified Figue tow, (c) TOCN, (d) TOCN-P, (e) TOCN-ODA and (f) TOCN-P-ODA.



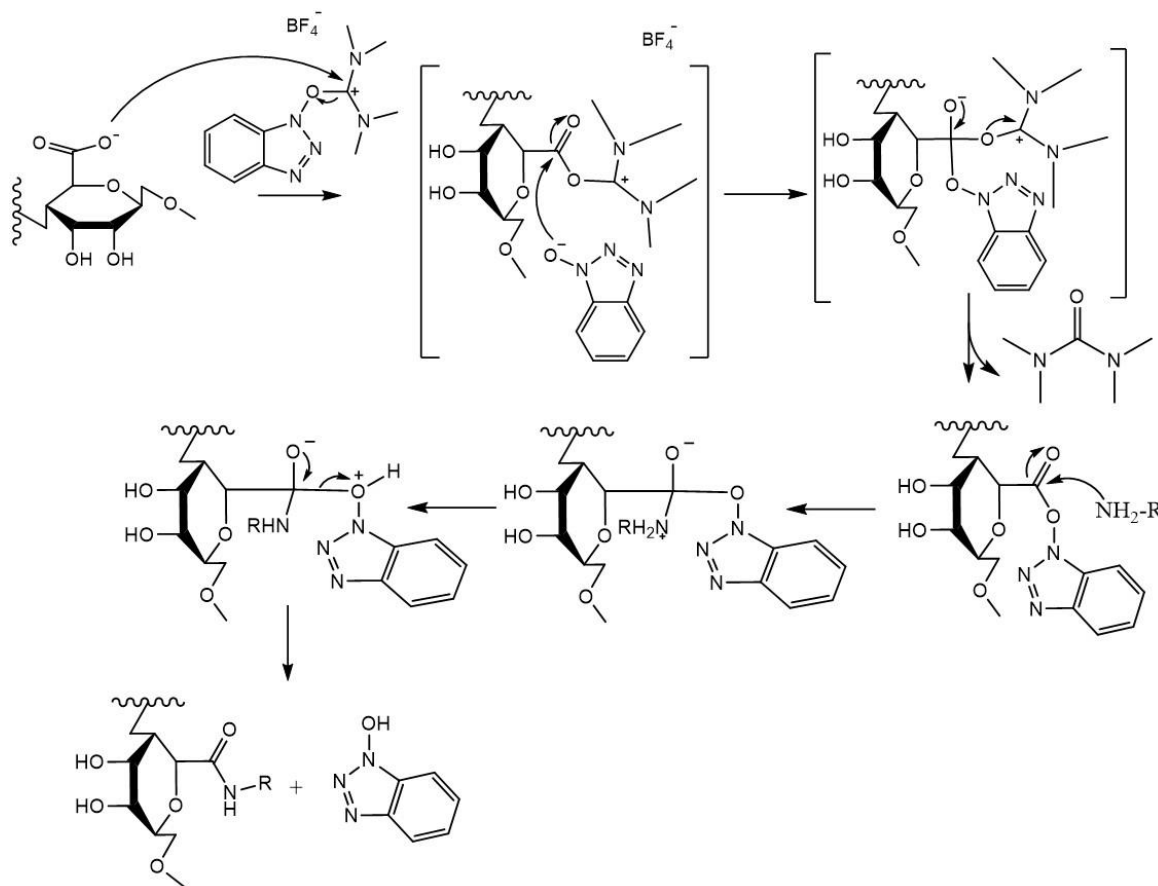
The surface modification of TOCN was achieved using the 'one-pot' amidation reaction reported by Gómez et al.³¹⁵. In this reaction, an "active ester" is produced *in situ* which forms the amidated product by reacting with a primary amine. The acylating agents most commonly used in amidation reactions are salts of phosphonium, iminium and uranium such as TBTU and HBTU which until now had only been used for the synthesis of proteins and peptides³¹⁶. In CNF amidation (Figure 16), the anion carboxylate of TOCN reacts with the electronically deficient uronium salt by removing an anionic species. This anion in turn reacts with the electrodeficient carbonyl carbon resulting from the previous stage to form an "active ester". Finally, the ester reacts with the primary amine forming the amide bond by nucleophilic addition³¹⁷.

³¹⁵ Gómez FN, Combariza MY, Blanco-Tirado C (2017) Facile cellulose nanofibrils amidation using a "one-pot" approach. *Cellulose* 24:717–730 . doi: 10.1007/s10570-016-1174-9

³¹⁶ Ibid.

³¹⁷ Ibid.

Figure 16. ‘One-pot’ TBTU amidation mechanism for TOCN surface modification. Adapted from Gómez et al.



Fuente: Gómez FN, Combariza MY, Blanco-Tirado C (2017) Facile cellulose nanofibrils amidation using a “one-pot” approach. *Cellulose* 24:717–730 . doi: 10.1007/s10570-016-1174-9

The variations on the chemical structure of the cellulose samples after their isolation and superficial chemical modification, were identified by IR-ATR spectroscopy. Figure 16a compares the IR spectra of untreated Figue tow, delignified Figue tow, TOCN and TOCN-P before and after the amidation reaction (TOCN-ODA and TOCN-P-ODA, respectively). In all spectra, common signals of cellulose were observed. A wide band in the region of $3000\text{--}3500\text{ cm}^{-1}$ attributed to O-H stretching vibrations³¹⁸. The 2896 , 1600 and $1426\text{--}1318\text{ cm}^{-1}$ peaks represent symmetric and asymmetric

³¹⁸ Iskalieva A, Yimmou BM, Gogate PR, et al (2012) Cavitation assisted delignification of wheat straw: a review. *Ultrason Sonochem* 19:984–93 . doi: 10.1016/j.ultsonch.2012.02.007

vibration of the C-H unit, the H-O-H stretching vibration of water absorbed in the carbohydrates and the C6-H₂ flexion of glucopyranose ring, respectively. The most intense band corresponds to glucosidic bond β (1→4) C-O-C stretching vibration between 1203 and 1108 cm⁻¹ and to the C-O vibration of C2, C3 and C6 at 1028 cm⁻¹. Finally, a small signal at 897 cm⁻¹ is originated from C1-H anomeric carbon³¹⁹. Figure 3.5b, a zoom of the IR spectra from 2000-1000 cm⁻¹, shows that after AHP treatment, signals at 1729 and 1239 cm⁻¹, assigned to the carboxyl groups of the acids, esters and acetyl groups of the hemicellulose and lignin³²⁰ and to the C-O-C stretching vibration of the aryl group in lignin, respectively, disappeared partially from the spectrum. This indicates that hemicellulose and lignin were removed successfully from Fique tow³²¹.

As result of the amidation in TOCN and TOCN-P, two characteristic signals of the amide group emerged: amide I and amide II in 1592 and 1520 cm⁻¹, respectively. The first one due to the C=O stretching of amide that overlaps with the stretching vibration of C=O of the remaining aldehydes and carboxylates in the same region and the second one represents the stretching and the NH deformation³²². For TOCN-P-ODA, amide I band is overlapped with another signal at 1617 cm⁻¹ assigned to the C=O stretching vibration of the free carboxylate groups that did not react with amines. In addition, the substitution of the carboxylic groups for amide bonds in TOCN and TOCN-R was verified by the intense signals at 2849 and 2916 cm⁻¹, which are attributed to the stretching vibration of the -CH₃ and -CH₂ groups of the aliphatic

³¹⁹ Chen W, Yu H, Liu Y, et al (2011) Individualization of cellulose nanofibers from wood using high-intensity ultrasonication combined with chemical pretreatments. *Carbohydr Polym* 83:1804–1811 . doi: 10.1016/j.carbpol.2010.10.040

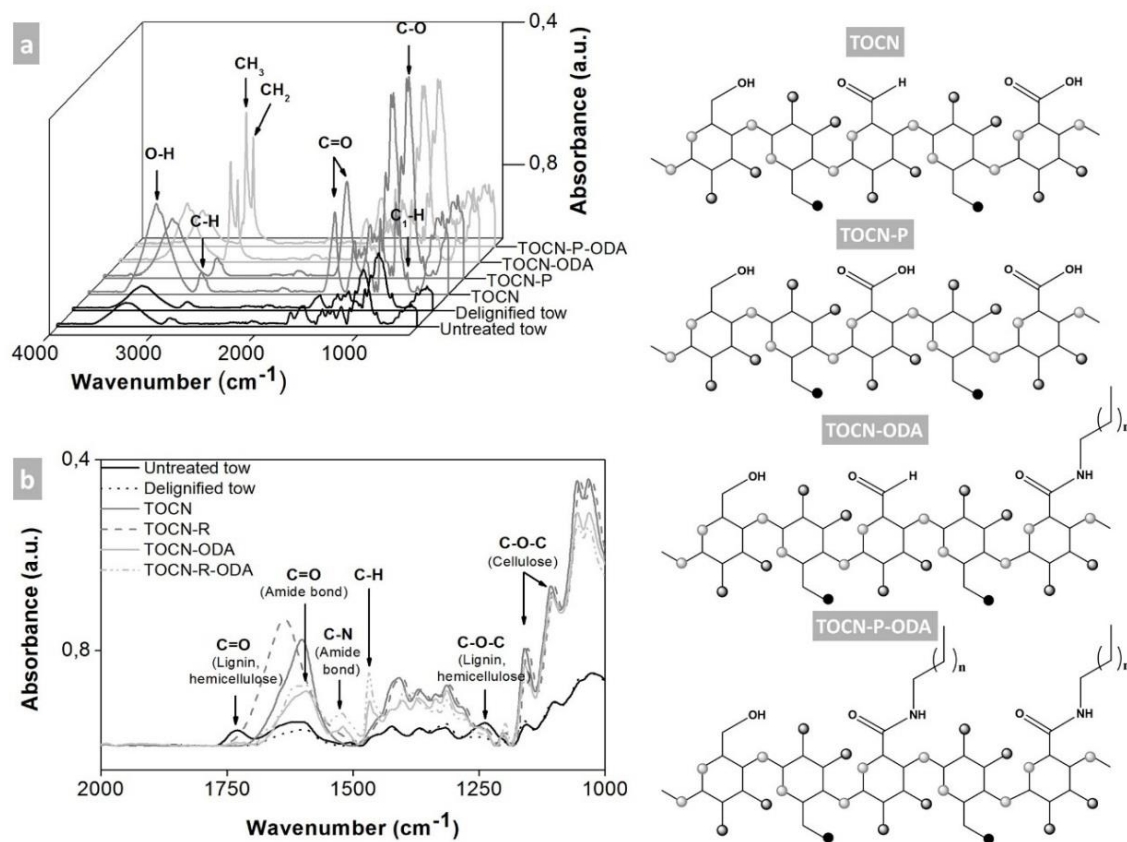
³²⁰ Wang B, Wang X, Feng H (2010) Deconstructing recalcitrant *Miscanthus* with alkaline peroxide and electrolyzed water. *Bioresour Technol* 101:752–760 . doi: 10.1016/j.biortech.2009.08.063

³²¹ Moriana R, Vilaplana F, Ek M (2015) Forest residues as renewable resources for bio-based polymeric materials and bioenergy: chemical composition, structure and thermal properties. *Cellulose* 22:3409–3423 . doi: 10.1007/s10570-015-0738-4

³²² Lasseguette E (2008) Grafting onto microfibrils of native cellulose. *Cellulose* 15:571–580 . doi: 10.1007/s10570-008-9200-1

chains. A new signal also appeared at 1468 cm^{-1} due to CH deformation of the C18 chain from ODA³²³.

Figure 17. (a) Complete and (b) zoomed IR-ATR spectra of Figue tow: untreated, delignified, TOCN, TOCN-P, TOCN-ODA and TOCN-P-ODA and representation of their chemical structure.



The crystallinity index (CrI) was used as a parameter to determine if crystallinity was affected by the different chemical and mechanical treatments during the process of isolation and modification of CNF. CrI shows the relative amount of crystalline and amorphous material in the cellulose structure according to the Segal method³²⁴.

³²³ Benkaddour A, Journoux-Lapp C, Jradi K, et al (2014) Study of the hydrophobization of TEMPO-oxidized cellulose gel through two routes: amidation and esterification process. *J Mater Sci* 49:2832–2843 . doi: 10.1007/s10853-013-7989-y

³²⁴ Segal L, Creely JJ, Martin AE, Conrad CM (1959) An Empirical Method for Estimating the Degree of Crystallinity of Native Cellulose Using the X-Ray Diffractometer. *Text Res J* 29:786–794 . doi: 10.1177/004051755902901003

Figure 16 shows X-ray diffraction profiles of the cellulose samples. The diffraction patterns coincide with the representative crystallographic planes of cellulose type I as reported by the Joint Committee on Powder Diffraction Standards (JCPDS file, No. 50-2241), space group P21 (No 4)^{325 326 327}. The first broad band at 15.32° corresponds to the overlapping of the signals of crystallographic plans (010) I α , (1-10) I β and (100) I α , (110) I β . The most intense signal at 22.5° represents the crystallographic plans (110) I α and (200) I β ^{328 329} and finally the weakest peak at 34.4° is due to multiple reflections including the (11-4) I α and (004) I β ^{330 331 332}. In addition, small signals corresponding to calcium oxalate were observed at 15°, 25°, 30° and 38° for untreated, delignified, TOCN and TOCN-P Fique tow³³³.

A significant increase in crystallinity was observed for the Fique tow after delignification (from 60 to 67%). The increase in crystallinity was undoubtedly due to the removal of amorphous materials such as hemicellulose and lignin³³⁴. It has been shown that after TEMPO-mediated oxidation, carboxyl groups are introduced mainly into the amorphous regions of cellulose as they are more reactive than crystalline

³²⁵ Morán JI, Alvarez VA, Cyras VP, Vázquez A (2008) Extraction of cellulose and preparation of nanocellulose from sisal fibers. *Cellulose* 15:149–159 . doi: 10.1007/s10570-007-9145-9

³²⁶ Mandal A, Chakrabarty D (2011) Isolation of nanocellulose from waste sugarcane bagasse (SCB) and its characterization. *Carbohydr Polym* 86:1291–1299

³²⁷ Sèbe G, Ham-Pichavant F, Ibarboure E, et al (2012) Supramolecular structure characterization of cellulose II nanowhiskers produced by acid hydrolysis of cellulose I substrates. *Biomacromolecules* 13:570–8 . doi: 10.1021/bm201777j

³²⁸ Okita Y, Saito T, Isogai A (2010) Entire surface oxidation of various cellulose microfibrils by TEMPO mediated oxidation. 1696–1700

³²⁹ French AD (2013) Idealized powder diffraction patterns for cellulose polymorphs. *Cellulose* 21:885–896 . doi: 10.1007/s10570-013-0030-4

³³⁰ Wada M, Kondo T, Okano T (2003) Thermally Induced Crystal Transformation from Cellulose I[α] to I[β]. *Polym J* 35:155–159 . doi: 10.1295/polymj.35.155

³³¹ Davidson TC, Newman RH, Ryan MJ (2004) Variations in the fibre repeat between samples of cellulose I from different sources. *Carbohydr Res* 339:2889–2893 . doi: 10.1016/j.carres.2004.10.005

³³² French AD (2013) Idealized powder diffraction patterns for cellulose polymorphs. *Cellulose* 21:885–896 . doi: 10.1007/s10570-013-0030-4

³³³ Ovalle-Serrano SA, Blanco-Tirado C, Combariza MY (2018a) Exploring the composition of raw and delignified Colombian fique fibers, tow and pulp. *Cellulose* 25:151–165 . doi: 10.1007/s10570-017-1599-9

³³⁴ Ibid.

regions³³⁵. The diffraction profile of TOCN derivatives did not show any change, which indicates that the crystalline structure of cellulose I was not altered by the modification treatments³³⁶. A remarkable decrease in the CrI was observed for TOCN and TOCN-P at 64% and 61%, respectively, due to the introduction of carboxylate groups on the surface of the CNF and to the mechanical treatment³³⁷. The higher decrease in the CrI for TOCN-P may be due to the higher carboxylate content. This makes the TOCN-P more hydrophilic than TOCN and therefore they can experience greater swelling in their nanofibers and decrease their structural rigidity. In the same way, the crystallinity index dropped to 53% and 51% for TOCN-ODA and TOCN-P-ODA, respectively. This effect was probably due to the coupling with long octadecylamine alkyl chains that destabilize the crystalline structure of cellulose without inducing significant changes in its final structure³³⁸.

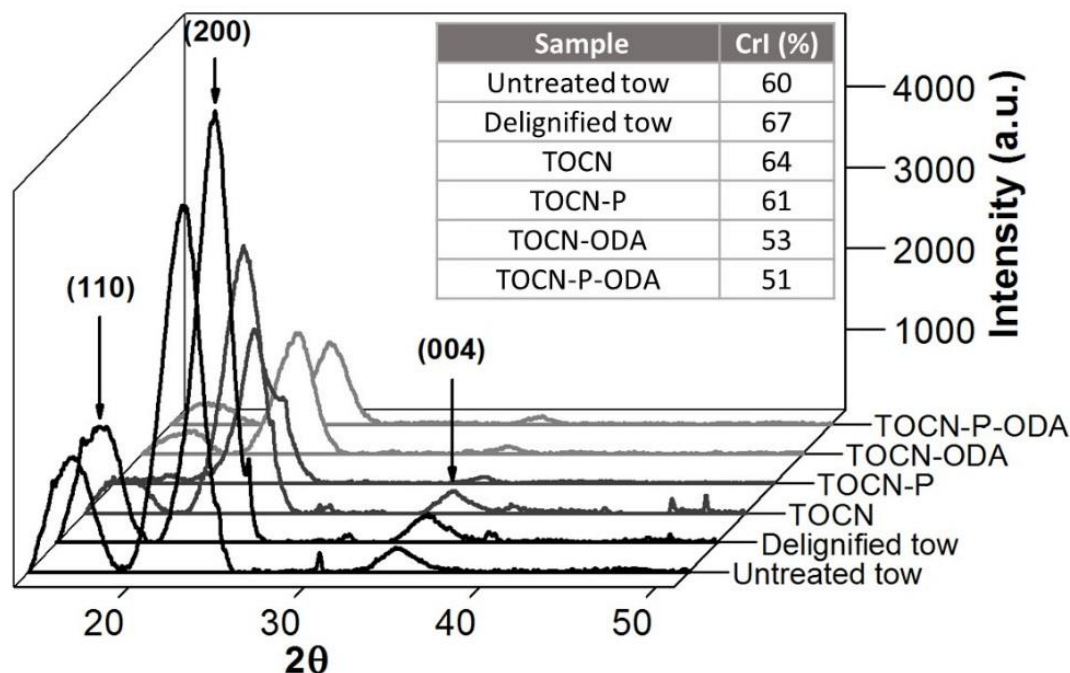
³³⁵ Benkaddour A, Journoux-Lapp C, Jradi K, et al (2014) Study of the hydrophobization of TEMPO-oxidized cellulose gel through two routes: amidation and esterification process. *J Mater Sci* 49:2832–2843 . doi: 10.1007/s10853-013-7989-y

³³⁶ Johnson RK, Zink-Sharp A, Glasser WG (2011) Preparation and characterization of hydrophobic derivatives of TEMPO-oxidized nanocelluloses. *Cellulose* 18:1599–1609 . doi: 10.1007/s10570-011-9579-y

³³⁷ Gómez FN, Combariza MY, Blanco-Tirado C (2017) Facile cellulose nanofibrils amidation using a “one-pot” approach. *Cellulose* 24:717–730 . doi: 10.1007/s10570-016-1174-9

³³⁸ Ibid.

Figure 18. X-ray diffraction profiles of Figue tow: untreated, delignified, TOCN, TOCN-P, TOCN-ODA and TOCN-P-ODA.



The DO, σ and DC are shown in Table 5. The DO calculated for untreated and delignified Figue tow were 0.04 and 0.07, respectively, indicating the presence of small amounts of carboxylic groups in the samples. This slight oxidation may correspond to carboxylic groups of the hemicellulose and/or lignin remaining in the tow and to the intensity of the mechanical treatment (ultrasonic irradiation) in its cleaning and delignification stages, as has been reported in previous studies³³⁹. The degree of oxidation of the TOCN obtained by the oxidation with TEMPO and post-oxidation with NaClO₂ were 0.29 and 0.39, which is equivalent to σ of 1.57 and 2.20 mmol/g of cellulose, respectively. This means that after the TEMPO-mediated oxidation, 1.57 mmol of hydroxymethyl groups per gram of cellulose were oxidized to carboxylate groups and about 0.63 mmol of the remaining aldehyde groups per

³³⁹ Chen W, Yu H, Liu Y, et al (2011) Individualization of cellulose nanofibers from wood using high-intensity ultrasonication combined with chemical pretreatments. *Carbohydr Polym* 83:1804–1811 . doi: 10.1016/j.carbpol.2010.10.040

gram of cellulose oxidized with TEMPO, were completely oxidized to their respective carboxylic form after treatment with NaClO₂. To our knowledge, the DO and σ we report for post-oxidized TOCN (0.39 and 2.2 mmol COOH/g cellulose) are the highest values reported so far^{340 341}. To make a broader idea about the carboxylate content, in 25 anhydroglucose monomer-repeating units in average, nine of them were oxidized during TEMPO-mediated oxidation (TOCN), but only six were completely oxidized to uronic acid and 3 were incompletely oxidized to aldehyde³⁴². After the coupling of TOCN and TOCN-P with TBTU and ODA, we obtained a similar degree of coupling (up to 70%) to that reported by Gómez et al.³⁴³. However, we reached a higher carboxyl content for Fique tow TOCN and TOCN-P (1.57 and 2.20 mmol/g cellulose, respectively) compared to the reported for commercial microcrystalline cellulose (1.25 mmol/g cellulose) so that the amount coupling was higher. This means 73% and 82% of the available COO⁻ groups reacted to form an amide, i.e., about 1.14 and 1.80 mmol of amide units were coupled to one gram of cellulose, respectively.

³⁴⁰ Mishra SP, Manent A-S, Chabot B, Daneault C (2012) The Use of Sodium Chlorite in Post-Oxidation of TEMPO-Oxidized Pulp: Effect on Pulp Characteristics and Nanocellulose Yield. *J Wood Chem Technol* 32:137–148 . doi: 10.1080/02773813.2011.624666

³⁴¹ Isogai A (2013) Wood nanocelluloses: fundamentals and applications as new bio-based nanomaterials. 449–459 . doi: 10.1007/s10086-013-1365-z

³⁴² Saito T, Okita Y, Nge TT, et al (2006) TEMPO-mediated oxidation of native cellulose: Microscopic analysis of fibrous fractions in the oxidized products. *Carbohydr Polym* 65:435–440 . doi: 10.1016/j.carbpol.2006.01.034

³⁴³ Gómez FN, Combariza MY, Blanco-Tirado C (2017) Facile cellulose nanofibrils amidation using a “one-pot” approach. *Cellulose* 24:717–730 . doi: 10.1007/s10570-016-1174-9

Table 5. Degree of oxidation (DO), degree of coupling after amidation process (DC), carboxylate content (σ) (by conductimetric titration and methylene blue adsorption (MBA)) and ζ -potential of Figue tow: untreated, delignified, TOCN, TOCN-R, TOCN-ODA and TOCN-R-ODA.

Material	Conductimetric titration				ζ -potential (mV)
	DO	DC	σ mmol COOH/g cellulose	C6-oxidized glucose units/ 25 glucose units	
Untreated tow	0.04	-	0.23	1	-
Delignified tow	0.07	-	0.43	~2	-
TOCN	0.29	-	1.57	~6	-56
TOCN-R	0.39	-	2.20	9	-64
TOCN-ODA	0.07	0.22	0.43	~2	-37
TOCN-R-ODA	0.06	0.33	0.40	~2	-31

ζ -potential values were -56 mV for TOCN and -64 mV for TOCN-P, confirming the increase in the oxidation degree as a consequence of the conversion of aldehyde groups to carboxylic acid. Both samples have a negative surface charge to form stable aqueous dispersion states. On the other hand, ζ -potential values decreased after amidation reaction to -36 mV and -31 mV for TOCN-ODA and TOCN-P-ODA, respectively. This results corroborate that a certain amount of carboxyl groups on the surface of TOCN and TOCN-R did not form covalent bonds with ODA and that the degree of substitution in TOCN-R-ODA was higher than in TOCN-ODA.

The hydrophobic character of TOCN-ODA and TOCN-R-ODA was checked by means of dispersion tests in non-polar organic solvents such as toluene. Figure 18a shows that when water was used as solvent, TOCN formed a stable translucent suspension for at least 3 months. However, precipitation was observed when it was dispersed in toluene (Figure 18b). The same results were observed for TOCN-P fibers. Stability of the charged nanofibrils can be explained by the sufficiently negative surface charge to form stable aqueous dispersions for a long period of time

due to the electrostatic repulsions, osmotic effects or a combination of both³⁴⁴. After chemical modification, TOCN-ODA and TOCN-P-ODA could not be dispersed in water and migrated to the surface of water (lower density) (Figure 18c). Conversely, these fibers formed a stable, homogeneous and turbid dispersion in a toluene solution (Figure 18d), demonstrated by the low transmittance as a result of light scattering by the amidated materials.

Figure 19. Images of (a) TOCN/water (b) TOCN/toluene (c) TOCN-ODA/water (d) TOCN-ODA/toluene and e) Light transmittance spectra of TOCN-(P) in water and TOCN-(P)-ODA in toluene dispersions.

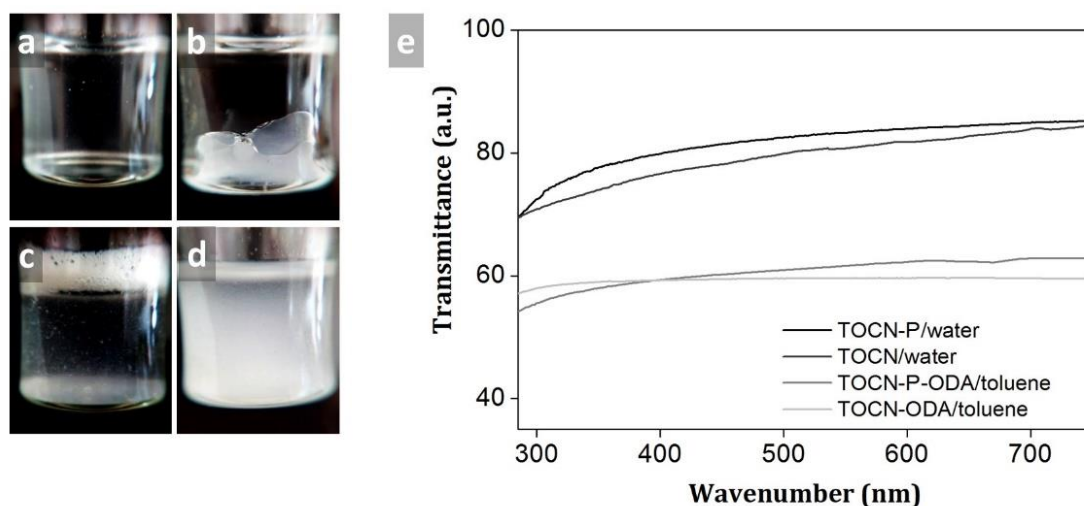


Figure 18e shows the light transmittance spectra of samples that formed stable dispersions in water and in toluene. TOCN and TOCN-P dispersions had high transmittances (above 70%) which depends on the wavelength and the nanofibrils' diameters³⁴⁵. As the light scattering is proportional to the cross-sectional area of the nanomaterial, for suspensions of nanofibers with greater diameter (TOCN-ODA and

³⁴⁴ Okita Y, Fujisawa S, Saito T, Isogai A (2011) TEMPO-Oxidized Cellulose Nanofibrils Dispersed in Organic Solvents. *Biomacromolecules* 12:518–522 . doi: 10.1021/bm101255x

³⁴⁵ Fukuzumi H (2012) Studies on structures and properties of TEMPO-oxidized cellulose nanofibril films. 博士論文 98

TOCN-P-ODA) the transmittance decreased around 55% as a consequence of the decrease in the intensity of the exit light due to the light scattering³⁴⁶.

Thermogravimetric analysis (TGA) was used to evaluate the thermal degradation process of cellulose samples, as shown in Figure 19. It has been proposed that the mechanism of thermal degradation of cellulose depends on the heating rate of pyrolysis. The process can opt for a dehydration pathway forming anhydrocellulose or for the depolymerization of cellulose producing mainly levoglucosan, which then forms tar above 400 °C³⁴⁷. Thermogravimetric curves (TG) and the corresponding derivative thermogravimetric (DTG) curves (Figure 19a and 19b) show three and two degradation steps for untreated and delignified Fique tow, respectively. The first degradation stage for both samples is shown in the region between 40 and 150 °C with a weight loss of 1.95% and 1.47% for untreated and delignified Fique tow, respectively, attributed to the dehydration of the fiber³⁴⁸. The second degradation temperature at 294 °C in untreated Fique tow, with a weight loss of 18.58%, represents the decomposition of hemicellulose into CO, CO₂, CH₄, CH₃COOH and HCOOH, among others³⁴⁹. The disappearance of this weight loss in the delignified Fique tow demonstrates the removal of hemicellulose as a result of AHP treatment³⁵⁰. The degradation temperature of cellulose between 320 °C and 400 °C is observed with a weight loss of 49.93% and 37.98% and maximum temperature at 355 °C and 340 °C for untreated and delignified Fique tow, respectively. The decrease in decomposition temperature in the delignified tow is due to the higher

³⁴⁶ Besbes I, Alila S, Boufi S (2011) Nanofibrillated cellulose from TEMPO-oxidized eucalyptus fibres: Effect of the carboxyl content. *Carbohydr Polym* 84:975–983 . doi: 10.1016/j.carbpol.2010.12.052

³⁴⁷ Lichtenstein K, Lavoine N (2017) Toward a deeper understanding of the thermal degradation mechanism of nanocellulose. *Polym Degrad Stab* 146:53–60 . doi: 10.1016/j.polymdegradstab.2017.09.018

³⁴⁸ Su Y, Du R, Guo H, et al (2015) Fractional pretreatment of lignocellulose by alkaline hydrogen peroxide: Characterization of its major components. *Food Bioprod Process* 94:322–330 . doi: 10.1016/j.fbp.2014.04.001

³⁴⁹ G.Maschio, C. Koufopoulos AL (1992) Pyrolysis, a promising route for biomass utilization. *Bioresour Technol* 42:219–231

³⁵⁰ Yang H, Yan R, Chen H, et al (2007) Characteristics of hemicellulose, cellulose and lignin pyrolysis. *Fuel* 86:1781–1788 . doi: 10.1016/j.fuel.2006.12.013

surface area of the fiber due to the delignification process which makes it more exposed during pyrolysis³⁵¹.

The degradation of unmodified TOCN and TOCN-P begin between 220 °C and 280 °C where the weight loss of 19.66% and 24.91% is attributed to the decarboxylation of sodium carboxylate groups and dehydration of the cellulose chains, followed by the formation of carbonyl compounds and beginning of the aromatization process³⁵². The next step is the collapse of the glycosidic structure between 280 °C and 350 °C with a weight loss of 27.06% and 24.01%, which involves the destruction of the crystalline and amorphous regions of the cellulose nanofibers, forming monomers of D-glucopyranose, further aromatization and decomposition of carbonyl compounds³⁵³. The presence of the carboxylate groups in TOCN and TOCN-R materials causes the degradation temperature of the cellulose to be lower (296 °C and 288 °C, respectively) than the degradation temperature of the starting material (340 °C for delignified Fique tow)³⁵⁴.

The TG results of TOCN-ODA and TOCN-P-ODA show higher thermal stability than TOCN and TOCN-P, indicating an increase in the hydrophobicity of nanofibers after their superficial chemical modification³⁵⁵. From an initial decomposition temperature of 296 °C and 288 °C for TOCN and TOCN-P, respectively, TOCN-ODA and TOCN-P-ODA were degraded at 335 °C and 348 °C, respectively. This effect can be

³⁵¹ Ovalle-Serrano SA, Blanco-Tirado C, Combariza MY (2018a) Exploring the composition of raw and delignified Colombian fique fibers, tow and pulp. *Cellulose* 25:151–165 . doi: 10.1007/s10570-017-1599-9

³⁵² Lichtenstein K, Lavoine N (2017) Toward a deeper understanding of the thermal degradation mechanism of nanocellulose. *Polym Degrad Stab* 146:53–60 . doi: 10.1016/j.polymdegradstab.2017.09.018

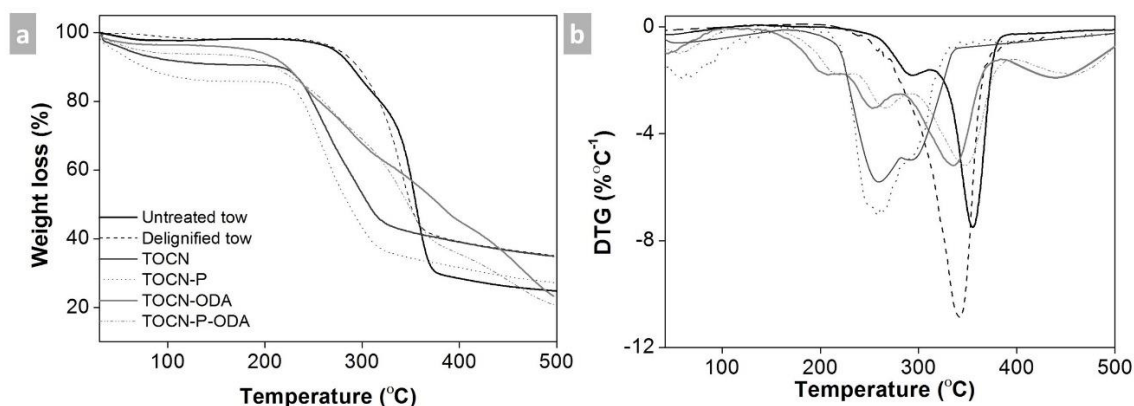
³⁵³ Fukuzumi H, Saito T, Okita Y, Isogai A (2010) Thermal stabilization of TEMPO-oxidized cellulose. *Polym Degrad Stab* 95:1502–1508 . doi: 10.1016/j.polymdegradstab.2010.06.015

³⁵⁴ Ovalle-Serrano SA, Gómez FN, Blanco-Tirado C, Combariza MY (2018b) Isolation and characterization of cellulose nanofibrils from Colombian Fique decortication by-products. *Carbohydr Polym* 189:169–177 . doi: 10.1016/j.carbpol.2018.02.031

³⁵⁵ Cunha AG, Freire CSR, Silvestre AJD, et al (2007) Highly hydrophobic biopolymers prepared by the surface pentafluorobenzoylation of cellulose substrates. *Biomacromolecules* 8:1347–1352 . doi: 10.1021/bm0700136

explained by the ability of the long chains of ODA to organize themselves on the surface of the TOCN providing them of a kind of shell that protects them during the heat treatment³⁵⁶. A higher thermal stability was observed for TOCN-P-ODA than for TOCN-ODA which can be explained by the greater degree of coupling after the amidation process as demonstrated before.

Figure 20. Thermogravimetical behavior of Figue tow: untreated, delignified, TOCN, TOCN-P, TOCN-ODA and TOCN-P-ODA. (a) TG and (b) DTG curves.



Contact angle (CA) refers to the angle formed between a solid surface and a liquid when they interact. The CA value depends on the cohesive forces of the water droplet and the adhesive forces between the outline of the contact surface and the liquid³⁵⁷. When the adhesive forces prevail over the cohesive forces, AC value varies between 0° and 90° and the surface is classified as hydrophilic. The high hydrophilic nature of the TOCN and TOCN-P, due to the -OH and -COOH groups (with higher -COOH content in TOCN-P), can be observed in the Figures 3.9a and 3.9b³⁵⁸. The

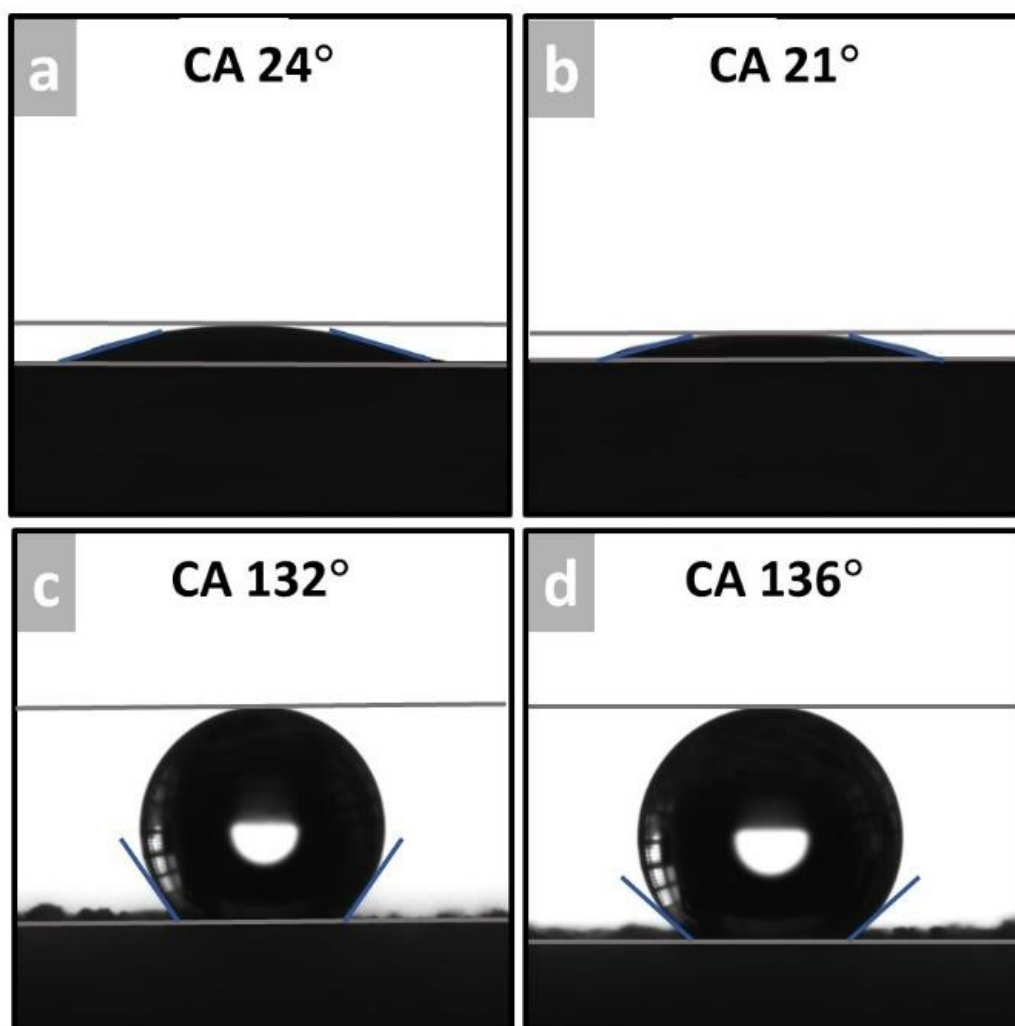
³⁵⁶ Missoum K, Bras J, Belgacem MN (2012) Organization of aliphatic chains grafted on nanofibrillated cellulose and influence on final properties. *Cellulose* 19:1957–1973 . doi: 10.1007/s10570-012-9780-7

³⁵⁷ Benkaddour A, Journoux-Lapp C, Jradi K, et al (2014) Study of the hydrophobization of TEMPO-oxidized cellulose gel through two routes: amidation and esterification process. *J Mater Sci* 49:2832–2843 . doi: 10.1007/s10853-013-7989-y

³⁵⁸ Benkaddour A, Journoux-Lapp C, Jradi K, et al (2014) Study of the hydrophobization of TEMPO-oxidized cellulose gel through two routes: amidation and esterification process. *J Mater Sci* 49:2832–2843 . doi: 10.1007/s10853-013-7989-y

high surface energy of both samples was demonstrated by a low contact angle (24° and 21° , respectively). Thanks to the increase of hydrophilicity in the surface of the TOCN after its complete oxidation, post-oxidation can be considered an interesting path towards the synthesis of superhydrophilic cellulose nanomaterials that have recently caused great impact in the textile industry and packaging area³⁵⁹.

Figure 21. Contact angle for a) TOCN, b) TOCN-P, c) TOCN-ODA and d) TOCN-P-ODA films.



³⁵⁹ Ibid.

On the other hand, a surface is classified as hydrophobic if the CA value goes between 90° and 180°. As shown in Figures 3.9c and 3.9d, the contact angle values of the TOCN-ODA and TOCN-P-ODA increased to 132° and 136°, respectively. This increase in hydrophobicity is attributed to the nonpolar octadecylamine alkyl chains that were coupled to TOCN and TOCN-P. This increase is more evident in TOCN-P-ODA due to the higher graft efficiency (82%) as demonstrated by conductimetric titration. However, these results could be affected by the characteristic surface porosity of the amidated samples contributing to a slightly increase in the CA values.

3.5 CONCLUSIONS

Along this chapter, it was studied the effect of post-oxidation in TOCN extracted from delignified Fique tow and its hydrophobization by means of a 'one-pot' amidation reaction. In agreement with previous chapters, AHP treatment was used to increase the efficiency in the TOCN extraction. The resulting TOCN had a web-like structure with high values of carboxylate content. The high carboxylate content was a key factor in the coupling of ODA on the surface of TOCN to form the amidated product. It showed that the more hydrophilic the starting material (TOCN-P), the more hydrophobic the amidated product (TOCN-P-ODA). Finally, the success of the amidation reaction was confirmed by spectroscopic, microscopic and thermal analysis techniques. The transition from hydrophilic to hydrophobic character of the synthesized materials was also evaluated by the evolution of the percentage of transmittance by means of UV-vis measurements for nanocellulose suspensions in different types of solvents and contact angle measurements.

4. PREPARATION OF FUNCTIONAL HYDRO/AEROGELS FROM COLOMBIAN FIQUE TOW CELLULOSE NANOFIBRILS

4.1 ABSTRACT

In this chapter, we report an environmentally benign 'one-pot' method for the production of functional hydro/aerogels by synthesizing silver nanoparticles in suspensions of TEMPO-oxidized cellulose nanofibers (TOCN) extracted from Fique tow, using only water as solvent. Hydrogels were prepared by adding AgNO₃ aqueous solutions into TOCN suspensions without stirring. The freeze-drying of the resultant hydrogels produced aerogels. Reaction parameters such as temperature and COOH:AgNO₃ molar ratios in the formation of hydrogels are studied. The morphology, chemical structure, crystallinity and thermal stability of TOCN hydro/aerogels were studied using UV-Vis, FESEM, IR-ATR, XRD and TGA. Results showed that higher AgNO₃ amounts increased the amount of silver nanoparticles and added some stability to the hydrogel. Raising the temperature at high values decreased the reaction time but produced some degradation and instability to the hydrogel.

4.2 INTRODUCTION

Cellulose, the most abundant natural polymer on Earth, is produced by many organism including plants, algae, bacteria and some animals (tunicate). As other polysaccharides, cellulose is a promising source of raw material for the synthesis of hydrogels due to its gelation ability. Additionally, it has attracted much attention thanks to its biodegradability, renewability, biocompatibility and high mechanical and thermal properties, resulting in hydrogels with high stiffness, great thermal stability,

high resistance upon solvent exchange of medium, among others, features hard to get with synthetic polymer gels or even other polysaccharide gels^{360 361}.

Cellulose can be extracted from crop residues and agricultural wastes, such as oil palm empty fruit bunches, rice husk, flax, Figue tow, and many more. It can be isolated into well-defined micro- and nano-scale structures known as nanocellulose, defined as cellulose particles with widths $<100\text{ nm}$ ^{362 363 364}. Nanocelluloses combine intrinsic properties of cellulose and specific features of nanoscale materials, having outstanding mechanical and thermal properties, biorenewability, light weight, large surface area-to-volume ratio and surface reactivity, which make them excellent nano-building blocks for ultra-light and highly porous hydro- and aerogels³⁶⁵. Nanocellulose is a general term that represents the main products from cellulose: cellulose nanocrystals (CNC) and cellulose nanofibers (CNF)³⁶⁶. CNC, shorter than CNF, are rod-like particles with a highly crystalline structure and can be used as reinforcement of various polymer composites owing to their high modulus. On the other hand, CNF commonly have a higher aspect ratio and ductility, providing an excellent resource for the preparation of hydro- and aerogels³⁶⁷.

³⁶⁰ Teow YH, Kam LM, Mohammad AW (2018) Synthesis of cellulose hydrogel for copper (II) ions adsorption. *J Environ Chem Eng* 6:4588–4597 . doi: 10.1016/j.jece.2018.07.010

³⁶¹ Isobe N, Komamiya T, Kimura S, et al (2018) Cellulose hydrogel with tunable shape and mechanical properties: From rigid cylinder to soft scaffold. *Int J Biol Macromol* 117:625–631 . doi: 10.1016/j.ijbiomac.2018.05.071

³⁶² Lee B-M, Jeun J-P, Kang P-H, et al (2017) Isolation and characterization of nanocrystalline cellulose from different precursor materials. *Fibers Polym* 18:272–277 . doi: 10.1007/s12221-017-6548-6

³⁶³ Isogai A, Bergström L (2018) Preparation of cellulose nanofibers using green and sustainable chemistry. *Curr Opin Green Sustain Chem* 12:15–21 . doi: 10.1016/j.cogsc.2018.04.008

³⁶⁴ Teow YH, Kam LM, Mohammad AW (2018) Synthesis of cellulose hydrogel for copper (II) ions adsorption. *J Environ Chem Eng* 6:4588–4597 . doi: 10.1016/j.jece.2018.07.010

³⁶⁵ Gu J, Hu C, Zhang W, Dichiaro AB (2018) Reagentless preparation of shape memory cellulose nanofibril aerogels decorated with Pd nanoparticles and their application in dye discoloration. *Appl Catal B Environ* 237:482–490 . doi: 10.1016/j.apcatb.2018.06.002

³⁶⁶ Malucelli LC, Lacerda LG, Dziedzic M, da Silva Carvalho Filho MA (2017) Preparation, properties and future perspectives of nanocrystals from agro-industrial residues: a review of recent research. *Rev Environ Sci Bio/Technology* 16:131–145 . doi: 10.1007/s11157-017-9423-4

³⁶⁷ Dong H, Snyder JF, Tran DT, Leadore JL (2013a) Hydrogel, aerogel and film of cellulose nanofibrils functionalized with silver nanoparticles. *Carbohydr Polym* 95:760–767 . doi: 10.1016/j.carbpol.2013.03.041

Inorganic nanoparticles have unique physical and chemical properties, with potential applications in electrical, optical and biomedical fields. However, they are unstable on their own due to their large active surface area, leading to self-aggregation and limiting their usage³⁶⁸. The typical synthesis of inorganic nanoparticles involves the use of capping agent, reducing agent, and reaction solvents, usually including toxic chemicals making necessary to reduce or eliminate the use of hazardous materials³⁶⁹. In this regard, preparing inorganic nanoparticles in CNF hydrogels is a great alternative to overcome these drawbacks.

In recent years, CNF hydro and aerogels have attracted much attention as matrixes in the synthesis of inorganic nanoparticles. Researchers have been reporting their use as both reducing agent and stabilizer for the synthesis of palladium, silver, gold and other metal nanoparticles³⁷⁰. CNF hydrogels are a three-dimensional network structure with functional groups (-COOH, -OH) and electron-rich oxygen atoms capable of interactions with metal ions. Besides, they are characterized by high hydrophilicity, insolubility, and high swelling ratio, facilitating the incorporation and dispersion of metal nanoparticles^{371 372}. It has been reported that hydroxyl groups as well as sulfate ester and/or carboxylate groups are a key factor in the reduction of metal species and are able to help controlling the growth of nanoparticles. The resultant bionanocomposite (CNF hydrogels-Ag nanoparticles) is reported to have a more efficient catalytic performance thanks to the improved diffusion of reactant through the matrix. Furthermore, morphology and size of metal nanoparticles might

³⁶⁸ Tang L, Tang F, Li M, Li L (2018) Facile synthesis of Ag@AgCl-contained cellulose hydrogels and their application. *Colloids Surfaces A Physicochem Eng Asp* 553:618–623 . doi: 10.1016/j.colsurfa.2018.06.016

³⁶⁹ Gu J, Hu C, Zhang W, Dichiara AB (2018) Reagentless preparation of shape memory cellulose nanofibril aerogels decorated with Pd nanoparticles and their application in dye discoloration. *Appl Catal B Environ* 237:482–490 . doi: 10.1016/j.apcatb.2018.06.002

³⁷⁰ Ibid.

³⁷¹ Zhu C, Xue J, He J (2009) Controlled In-Situ Synthesis of Silver Nanoparticles in Natural Cellulose Fibers Toward Highly Efficient Antimicrobial Materials. *J Nanosci Nanotechnol* 9:3067–3074 . doi: 10.1166/jnn.2009.212

³⁷² Teow YH, Kam LM, Mohammad AW (2018) Synthesis of cellulose hydrogel for copper (II) ions adsorption. *J Environ Chem Eng* 6:4588–4597 . doi: 10.1016/j.jece.2018.07.010

be controlled by varying experimental parameters such as amount of reactants, functional groups in CNF, reaction time, among others. These features make CNF hydro- and aerogels great templates for metal nanoparticles preparation^{373 374}.

Cellulose hydro- and aerogels are prepared by direct cellulose dissolution. Cellulose hydrogels are usually fabricated from a cellulose solution through physical cross-linking due to its facility to form hydrogen bonding linked networks. Preparation of cellulose aerogels consist in a solvent exchange and a drying process after cellulose dissolution. However, cellulose dissolution requires uncommon and environmentally unfriendly solvents such as alkali/urea or lithium chloride/dimethylacetamide solutions³⁷⁵. On the other hand, hydro- and aerogels preparation from CNF is an effective alternative to these drawbacks. The charged interface of CNF is highly useful in their use as building blocks of hydro- or aerogels. The charged interface is used to stabilize the reinforcing agent by improving the dispersibility of the filler in the matrix and to promote through electrostatic interactions or hydrogen bonds between gel components to lower the effective threshold for CNF gelation³⁷⁶.

CNF hydro- and aerogels can be prepared by a wide range of processing methods. Hydrogels are commonly prepared by free radical polymerization of a CNF/ polymer precursor solution by chemically crosslinking the main polymer component around the nanocellulose. Hydrogels from TEMPO-oxidized cellulose nanofibers (TOCN) can also be prepared by the addition of strong acids to protonate the carboxylate groups on the TOCN or even by mixing the TOCN suspension, generating

³⁷³ Tang L, Tang F, Li M, Li L (2018) Facile synthesis of Ag@AgCl-contained cellulose hydrogels and their application. *Colloids Surfaces A Physicochem Eng Asp* 553:618–623 . doi: 10.1016/j.colsurfa.2018.06.016

³⁷⁴ Gu J, Hu C, Zhang W, Dichiara AB (2018) Reagentless preparation of shape memory cellulose nanofibril aerogels decorated with Pd nanoparticles and their application in dye discoloration. *Appl Catal B Environ* 237:482–490 . doi: 10.1016/j.apcatb.2018.06.002

³⁷⁵ Dong H, Snyder JF, Tran DT, Leadore JL (2013a) Hydrogel, aerogel and film of cellulose nanofibrils functionalized with silver nanoparticles. *Carbohydr Polym* 95:760–767 . doi: 10.1016/j.carbpol.2013.03.041

³⁷⁶ De France KJ, Hoare T, Cranston ED (2017) Review of Hydrogels and Aerogels Containing Nanocellulose. *Chem Mater* 29:4609–4631 . doi: 10.1021/acs.chemmater.7b00531

impressive properties such as injectability and self-healing. Regarding CNF aerogels, procedures for their fabrication involve freeze-drying or supercritical CO₂ drying from CNF suspensions. In this case, the aqueous phase is replaced with air and the porosities can get as high as 99.5%. Aerogels and hydrogels are then somehow interconvertible since aerogels can be rehydrated to produce hydrogels and hydrogels can be freeze-dried to produce aerogels^{377 378 379}

The intrinsic properties of NFC hydro- and aerogels functionalized with silver nanoparticles justify its utilization in many applications, including use in food, cosmetic, pharmaceutical and material industry³⁸⁰. However, petroleum-based raw material are still the most used in the synthesis of hydro- and aerogels³⁸¹. In addition, the development of greener methods to produce metal nanoparticles is still a task at hand.

This chapter deals with an environmentally friendly approach to functionalize highly porous TOCN (extracted from Figue tow) hydrogels with silver nanoparticles. We propose a 'one-pot' green synthesis method with only water as solvent where TOCN substitutes both capping and reducing agents in silver nanoparticle synthesis, preventing their aggregation while maintaining its reactivity. Additionally, a TOCN aerogel is prepared by freeze-drying the TOCN hydrogel. The functional hydro- and aerogels produced were characterized by means of UV-Vis spectroscopy, field emission scanning electron microscopy (FESEM), attenuated total reflectance

³⁷⁷ Dong H, Snyder JF, Tran DT, Leadore JL (2013a) Hydrogel, aerogel and film of cellulose nanofibrils functionalized with silver nanoparticles. *Carbohydr Polym* 95:760–767 . doi: 10.1016/j.carbpol.2013.03.041

³⁷⁸ De France KJ, Hoare T, Cranston ED (2017) Review of Hydrogels and Aerogels Containing Nanocellulose. *Chem Mater* 29:4609–4631 . doi: 10.1021/acs.chemmater.7b00531

³⁷⁹ Yao Q, Fan B, Xiong Y, et al (2017) Stress sensitive electricity based on Ag/cellulose nanofiber aerogel for self-reporting. *Carbohydr Polym* 168:265–273 . doi: 10.1016/j.carbpol.2017.03.089

³⁸⁰ Dong H, Snyder JF, Tran DT, Leadore JL (2013a) Hydrogel, aerogel and film of cellulose nanofibrils functionalized with silver nanoparticles. *Carbohydr Polym* 95:760–767 . doi: 10.1016/j.carbpol.2013.03.041

³⁸¹ Teow YH, Kam LM, Mohammad AW (2018) Synthesis of cellulose hydrogel for copper (II) ions adsorption. *J Environ Chem Eng* 6:4588–4597 . doi: 10.1016/j.jece.2018.07.010

infrared spectroscopy (ATR-IR), X-ray diffraction (XRD) and thermogravimetric analyses (TGA).

4.3 EXPERIMENTAL

4.3.1 Materials. Fique tow (*Furcraea macrophylla*) was collected from Fique leaves decortication in the rural area of San Joaquín, Santander, Colombia. 2,2,6,6-Tetramethyl-piperidin-1-oxyl (TEMPO) was purchased from Sigma Aldrich (Saint Louis, MO, USA) and sodium hypochlorite (NaClO, 15%) and silver nitrate (AgNO₃) from Carlo Erba Reagents (Milan, Italy). Sodium bromide (NaBr), hydrogen peroxide (H₂O₂), sodium hydroxide (NaOH), ethanol (EtOH) and hydrochloric acid (HCl, 37%) were purchased from Merck (Darmstadt, Germany). All chemical reagents were used with no further purification. Aqueous solutions and suspensions were prepared with ultrapure water (18 MΩ·cm @ 25 °C).

4.3.2 Fique tow treatment, delignification and TOCN extraction. We followed the procedures discussed in Chapters 1 and 2. Fique tow was immersed in an ultrasound bath (Bransonic CPX3800, 40 kHz, 130 Watt) with distilled water for 60 min at 40 °C to remove impurities. Fique tow was then dried in an oven at 60 °C for 24 h³⁸². To remove hemicellulose and lignin, untreated Fique tow was cut into short lengths (1 cm) and 8 g were immersed in 100 mL of a H₂O₂ solution (10% w/w) at pH 11.5. The mixture was kept in an ultrasonic bath for 2 h at 70 °C. Then, delignified tow was washed by filtration with distilled water and dried at 60 °C for 24 h³⁸³.

For TOCN extraction, 1 g of delignified Fique tow was suspended in 100 mL of water. TEMPO (16 mg) and sodium bromide (100 mg) were dissolved in distilled water and added slowly to the suspension. Then, NaClO (0.037 mol) was added dropwise to

³⁸² Ovalle-Serrano SA, Blanco-Tirado C, Combariza MY (2018a) Exploring the composition of raw and delignified Colombian fique fibers, tow and pulp. *Cellulose* 25:151–165 . doi: 10.1007/s10570-017-1599-9

³⁸³ Ibid.

start the oxidation reaction which was carried out in an ultrasonic bath (Bransonic CPX3800, 40 kHz, 130 Watt), keeping the pH at 10.5 with a 0.5 N NaOH solution at room temperature. When no more NaOH was needed the reaction was stopped by the addition of ethanol. The oxidized cellulose was centrifuged several times at 4700 rpm for 15 min with ultrapure water until neutral pH to remove unreacted chemicals and separate the TOCN. Fique tow TOCN aqueous suspensions of 0.5% wt were mechanically disintegrated by sonication in an Ultrasonic Processor (Sonics vibra-cell VC750, 20 kHz, 750 Watt) for 10 min (1:1 pulses) at 40% amplitude. Finally, the product was centrifuged again under the aforementioned conditions³⁸⁴

After TEMPO-mediated regioselective oxidation of Fique tow, the superficial carboxyl groups in the TOCN are as a sodium carboxylate salt (-COONa). To convert the sodium carboxylates into the free acid form (-COOH) a HCl solution (0.5 N) was added to an aqueous dispersion of Fique tow TOCN (0.5% wt.) until pH 2 under magnetic stirring during 0.5 h. After ion exchange the solution of Fique tow TOCN became a translucent gel by the conversion of the -COONa groups to -COOH. To remove the excess acid, the gel was washed until pH 4 with distilled water, using vacuum filtration, and then it was re-dispersed in water³⁸⁵.

4.3.3 Preparation of hydro/aerogels. Functional hydrogels were prepared by adding a AgNO₃ aqueous solution into a 0.8% wt. TOCN (1.6 mmol -COOH/g cellulose) aqueous suspension. Initially, 10 mL of a recently degasified and sonicated TOCN suspension were put in a test tube and 5 mL of deionized water were added dropwise on top, without stirring. Then, 5 mL of the AgNO₃ aqueous solution was added dropwise along the sidewall of the test tube into the TOCN suspension without stirring. The COOH:AgNO₃ molar ratios used in the hydrogel

³⁸⁴ Ovalle-Serrano SA, Gómez FN, Blanco-Tirado C, Combariza MY (2018b) Isolation and characterization of cellulose nanofibrils from Colombian Fique decortication by-products. *Carbohydr Polym* 189:169–177 . doi: 10.1016/j.carbpol.2018.02.031

³⁸⁵ Fujisawa S, Okita Y, Fukuzumi H, et al (2011) Preparation and characterization of TEMPO-oxidized cellulose nanofibril films with free carboxyl groups. *Carbohydr Polym* 84:579–583 . doi: 10.1016/j.carbpol.2010.12.029

formation were 1:1, 1:2 and 1:3, to ensure a complete saturation of the carboxylate groups with Ag⁺ ions in the TOCN. The same methodology was followed at room temperature and at 60 °C for 8 days and 28 hours, respectively, to determine the role of temperature in the reaction time and in nanoparticles formation. Finally, the functional hydrogel was washed thoroughly with deionized water to remove the unattached Ag⁺ ions³⁸⁶. Functional aerogels were produced by the freeze-drying of functional hydrogels. In this process, hydrogels were put in a freezer at -15 °C for 4 hours and then were lyophilized in a Labconco FreeZone Plus 6 under vacuum (0.060 mBar) at -83 °C for 24 hours.

4.3.4 Characterization. Absorbance measurements from 200 to 600 nm using a Shimadzu UV-Vis spectrophotometer (UV-2401PC) were used to determine the presence of silver nanoparticles in the hydrogels. Field emission scanning electron microscopy (FESEM) images were taken on a FEI QUANTA FEG 650 (Oregon, USA) instrument equipped with a large field detector. Hydrogels were air-dried and freeze-dried (aerogel) and coated with a thin layer of gold (around 20 nm) before imaging and the micrographs were taken at 10 kV. For attenuated total reflectance (ATR-IR) measurements a Bruker Tensor 27 (Billerica, MA) FTIR instrument equipped with a Platinum Diamond ATR unit A225/Q (Billerica, MA) was used at a resolution of 2 cm⁻¹ and 32 scans were accumulated for each spectrum. X-Ray diffraction (XRD) analyses were performed on a Bruker D8 DISCOVER X-ray diffractometer (Billerica, MA) with a DaVinci geometry, using a CuK α 1 radiation source (40 kV and 30 mA), an area detector VANTEC-500, and a poly(methyl methacrylate) sample holder. Thermogravimetric (TGA) analyses of freeze-dried samples (10 mg) were investigated using a STA 449 F5 Jupiter instrument (São Paulo, Brazil) under nitrogen flow (50 mL/min). The samples were scanned from room temperature up to 500 °C at a heating rate of 10 °C/min. ζ potential was

³⁸⁶ Dong H, Snyder JF, Tran DT, Leadore JL (2013a) Hydrogel, aerogel and film of cellulose nanofibrils functionalized with silver nanoparticles. *Carbohydr Polym* 95:760–767 . doi: 10.1016/j.carbpol.2013.03.041

measured with a Malvern Zetasizer Nano ZS90 instrument (Worcestershire, UK), equipped with a capillary cell 1070.

4.4 RESULTS AND DISCUSSION

As stated in the previous chapters, raw Fique tow (Figure 20a) is characterized by a light yellow color, due to its lignin content. However, the alkaline hydrogen peroxide process removes lignin and hemicelluloses, bleaching the material to a white color (Figure 20b). This process takes place in two stages: 1) bleaching via formation of the hydroperoxide ion, HOO^- , which transform chromophoric groups in lignin into nonchromophoric species, and 2) delignification through generation of hydroxyl ($\text{HO}\cdot$) and superoxide anion ($\text{O}_2^-\cdot$) radicals, some of the most important species in oxidation reactions³⁸⁷, which attack lignin side-chains and produce low-molecular-weight and water-soluble oxidation products^{388 389 390}.

Delignified Fique tow was used for the production of CNF by the addition of NaClO (primary oxidant) to aqueous suspensions of cellulose containing the 2,2,6,6-tetramethylpiperidine-1-oxyl radical (TEMPO) and NaBr (co-oxidant) under basic conditions. The TEMPO-mediated oxidation of CNF produces TEMPO-oxidized cellulose nanofibers (TOCN) by the selective oxidation to carboxylate groups of hydroxyl groups of C6 of the monomeric D-anhydroglucose unit of cellulose³⁹¹. The presence of $-\text{COO}^-$ groups on the surface of cellulose inhibits hydrogen bond

³⁸⁷ Xiang Q, Lee YY (2000) Oxidative Cracking of Precipitated Hardwood Lignin by Hydrogen Peroxide. *Appl Biochem Biotechnol* 84–86:153–162 . doi: 10.1385/ABAB:84-86:1-9:153

³⁸⁸ Sun RC, Fang JM, Tomkinson J (2000) Delignification of rye straw using hydrogen peroxide. *Ind Crops Prod* 12:71–83 . doi: 10.1016/S0926-6690(00)00039-X

³⁸⁹ Perez-Pimienta JA, Poggi-Varaldo HM, Ponce-Noyola T, et al (2016) Fractional pretreatment of raw and calcium oxalate-extracted agave bagasse using ionic liquid and alkaline hydrogen peroxide. *Biomass and Bioenergy* 91:48–55 . doi: 10.1016/j.biombioe.2016.05.001

³⁹⁰ Dutra ED, Santos FA, Alencar BRA, et al (2017) Alkaline hydrogen peroxide pretreatment of lignocellulosic biomass: status and perspectives. *Biomass Convers Biorefinery*. doi: 10.1007/s13399-017-0277-3

³⁹¹ Saito T, Okita Y, Nge TT, et al (2006) TEMPO-mediated oxidation of native cellulose: Microscopic analysis of fibrous fractions in the oxidized products. *Carbohydr Polym* 65:435–440 . doi: 10.1016/j.carbpol.2006.01.034

formation between CNF by Coulombic repulsion. Thus, the higher the amount of carboxylate groups in cellulose, the higher the stability of the TOCN suspension. The resultant TOCN suspensions (Figure 20c) are typically translucent gels, highly hydrophilic and insoluble in polar aprotic organic solvents^{392 393 394 395}. Aqueous TOCN suspensions can be turned into hydrogel-like structures by converting carboxylate groups to their carboxylic form. The $-\text{COO}^-\text{Na}^+$ units are transformed into $-\text{COOH}$ by ion exchange using HCl. Thus, the fluid TOCN suspension becomes a homogeneous, non-flowable and translucent gel (Figure 21b). The increase in viscosity of TOCN suspensions is probably due to the formation of intra- and inter-nanofibril hydrogen bonds, making TOCN-COOH less hydrophilic than TOCN-COO⁻Na⁺³⁹⁶. Figure 20d is a picture of TOCN aerogels, prepared by the freeze-drying of TOCN suspensions. In the drying process, TOCN aerogels take the shape of the vessel used during the lyophilization.

³⁹² Saito T, Isogai A (2004) TEMPO-Mediated Oxidation of Native Cellulose. The Effect of Oxidation Conditions on Chemical and Crystal Structures of the Water-Insoluble Fractions. *Biomacromolecules* 5:1983–1989 . doi: 10.1021/bm0497769

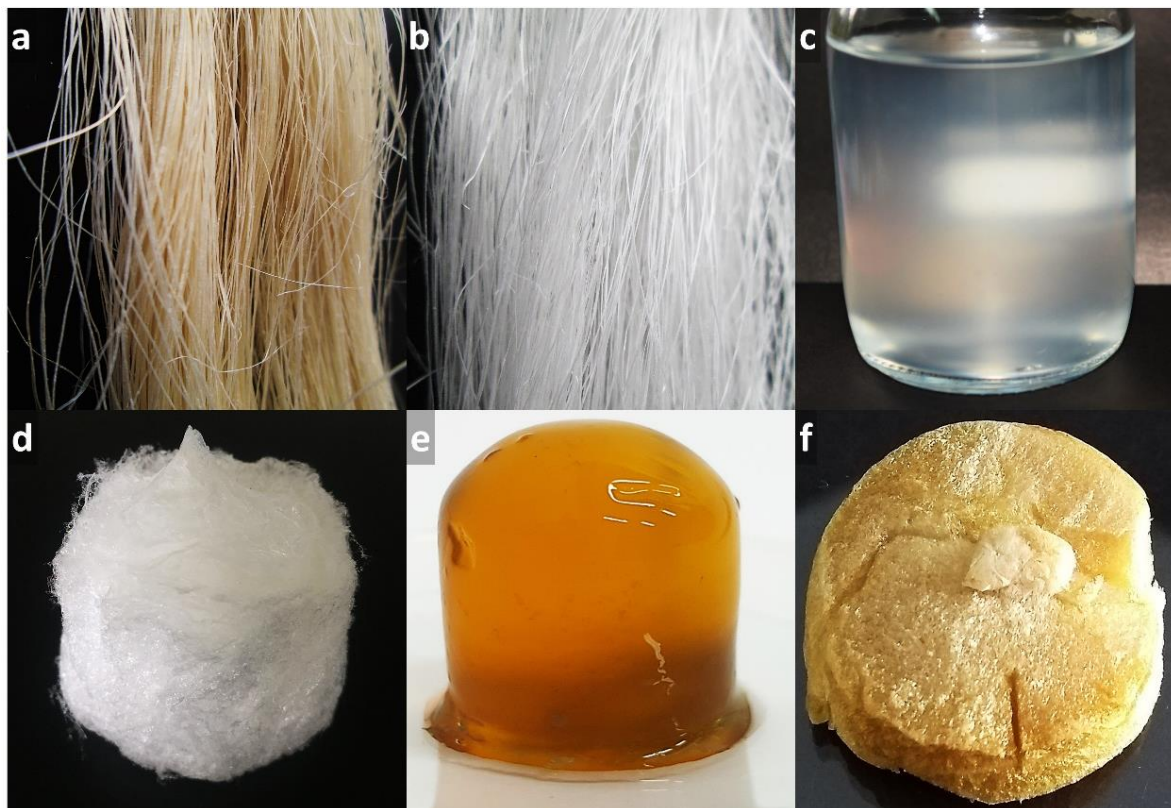
³⁹³ Saito T, Okita Y, Nge TT, et al (2006) TEMPO-mediated oxidation of native cellulose: Microscopic analysis of fibrous fractions in the oxidized products. *Carbohydr Polym* 65:435–440 . doi: 10.1016/j.carbpol.2006.01.034

³⁹⁴ Tang Z, Li W, Lin X, et al (2017) TEMPO-Oxidized cellulose with high degree of oxidation. *Polymers (Basel)* 9:3–4 . doi: 10.3390/polym9090421

³⁹⁵ Hamou K Ben, Kaddami H, Dufresne A, et al (2018) Impact of TEMPO-oxidization strength on the properties of cellulose nanofibril reinforced polyvinyl acetate nanocomposites. *Carbohydr Polym* 181:1061–1070 . doi: 10.1016/j.carbpol.2017.11.043

³⁹⁶ Fujisawa S, Okita Y, Fukuzumi H, et al (2011) Preparation and characterization of TEMPO-oxidized cellulose nanofibril films with free carboxyl groups. *Carbohydr Polym* 84:579–583 . doi: 10.1016/j.carbpol.2010.12.029

Figure 22. Optical images of (a) raw and (b) delignified Figue tow, (c) TOCN aqueous suspension, (d) TOCN aerogel, (e) TOCN-Ag NPs hydrogel and (f) TOCN-Ag NPS aerogel.



Addition of the AgNO_3 aqueous solution to the TOCN suspension resulted in a strong yellow-like colored gel with a shape defined by the vessel used for the reaction (Figure 20e). The yellow-like color indicates the presence of Ag NPs³⁹⁷. Unlike TOCN suspensions (Figure 20c), the TOCN-Ag NPS hydrogels had no fluidity and were strong enough to be picked up and stay in a freestanding form³⁹⁸. The freeze-drying of the TOCN-Ag NPS hydrogel produced a yellow-like TOCN-Ag NPS aerogel (Figure 20f). The aerogel had a cylindrical form, shaped by the vessels used during

³⁹⁷ Dong H, Snyder JF, Tran DT, Leadore JL (2013a) Hydrogel, aerogel and film of cellulose nanofibrils functionalized with silver nanoparticles. *Carbohydr Polym* 95:760–767 . doi: 10.1016/j.carbpol.2013.03.041

³⁹⁸ Dong H, Snyder JF, Williams KS, Andzelm JW (2013b) Cation-Induced Hydrogels of Cellulose Nanofibrils with Tunable Moduli. *Biomacromolecules* 14:3338–3345 . doi: 10.1021/bm400993f

the freeze-drying process. As reported for other CNF-NPs aerogels, it had a porous internal structure with a rough external surface³⁹⁹.

Gu et al.⁴⁰⁰ have reported that in TOCN suspensions not only hydroxyl groups play a key role in the reduction of Ag⁺ ions process, but also the aldehyde groups produced after the TEMPO-mediated oxidation. To check this information, we repeated the post-oxidation process described in Chapter 3 and used the post-oxidized TOCN suspension for the synthesis of Ag NPs with a molar ratio of COOH:AgNO₃ 1:2 at 60 °C. As explained before, we increased the carboxylate content from 1.6 to 2.2 mmol COOH/g cellulose with the post-oxidation reaction. However, after 28 hours of reaction the suspension was just starting to change to a grey-brownish color with no obvious gelification, probably indicating the formation of Ag in bulk and not Ag NPs. This is in agreement with the reported by Gu et al.⁴⁰¹ and might indicate that aldehyde groups are essential in the synthesis of silver NPs in TOCN suspension at least when the procedure used in this work is followed. Additionally, the post-oxidation process might oxidize some reducing ends hemiacetal groups in TOCN, decreasing its redox potential^{402 403}. In this way, the formation mechanism of Ag NPs might works as proposed in Figure 4.2. TOCN-Ag NPS hydrogels were produce by diffusion of metal cations Ag⁺ into the TOCN suspension. The high dispersion, high surface area and functional groups in the surface (hydroxyl, aldehyde and carboxylate groups), make the TOCN suspensions

³⁹⁹ Gu J, Hu C, Zhang W, Dichiara AB (2018) Reagentless preparation of shape memory cellulose nanofibril aerogels decorated with Pd nanoparticles and their application in dye discoloration. *Appl Catal B Environ* 237:482–490 . doi: 10.1016/j.apcatb.2018.06.002

⁴⁰⁰ Ibid.

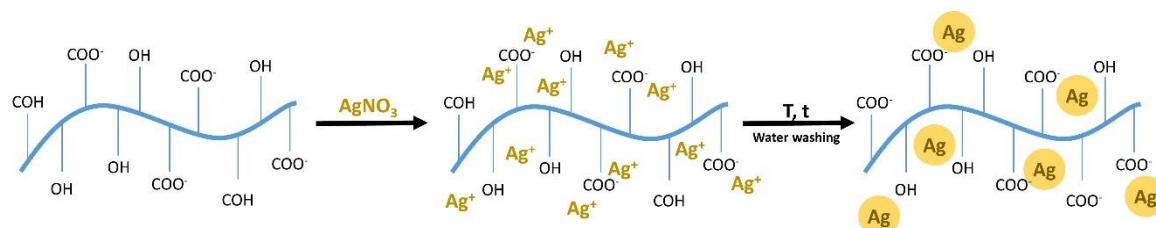
⁴⁰¹ Ibid.

⁴⁰² Isogai T, Saito T, Isogai A (2010) TEMPO electromediated oxidation of some polysaccharides including regenerated cellulose fiber. *Biomacromolecules* 11:1593–1599 . doi: 10.1021/bm1002575

⁴⁰³ Mishra SP, Manent A-S, Chabot B, Daneault C (2012) The Use of Sodium Chlorite in Post-Oxidation of TEMPO-Oxidized Pulp: Effect on Pulp Characteristics and Nanocellulose Yield. *J Wood Chem Technol* 32:137–148 . doi: 10.1080/02773813.2011.624666

suitable reducing and stabilizing agents for Ag^+ ions to form Ag NPs^{404 405 406 407}. In the synthesis of Ag NPs in TOCN suspensions, Ag^+ ions are attached to negatively charged groups (carboxylate groups) in TOCN surface via ion-dipole interactions to be subsequently reduced to Ag NPs by aldehyde and some hydroxyl groups. Finally, carboxylate groups and the newly formed ketone groups may immobilize and stabilize the Ag NPs by electrostatic interactions^{408 409}.

Figure 23. Scheme for the synthesis of Ag NPs in TOCN suspensions.



Fuente: Adapted from Ogundare and van Zyl 2018 (Ogundare and van Zyl 2018).

Degasification and sonication were a key step in the hydrogel preparation. Stored TOCN suspensions form aggregates in time, despite the electrostatic repulsion caused by carboxylate groups. When no-sonicated TOCN suspensions were used in the synthesis of silver nanoparticles, there was no formation of hydrogel-like structures. Nevertheless, sonication produced the disentanglement and fragmentation of aggregate fibers in TOCN suspension, increasing the surface area

⁴⁰⁴ Cao X, Ding B, Yu J, Al-Deyab SS (2013) In situ growth of silver nanoparticles on TEMPO-oxidized jute fibers by microwave heating. *Carbohydr Polym* 92:571–576 . doi: 10.1016/j.carbpol.2012.08.091

⁴⁰⁵ Dong H, Snyder JF, Tran DT, Leadore JL (2013a) Hydrogel, aerogel and film of cellulose nanofibrils functionalized with silver nanoparticles. *Carbohydr Polym* 95:760–767 . doi: 10.1016/j.carbpol.2013.03.041

⁴⁰⁶ Dong H, Snyder JF, Williams KS, Andzelm JW (2013b) Cation-Induced Hydrogels of Cellulose Nanofibrils with Tunable Moduli. *Biomacromolecules* 14:3338–3345 . doi: 10.1021/bm400993f

⁴⁰⁷ Ogundare SA, van Zyl WE (2018) Nanocrystalline cellulose as reducing- and stabilizing agent in the synthesis of silver nanoparticles: Application as a surface-enhanced Raman scattering (SERS) substrate. *Surfaces and Interfaces* 13:1–10 . doi: 10.1016/j.surfin.2018.06.004

⁴⁰⁸ Gu J, Hu C, Zhang W, Dichiara AB (2018) Reagentless preparation of shape memory cellulose nanofibril aerogels decorated with Pd nanoparticles and their application in dye discoloration. *Appl Catal B Environ* 237:482–490 . doi: 10.1016/j.apcatb.2018.06.002

⁴⁰⁹ Ogundare SA, van Zyl WE (2018) Nanocrystalline cellulose as reducing- and stabilizing agent in the synthesis of silver nanoparticles: Application as a surface-enhanced Raman scattering (SERS) substrate. *Surfaces and Interfaces* 13:1–10 . doi: 10.1016/j.surfin.2018.06.004

by breaking hydrogen bonds between TOCN. Thus, Ag⁺ ions could easily interact with the nanofibers and induce the gelation of the suspension⁴¹⁰. The mechanism for cation-induced gelation of TOCN starts with the screening of the electrostatic repulsion in the nanofibers by the ionic interactions of Ag⁺ ions. Enough screening allows the nanofibers to come closer and let the van der Waals forces to dominate. The screening tends to be more effective by increasing both the valence and concentration of counterions so that rising up any of them could promote more rapid gelation and more stable gels^{411 412}. Our results are in agreement with this information because we observed that higher Ag⁺ ions concentration (COOH:AgNO₃ molar ratio 1:3) produced more stable hydrogels compared to lower Ag⁺ ions concentration (molar ratios COOH:AgNO₃ 1:1) since the last were more affected by shaking.

We performed previous experiments for the preparation of TOCN-Ag NPs hydrogels with temperatures higher than 60 °C. At higher temperatures the reduction of Ag⁺ ions started sooner but the yellow-like color of Ag NPs stayed in the top of reaction mixture, suggesting the Ag NPs were being formed only there. Additionally, the degradation of the materials started before any gelation process, probably because the high temperature and the short time prevented the interaction between Ag⁺ ions and the TOCN suspension⁴¹³.

The spontaneous reduction of Ag⁺ ions by TOCN and formation of Ag nanoparticles

⁴¹⁰ Maestri CA, Abrami M, Hazan S, et al (2017) Role of sonication pre-treatment and cation valence in the sol-gel transition of nano-cellulose suspensions. *Sci Rep* 7:11129 . doi: 10.1038/s41598-017-11649-4

⁴¹¹ Dong H, Snyder JF, Tran DT, Leadore JL (2013a) Hydrogel, aerogel and film of cellulose nanofibrils functionalized with silver nanoparticles. *Carbohydr Polym* 95:760–767 . doi: 10.1016/j.carbpol.2013.03.041

⁴¹² Dong H, Snyder JF, Williams KS, Andzelm JW (2013b) Cation-Induced Hydrogels of Cellulose Nanofibrils with Tunable Moduli. *Biomacromolecules* 14:3338–3345 . doi: 10.1021/bm400993f

⁴¹³ Maestri CA, Abrami M, Hazan S, et al (2017) Role of sonication pre-treatment and cation valence in the sol-gel transition of nano-cellulose suspensions. *Sci Rep* 7:11129 . doi: 10.1038/s41598-017-11649-4

was observed by naked eyes and monitored by UV-Vis spectroscopy. Figure 4.3 shows the UV-Vis spectra of TOCN suspensions and hydrogels prepared at 60 °C with different COOH:AgNO₃ molar ratios. Similar results were observed when the hydrogel preparation was made at room temperature. TOCN dispersions exhibited minimal UV and visible absorption. The TOCN-Ag NPs hydrogels had an obvious absorption peak at 413 nm, typical of the surface plasmon resonance absorption of metallic Ag NPs. The color of the hydrogels turned darker as the absorbance did with higher Ag⁺ ions concentrations, indicating more Ag NPs were deposited in the surface of the TOCN^{414 415}. A comparable increase in color intensity was observed with longer reaction times. The wavelength of maximum absorption is related to the diameter of Ag NPs, with longer wavelengths corresponding to larger Ag NPs. The width of the absorption peak represents the size distribution of Ag NPs. However, nor the temperature, reaction time or COOH:AgNO₃ molar ratio used in this work shifted the absorption maximum or significantly changed its width, indicating most of the nanoparticles had similar size ranges and that these parameters affected mainly the amount of Ag NPs synthesized^{416 417}.

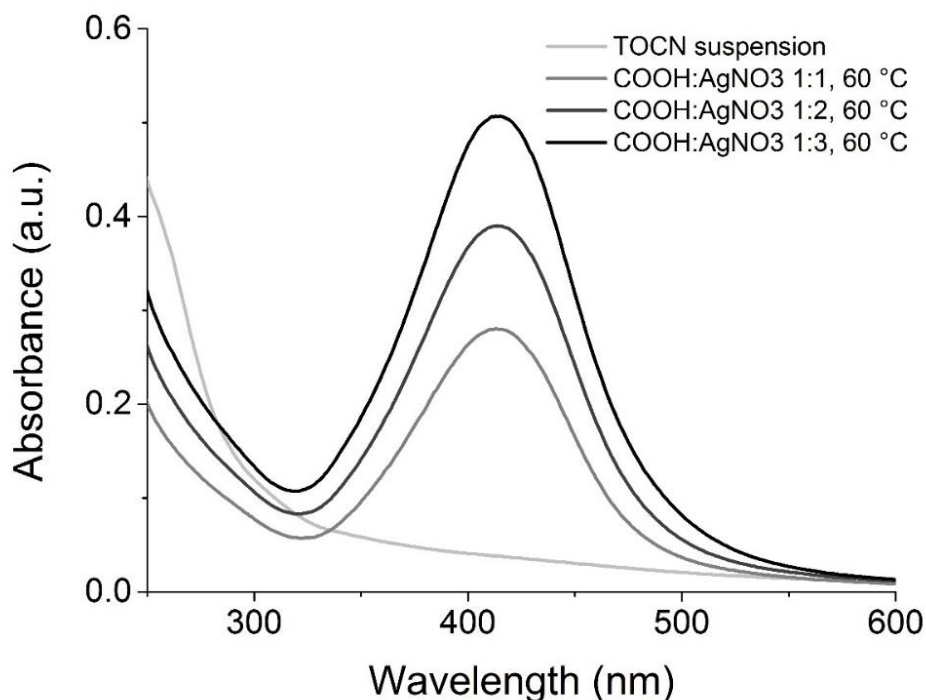
⁴¹⁴ Dong H, Snyder JF, Tran DT, Leadore JL (2013a) Hydrogel, aerogel and film of cellulose nanofibrils functionalized with silver nanoparticles. *Carbohydr Polym* 95:760–767 . doi: 10.1016/j.carbpol.2013.03.041

⁴¹⁵ Ogundare SA, van Zyl WE (2018) Nanocrystalline cellulose as reducing- and stabilizing agent in the synthesis of silver nanoparticles: Application as a surface-enhanced Raman scattering (SERS) substrate. *Surfaces and Interfaces* 13:1–10 . doi: 10.1016/j.surfin.2018.06.004

⁴¹⁶ Araki J, Hida Y (2018) Comparison of methods for quantitative determination of silver content in cellulose nanowhisker/silver nanoparticle hybrids. *Cellulose* 25:1065–1076 . doi: 10.1007/s10570-017-1640-z

⁴¹⁷ Ogundare SA, van Zyl WE (2018) Nanocrystalline cellulose as reducing- and stabilizing agent in the synthesis of silver nanoparticles: Application as a surface-enhanced Raman scattering (SERS) substrate. *Surfaces and Interfaces* 13:1–10 . doi: 10.1016/j.surfin.2018.06.004

Figure 24. UV-Vis spectra of TOCN suspensions and TOCN-Ag NPs hydrogels prepared at 60 °C.



FESEM images are shown in Figure 22. Micrographs of untreated (Figure 22a) and delignified (Figure 22b) Figue tow show the structural changes after the alkaline hydrogen peroxide process. The delignification removes non-cellulosic material such as hemicellulose and lignin, allowing to identify the individual microfibrils^{418 419 420}. Air-dried TOCN suspensions (Figure 22c) reveal interconnected nanofibrils, with diameters around 100 nm forming a three-dimensional and highly porous network

⁴¹⁸ Ouchi A (2008) Efficient total halogen-free photochemical bleaching of kraft pulps using alkaline hydrogen peroxide. *J Photochem Photobiol A Chem* 200:388–395 . doi: 10.1016/j.jphotochem.2008.09.006

⁴¹⁹ Su Y, Du R, Guo H, et al (2015) Fractional pretreatment of lignocellulose by alkaline hydrogen peroxide: Characterization of its major components. *Food Bioprod Process* 94:322–330 . doi: 10.1016/j.fbp.2014.04.001

⁴²⁰ Ovalle-Serrano SA, Blanco-Tirado C, Combariza MY (2018a) Exploring the composition of raw and delignified Colombian fique fibers, tow and pulp. *Cellulose* 25:151–165 . doi: 10.1007/s10570-017-1599-9

made by elongated and highly entangled structures^{421 422 423}. On the other hand, freeze-drying of the TOCN suspensions (Figure 22d) produced TOCN aerogels with extended sheet-like structures made of nanofibers, with higher bulk density and lower surface area than hydrogels⁴²⁴. Similar results were obtained for freeze-dried TOCN-Ag NPs aerogels⁴²⁵. Higher magnification of the TOCN-Ag NPs aerogels (Figure 22e) showed the presence of spherical Ag NPs with diameters ranging from 30-90 nm. Furthermore, at higher Ag⁺ ions concentration, cubic Ag particles with diameters around 1 μm could also be found with TOCN entangled around them (Figure 22f).

It has been reported that hydrogels can be prepared by five main approaches: 1) hydrogel formation in a nanoparticle suspension, 2) physically embedding the nanoparticles into hydrogel matrix after gelation, 3) reactive nanoparticles formation within a preformed gel, 4) cross-linking using nanoparticles to form hydrogels, and 5) gel formation using nanoparticles, polymers and distinct gelator molecules. Approaches 1, 2, 4 y 5 involve the use of previously prepared nanoparticles while approach 3 consists in the synthesis *in situ* of nanoparticles. We believe the procedure reported in this chapter can be included in the approach number 3. However, as seen in the micrograph of the Figure 22f, it seems that at higher Ag⁺ ions concentration (molar ratios COOH:AgNO₃ 1:3) Ag NPs aggregate in some regions and start working as cross-linkers in the hydrogels as proposed in the

⁴²¹ Dong H, Snyder JF, Williams KS, Andzelm JW (2013b) Cation-Induced Hydrogels of Cellulose Nanofibrils with Tunable Moduli. *Biomacromolecules* 14:3338–3345 . doi: 10.1021/bm400993f

⁴²² Liu C, Li B, Du H, et al (2016) Properties of nanocellulose isolated from corncob residue using sulfuric acid, formic acid, oxidative and mechanical methods. *Carbohydr Polym* 151:716–724 . doi: 10.1016/j.carbpol.2016.06.025

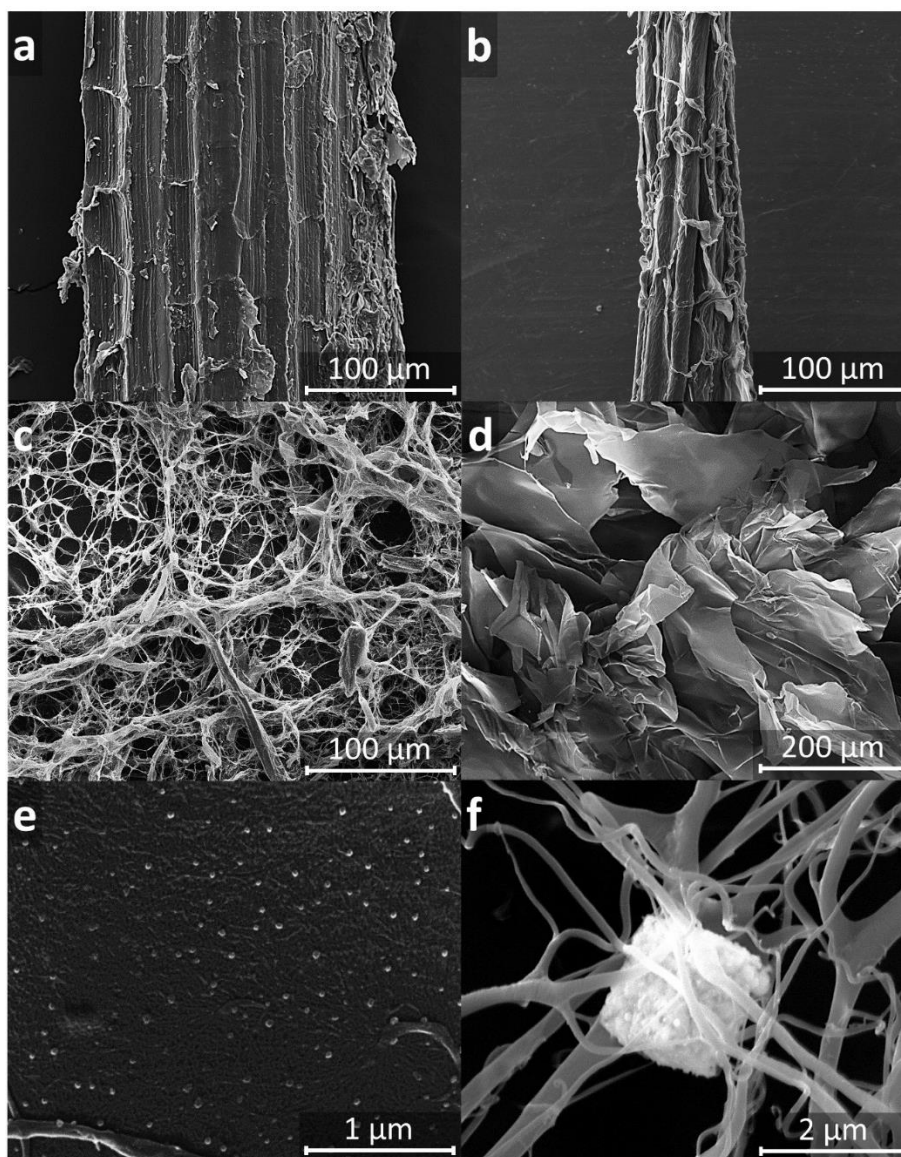
⁴²³ Ovalle-Serrano SA, Gómez FN, Blanco-Tirado C, Combariza MY (2018b) Isolation and characterization of cellulose nanofibrils from Colombian Figue decortication by-products. *Carbohydr Polym* 189:169–177 . doi: 10.1016/j.carbpol.2018.02.031

⁴²⁴ De France KJ, Hoare T, Cranston ED (2017) Review of Hydrogels and Aerogels Containing Nanocellulose. *Chem Mater* 29:4609–4631 . doi: 10.1021/acs.chemmater.7b00531

⁴²⁵ Dong H, Snyder JF, Tran DT, Leadore JL (2013a) Hydrogel, aerogel and film of cellulose nanofibrils functionalized with silver nanoparticles. *Carbohydr Polym* 95:760–767 . doi: 10.1016/j.carbpol.2013.03.041

approach number 4. This might be another reason for the more stable structure in the hydrogels prepared with COOH:AgNO₃ molar ratios 1:3 compared to 1:1⁴²⁶

Figure 25. FESEM images of (a) raw and (b) delignified Figue tow, (c) air-dried TOCN suspension, (d) TOCN aerogels and (e) and (f) TOCN-Ag NPs aerogels.



⁴²⁶ Thoniyot P, Tan MJ, Karim AA, et al (2015) Nanoparticle-Hydrogel Composites: Concept, Design, and Applications of These Promising, Multi-Functional Materials. *Adv Sci* 2:1400010 . doi: 10.1002/adv.201400010

Figure 23a shows the IR spectra of raw and delignified Fique tow, TOCN suspension and TOCN-Ag NPs hydrogels. All the spectra show typical bands of cellulose. The main absorption band at 3000-3500 cm^{-1} corresponds to the stretching of hydroxyl groups. Peaks at 2897, 1030 and 1643 cm^{-1} are due to CH_2 , C-OH and the H-O-H stretching vibration of water absorbed in the carbohydrates, respectively. The most intense band corresponds to glucosidic bond β (1 \rightarrow 4) C-O-C stretching vibration between 1203 and 1108 cm^{-1} and to the C-O vibration of C2, C3 and C6 at 1028 cm^{-1} ^{427 428}. Additionally, band around 900 cm^{-1} represents the vibration signal of the anomeric carbon C1-H⁴²⁹. After the alkaline hydrogen peroxide process, due to the removal of non-cellulosic components, signals at 1729 and 1239 cm^{-1} assigned to the stretching vibration of carbonyl units (C=O) characteristic of lignin and hemicellulose and C-O-C vibrations of aromatic ether linkages in lignin^{430 431}, respectively, decrease in the delignified Fique tow. TOCN spectrum exhibits a characteristic signal at 1600 cm^{-1} due to the C=O carbonyl stretching vibrations⁴³².

X-ray patterns of raw and delignified Fique tow, TOCN suspensions and TOCN-Ag NPs hydrogels are similar, as seen in Figure 23b. Typical cellulose I peaks at $2\theta=15.8^\circ$, 22.5° and 34.5° , where the broad band at 15.8° is due to overlapping of signals at $2\theta = 14.8^\circ$ and 16.8° characteristic of crystallographic planes (1 -1 0) and

⁴²⁷ Chen W, Yu H, Liu Y, et al (2011) Individualization of cellulose nanofibers from wood using high-intensity ultrasonication combined with chemical pretreatments. *Carbohydr Polym* 83:1804–1811 . doi: 10.1016/j.carbpol.2010.10.040

⁴²⁸ Muthulakshmi L, Rajini N, Nellaiah H, et al (2017) Experimental Investigation of Cellulose/Silver Nanocomposites Using In Situ Generation Method. *J Polym Environ* 25:1021–1032 . doi: 10.1007/s10924-016-0871-7

⁴²⁹ Pretsch E, Bühlmann P, Badertscher M (2009) *Structure Determination of Organic Compounds*. Springer Berlin Heidelberg, Berlin, Heidelberg

⁴³⁰ Abraham E, Deepa B, Pothan LA, et al (2011) Extraction of nanocellulose fibrils from lignocellulosic fibres: A novel approach. *Carbohydr Polym* 86:1468–1475

⁴³¹ Ramadoss G, Muthukumar K (2016) Mechanistic study on ultrasound assisted pretreatment of sugarcane bagasse using metal salt with hydrogen peroxide for bioethanol production. *Ultrason Sonochem* 28:207–217 . doi: 10.1016/j.ultsonch.2015.07.006

⁴³² Muthulakshmi L, Rajini N, Nellaiah H, et al (2017) Experimental Investigation of Cellulose/Silver Nanocomposites Using In Situ Generation Method. *J Polym Environ* 25:1021–1032 . doi: 10.1007/s10924-016-0871-7

(1 1 0), respectively, and the signals in 22.7° and 34.6° correspond to the crystallographic planes (2 0 0) and (0 0 4) coincide with characteristic signals of cellulose I crystallographic planes as reported by the Joint Committee on Powder Diffraction Standards (JCPDS file, No. 50-2241), space group P21 (No 4)^{433 434}. This indicates that the deposition of Ag NPs in TOCN did not change the cellulose crystalline structure⁴³⁵. For TOCN-Ag NPs hydrogels there are also some obvious peaks at 38.1°, 44.2° and 64.1°, attributed to silver crystal with a face centered cubic structure (JCPDS card: 04-0783) corresponding to (1 1 1), (2 0 0) and (2 2 0) planes, respectively^{436 437}. However, there can be seen other peaks at 27.7°, 32.1 and 46.1° corresponding to (1 1 1), (2 0 0) and (2 2 0) planes, respectively, which indicate the presence of the face centered cubic structure of AgCl crystals (JCPDS card 85-1355)^{438 439 440}. AgCl NPs are probably due to the presence of remaining Cl after the TEMPO-mediated oxidation redaction, as was shown by some EDS analyses. Additionally, the amount of AgCl NPs formed is so low that peaks with lower intensities than 27.7°, 32.1 and 46.1°, which should be at 2θ of 55° and 57°, couldn't be identified in the XRD patterns.

⁴³³ Mandal A, Chakrabarty D (2011) Isolation of nanocellulose from waste sugarcane bagasse (SCB) and its characterization. *Carbohydr Polym* 86:1291–1299

⁴³⁴ Sèbe G, Ham-Pichavant F, Ibarboure E, et al (2012) Supramolecular structure characterization of cellulose II nanowhiskers produced by acid hydrolysis of cellulose I substrates. *Biomacromolecules* 13:570–8 . doi: 10.1021/bm201777j

⁴³⁵ Gu J, Hu C, Zhang W, Dichiara AB (2018) Reagentless preparation of shape memory cellulose nanofibril aerogels decorated with Pd nanoparticles and their application in dye discoloration. *Appl Catal B Environ* 237:482–490 . doi: 10.1016/j.apcatb.2018.06.002

⁴³⁶ Yao Q, Fan B, Xiong Y, et al (2017) Stress sensitive electricity based on Ag/cellulose nanofiber aerogel for self-reporting. *Carbohydr Polym* 168:265–273 . doi: 10.1016/j.carbpol.2017.03.089

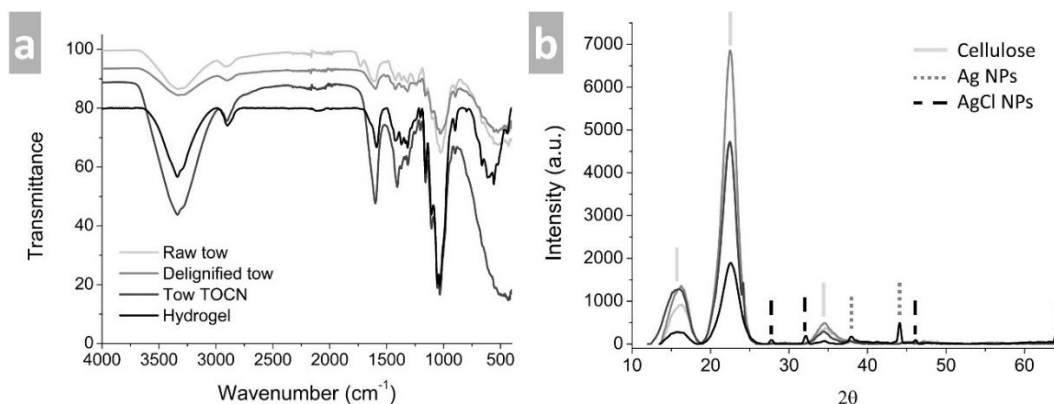
⁴³⁷ Chook SW, Yau SX, Chia CH, et al (2017) Carboxylated-nanocellulose as a template for the synthesis of silver nanoprism. *Appl Surf Sci* 422:32–38 . doi: 10.1016/j.apsusc.2017.05.242

⁴³⁸ Awwad AM, Salem NM, Ibrahim QM, Abdeen AO (2015) Phytochemical Fabrication And Characterization Of Silver/ Silver Chloride Nanoparticles Using Albizia Julibrissin Flowers Extract. *Adv Mater Lett* 6:726–730 . doi: 10.5185/amlett.2015.5816

⁴³⁹ Trinh ND, Nguyen TTB, Nguyen TH (2015) Preparation and characterization of silver chloride nanoparticles as an antibacterial agent. *Adv Nat Sci Nanosci Nanotechnol* 6:1–6 . doi: 10.1088/2043-6262/6/4/045011

⁴⁴⁰ Tang L, Tang F, Li M, Li L (2018) Facile synthesis of Ag@AgCl-contained cellulose hydrogels and their application. *Colloids Surfaces A Physicochem Eng Asp* 553:618–623 . doi: 10.1016/j.colsurfa.2018.06.016

Figure 26. (a) IR spectra and (b) XRD patterns of Raw and delignified Fique tow, TOCN suspensions and TOCN-Ag NPs hydrogels.



TGA analyses (Figure 24) of raw and delignified Fique tow, TOCN suspension and TOCN-Ag NPs hydrogels showed an initial weight loss of about 5% between 25-120 °C attributed to humidity on the surfaces of the samples. Raw Fique tow registered an additional weight loss (18%) at 298 °C due to hemicellulose decomposition⁴⁴¹. This weight loss disappeared in delignified Fique tow, suggesting the effective removal of hemicellulose from the material⁴⁴². Cellulose, being a linear polymer, presents higher thermal stability than hemicellulose. In raw and delignified Fique tow, the point for maximum cellulose decomposition was 369 and 340 °C, respectively, probably due to smaller fiber dimensions compared to raw fibers, leading to high surface areas exposure to heat⁴⁴³.

Thermal degradation of tow TOCN showed lower cellulose decomposition temperature (300 °C) compared to raw and delignified Fique tow. Additionally, the curve shows a slight shoulder at 255 °C attributed to decomposition of carboxylic

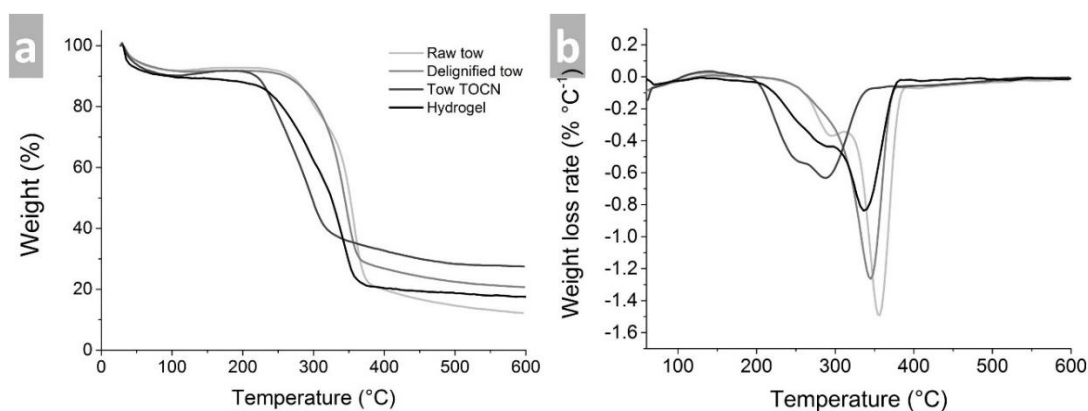
⁴⁴¹ Morán JI, Alvarez VA, Cyras VP, Vázquez A (2008) Extraction of cellulose and preparation of nanocellulose from sisal fibers. *Cellulose* 15:149–159 . doi: 10.1007/s10570-007-9145-9

⁴⁴² Ovalle-Serrano SA, Blanco-Tirado C, Combariza MY (2018a) Exploring the composition of raw and delignified Colombian fique fibers, tow and pulp. *Cellulose* 25:151–165 . doi: 10.1007/s10570-017-1599-9

⁴⁴³ Jiang F, Hsieh Y-L (2013) Chemically and mechanically isolated nanocellulose and their self-assembled structures. *Carbohydr Polym* 95:32–40 . doi: 10.1016/j.carbpol.2013.02.022

units on TOCN surface. As described in Chapters 2 and 3, tow TOCN lower cellulose decomposition is explained by the higher surface area exposed to the heat and by the presence of carboxylic units which facilitate direct solid-to-gas phase transitions through decarboxylation reactions^{444 445}. As for TOCN-Ag NPs hydrogels DTG curves (Figure 24b), there are two bands at 293 °C and 332 °C. The first one possibly due to thermal degradation of the metallic anhydroglucuronate units and the second one to cellulose decomposition⁴⁴⁶. There can be seen that after hydrogel formation the cellulose decomposition temperature shifted from 300 °C in TOCN to 332 °C in TOCN-Ag NPs hydrogel, indicating that formation of Ag NPs in TOCN increased the thermal stability of the final product⁴⁴⁷.

Figure 27. (a) TGA curves and (b) DTG curves for raw Fique tow, delignified Fique tow, TOCN and TOCN-Ag NPs hydrogels.



⁴⁴⁴ Jiang F, Hsieh Y-L (2013) Chemically and mechanically isolated nanocellulose and their self-assembled structures. *Carbohydr Polym* 95:32–40 . doi: 10.1016/j.carbpol.2013.02.022

⁴⁴⁵ Ovalle-Serrano SA, Gómez FN, Blanco-Tirado C, Combariza MY (2018b) Isolation and characterization of cellulose nanofibrils from Colombian Fique decortication by-products. *Carbohydr Polym* 189:169–177 . doi: 10.1016/j.carbpol.2018.02.031

⁴⁴⁶ Cao X, Ding B, Yu J, Al-Deyab SS (2013) In situ growth of silver nanoparticles on TEMPO-oxidized jute fibers by microwave heating. *Carbohydr Polym* 92:571–576 . doi: 10.1016/j.carbpol.2012.08.091

⁴⁴⁷ López-Carballo G, Higuera L, Gavara R, Hernández-Muñoz P (2013) Silver Ions Release from Antibacterial Chitosan Films Containing in Situ Generated Silver Nanoparticles. *J Agric Food Chem* 61:260–267 . doi: 10.1021/jf304006y

4.5 CONCLUSIONS

In this chapter we described an environmentally benign 'one-pot' method for the preparation of functional hydro/aerogels from TOCN (extracted from Figue tow) and Ag NPs, using only water as solvent. We investigated the effect of temperature and COOH:AgNO₃ molar ratio in the preparation of the TOCN-Ag NPs hydro/aerogels. TOCN suspensions can be subjected to a sol-gel transition by exchanging Na⁺ by H⁺ ions since the resultant carboxylic acid in TOCN facilitates the formation of inter- and intramolecular hydrogen bonds in the structure. Results also showed the importance of sonication before the sol-gel transition process. Temperature influenced mainly the reaction time: 8 days at room temperature and 28 h at 60 °C. COOH:AgNO₃ molar ratios (1:1, 1:2 and 1:3) affected mostly the amount of Ag NPs, producing higher amounts of Ag NPs at higher COOH:AgNO₃ molar ratios. Additionally, FESEM showed that higher COOH:AgNO₃ molar ratios might induce aggregation of spherical Ag NPs into cubic Ag particles. However, high Ag⁺ ions concentrations strongly affect the assembly of TOCN-Ag NPs hydrogels, since at lower COOH:AgNO₃ molar ratios the hydrogels had a poor stability. On the other hand, we performed the same procedure with a post-oxidized TOCN. The results suggested that high carboxylate content TOCN (2.2 mmol COOH/g cellulose) are not a suitable matrix for the reduction of Ag⁺ to Ag NPs, since aldehydes are oxidized in the post-oxidation process, decreasing TOCN redox potential. TOCN form gels due to hydrogen bonds and the strong electrostatic interactions between cations and carboxyl groups. Hydrogels stability can be improved following the procedure described in this chapter by increasing the Ag⁺ ions concentration in the reaction and, as reported in the literature, by adding cations with higher valence.

5. CONCLUSIONES

Fique decortication by-products (tow and pulp), have cellulose contents of 52.3% and 30.5%, respectively. The cellulose in tow has the same physicochemical and spectroscopic characteristics than that of long Fique fibers. On the other hand, Fique pulp is composed of two distinctive materials: cellulose filaments from secondary cell walls and leaf epidermis. Cellulose filaments in Fique pulp are highly amorphous exhibiting low crystallinity; while the epidermis shows the presence of oxalates and waxes, common to the leaf cuticle. The pretreatment of Fique decortication by-products with AHP was effective in the removal of non-cellulosic compounds such as hemicellulose and lignin. Optimal conditions for the delignification of Fique fibers and tow were reached when the samples were subjected to 120 min treatment at 70 °C with a H₂O₂ concentration of 10% w/w at pH 11.5 in the presence of ultrasound. The maximum lignin removal in Fique fibers and tow achieved with this procedure was around 88%, while for Fique pulp the lignin removal was of about 79%. After AHP, IR spectra showed the decrease, or absence, of signals attributed to hemicellulose and lignin, while XRD patterns showed increased crystallinity indexes. Thermal analyses corroborated the removal of components other than cellulose and FESEM pictures showed how the lamellar structure in the macro fiber is disrupted by the removal of hemicellulose, lignin and ground tissue, leaving cellulose microfibrils exposed. As the first in-depth report on Fique by-products characterization, our analyses indicate that alternative uses for Fique by-products such as pulp and tow are highly feasible due to the physicochemical characteristics of these residues and their significant content of crystalline and amorphous cellulose. Furthermore, Fique pulp and tow are produced in greater excess (five times more) than Fique fibers, which make them an alternative source for extracting cellulose because of their wide availability and low cost.

Cellulose nanofibrils (CNF) were successfully extracted from delignified Fique tow through TEMPO oxidation assisted with ultrasonic radiation. We observed TOCN

with 'rod-like' structures and diameters around 100 nm and lengths of several micrometers. These CNF, with a carboxylate content of 1.6 mmol -COOH/g cellulose, corresponding to 35% -COOH functional groups, formed stable aqueous suspensions with ζ potential of -53 mV as a result of electrostatic repulsion. Such stability was also confirmed by optical birefringence phenomenon of aqueous suspensions of TOCN. Crystallinity index of these CNF was higher than 60% and thermal degradation temperatures did not vary significantly upon oxidation when compared to the raw Fique tow and delignified Fique tow. We also show the significant effect of the delignification pretreatment and the use of ultrasound in the TEMPO oxidation reaction. A degree of oxidation of 0.27 and a carboxylate content of 1.6 mmol/g were measured for CNF from delignified Fique tow when the TEMPO reaction was carried out in the presence of ultrasonic energy. In absence of sonication, we registered a degree of oxidation of 0.21 and a carboxylate content of 1.2 mmol/g. In addition, when raw Fique tow was used in the TEMPO-oxidation reaction, the degree of oxidation was 0.17 and the carboxylate content was 1.0 mmol/g. Clearly, delignification and use of ultrasound increase degree of oxidation in TOCN up to 37 and 22%, respectively. Finally, Fique CNF exhibit similar physicochemical, thermal and microscopic behaviors than CNF from different sources such as hemp bast, commercial bamboo pulp, bagasse bleached Kraft pulp, palm oil empty bunches, rice straw, jute, sisal and abaca, among others. To the best of our knowledge, this contribution reported for the first time the extraction and characterization of nanocellulose from Colombian Fique lignocellulosic biomass.

We also studied the effect of post-oxidation in TOCN extracted from delignified Fique tow and its hydrophobization by means of a 'one-pot' amidation reaction. In agreement with previous chapters, AHP treatment was used to increase the efficiency in the TOCN extraction. The resulting TOCN had a web-like structure with high values of carboxylate content. The high carboxylate content was a key factor in the coupling of ODA on the surface of TOCN to form the amidated product. It showed that the more hydrophilic the starting material (TOCN-P), the more hydrophobic the

amidated product (TOCN-P-ODA). Finally, the success of the amidation reaction was confirmed by spectroscopic, microscopic and thermal analysis techniques. The transition from hydrophilic to hydrophobic character of the synthesized materials was also evaluated by the evolution of the percentage of transmittance by means of UV-vis measurements for nanocellulose suspensions in different types of solvents and contact angle measurements.

Finally, we described an environmentally benign 'one-pot' method for the preparation of functional hydro/aerogels from TOCN (extracted from Fique tow) and Ag NPs, using only water as solvent. We investigated the effect of temperature and COOH:AgNO₃ molar ratio in the preparation of the TOCN-Ag NPs hydro/aerogels. TOCN suspensions can be subjected to a sol-gel transition by exchanging Na⁺ by H⁺ ions since the resultant carboxylic acid in TOCN facilitates the formation of inter- and intramolecular hydrogen bonds in the structure. Results also showed the importance of sonication before the sol-gel transition process. Temperature influenced mainly the reaction time: 8 days at room temperature and 28 h at 60 °C. COOH:AgNO₃ molar ratios (1:1, 1:2 and 1:3) affected mostly the amount of Ag NPs, producing higher amounts of Ag NPs at higher COOH:AgNO₃ molar ratios. Additionally, FESEM showed that higher COOH:AgNO₃ molar ratios might induce aggregation of spherical Ag NPs into cubic Ag particles. However, high Ag⁺ ions concentrations strongly affect the assembly of TOCN-Ag NPs hydrogels, since at lower COOH:AgNO₃ molar ratios the hydrogels had a poor stability. On the other hand, we performed the same procedure with a post-oxidized TOCN. The results suggested that high carboxylate content TOCN (2.2 mmol COOH/g cellulose) are not a suitable matrix for the reduction of Ag⁺ to Ag NPs, since aldehydes are oxidized in the post-oxidation process, decreasing TOCN redox potential. TOCN form gels due to hydrogen bonds and the strong electrostatic interactions between cations and carboxyl groups. Hydrogels stability can be improved following the procedure described in this chapter by increasing the Ag⁺ ions concentration in the reaction and, as reported in the literature, by adding cations with higher valence.

BIBLIOGRAFIA

Abdul Khalil, H. P. S., Davoudpour, Y., Islam, M. N., Mustapha, A., Sudesh, K., Dungani, R., et al. (2014). Production and modification of nanofibrillated cellulose using various mechanical processes: a review. *Carbohydrate Polymers*, 99, 649–65. <https://doi.org/10.1016/j.carbpol.2013.08.069>

Abe K, Yano H (2011) Formation of hydrogels from cellulose nanofibers. *Carbohydr Polym* 85:733–737 . doi: 10.1016/j.carbpol.2011.03.028

Abraham, E., Deepa, B., Pothan, L. A., Jacob, M., Thomas, S., Cvelbar, U., et al. (2011). Extraction of nanocellulose fibrils from lignocellulosic fibres: A novel approach. *Carbohydrate Polymers*, 86, 1468–1475.

Ahmadi M, Madadlou A, Sabouri AA (2015) Isolation of micro- and nano-crystalline cellulose particles and fabrication of crystalline particles-loaded whey protein cold-set gel. *Food Chem* 174:97–103. doi: 10.1016/j.foodchem.2014.11.038

Alila, S., Besbes, I., Vilar, M. R., Mutjé, P., & Boufi, S. (2013). Non-woody plants as raw materials for production of microfibrillated cellulose (MFC): A comparative study. *Industrial Crops and Products*, 41, 250–259. <https://doi.org/10.1016/j.indcrop.2012.04.028>

Annadurai G, Juang R-S, Lee D-J (2002) Use of cellulose-based wastes for adsorption of dyes from aqueous solutions. *J Hazard Mater* 92:263–274. doi: 10.1016/S0304-3894(02)00017-1

Araki J, Hida Y (2018) Comparison of methods for quantitative determination of silver content in cellulose nanowhisker/silver nanoparticle hybrids. *Cellulose* 25:1065–1076 . doi: 10.1007/s10570-017-1640-z

Argun, H., & Onaran, G. (2015). Delignification of vineyard pruning residues by alkaline peroxide treatment. *Industrial Crops and Products*, 74, 697–702. <https://doi.org/10.1016/j.indcrop.2015.05.031>

Awwad AM, Salem NM, Ibrahim QM, Abdeen AO (2015) Phytochemical Fabrication And Characterization Of Silver/ Silver Chloride Nanoparticles Using Albizia Julibrissin Flowers Extract. *Adv Mater Lett* 6:726–730 . doi: 10.5185/amlett.2015.5816

Azizi Samir, M. A. S., Alloin, F., & Dufresne, A. (2005). Review of recent research into cellulosic whiskers, their properties and their application in nanocomposite field. *Biomacromolecules*, 6(2), 612–626. <https://doi.org/10.1021/bm0493685>

Barreto ACH, Rosa DS, Fachine PBA, Mazzetto SE (2011) Properties of sisal fibers treated by alkali solution and their application into cardanol-based biocomposites. *Compos Part A Appl Sci Manuf* 42:492–500. doi: 10.1016/j.compositesa.2011.01.008

Belaadi A, Bezazi A, Bourchak M, et al. (2014) Thermochemical and statistical mechanical properties of natural sisal fibres. *Compos Part B Eng* 67:481–489. doi: 10.1016/j.compositesb.2014.07.029

Benkaddour A, Journoux-Lapp C, Jradi K, et al (2014) Study of the hydrophobization of TEMPO-oxidized cellulose gel through two routes: amidation and esterification process. *J Mater Sci* 49:2832–2843 . doi: 10.1007/s10853-013-7989-y

Besbes I, Alila S, Boufi S (2011) Nanofibrillated cellulose from TEMPO-oxidized eucalyptus fibres: Effect of the carboxyl content. *Carbohydr Polym* 84:975–983 . doi: 10.1016/j.carbpol.2010.12.052

Besemer A (1993) The bromide catalized hypochlorite oxidation of starch and inulin. Delft University of Technology

Bhatnagar A (2005) Processing of Cellulose Nanofiber-reinforced Composites. *J Reinf Plast Compos* 24:1259–1268 . doi: 10.1177/0731684405049864

Bledzki AK, Mamun AA, Lucka-Gabor M, Gutowski VS (2008) The effects of acetylation on properties of flax fibre and its polypropylene composites. *Express Polym Lett* 2:413–422 . doi: 10.3144/expresspolymlett.2008.50

Bragd PL, Besemer AC, Van Bekkum H (2000) Bromide-free TEMPO-mediated oxidation of primary alcohol groups in starch and methyl α -D-glucopyranoside. *Carbohydr Res* 328:355–363 . doi: 10.1016/S0008-6215(00)00109-9

Brahim M, El Kantar S, Boussetta N, et al. (2016) Delignification of rapeseed straw using innovative chemo-physical pretreatments. *Biomass and Bioenergy* 95:92–98. doi: 10.1016/j.biombioe.2016.09.019

Brett CT (2000) Cellulose microfibrils in plants: biosynthesis, deposition, and integration into the cell wall. *Int Rev Cytol* 199:161–199. doi: 10.1016/s0074-7696(00)99004-1

Browning BL (1967) No Title. *Methods Wood Chem. Vol II*. John Wiley & Sons, New York, USA, pp 406–727

Bussemaker MJ, Xu F, Zhang D (2013) Manipulation of ultrasonic effects on lignocellulose by varying the frequency, particle size, loading and stirring. *Bioresour Technol* 148:15–23. doi: 10.1016/j.biortech.2013.08.106

Bussemaker MJ, Zhang D (2013) Effect of ultrasound on lignocellulosic biomass as a pretreatment for biorefinery and biofuel applications. *Ind Eng Chem Res* 52:3563–3580. doi: 10.1021/ie3022785

Cao X, Ding B, Yu J, Al-Deyab SS (2012) Cellulose nanowhiskers extracted from TEMPO-oxidized jute fibers. *Carbohydr Polym* 90:1075–80. doi: 10.1016/j.carbpol.2012.06.046

Cao X, Ding B, Yu J, Al-Deyab SS (2013) In situ growth of silver nanoparticles on TEMPO-oxidized jute fibers by microwave heating. *Carbohydr Polym* 92:571–576. doi: 10.1016/j.carbpol.2012.08.091

Cao, Y., Jiang, Y., Song, Y., Cao, S., Miao, M., Feng, X., et al. (2015). Combined bleaching and hydrolysis for isolation of cellulose nanofibrils from waste sackcloth. *Carbohydrate Polymers*, 131, 152–158. <https://doi.org/10.1016/j.carbpol.2015.05.063>

Castellanos D. OF, Torres P. LM, Rojas L. JC (2009) *Agenda prospectiva de investigación y desarrollo tecnológico para la cadena productiva de Fique en Colombia*. Ministerio de agricultura y desarrollo rural, Bogotá

Castellanos LJ, Blanco-Tirado C, Hinestroza JP, Combariza MY (2012) In situ synthesis of gold nanoparticles using Fique natural fibers as template. *Cellulose* 19:1933–1943. doi: 10.1007/s10570-012-9763-8

Chacón-Patiño ML, Blanco-Tirado C, Hinestroza JP, Combariza MY (2013) Biocomposite of nanostructured MnO₂ and Fique fibers for efficient dye degradation. *Green Chem* 15:2920. doi: 10.1039/c3gc40911b

Chaudhary G, Singh LK, Ghosh S (2012) Alkaline pretreatment methods followed by acid hydrolysis of *Saccharum spontaneum* for bioethanol production. *Bioresour Technol* 124:111–118 . doi: 10.1016/j.biortech.2012.08.067

Chen W, Yu H, Liu Y, et al (2011) Individualization of cellulose nanofibers from wood using high-intensity ultrasonication combined with chemical pretreatments. *Carbohydr Polym* 83:1804–1811 . doi: 10.1016/j.carbpol.2010.10.040

Chen W, Yu H, Liu Y, et al (2011) Individualization of cellulose nanofibers from wood using high-intensity ultrasonication combined with chemical pretreatments. *Carbohydr Polym* 83:1804–1811 . doi: 10.1016/j.carbpol.2010.10.040

Chen W, Yu H, Liu Y, et al. (2011) Isolation and characterization of cellulose nanofibers from four plant cellulose fibers using a chemical-ultrasonic process. *Cellulose* 18:433–442. doi: 10.1007/s10570-011-9497-z

Chen, W., Yu, H., Liu, Y., Chen, P., Zhang, M., & Hai, Y. (2011). Individualization of cellulose nanofibers from wood using high-intensity ultrasonication combined with chemical pretreatments. *Carbohydrate Polymers*, 83(4), 1804–1811. <https://doi.org/10.1016/j.carbpol.2010.10.040>

Chook SW, Yau SX, Chia CH, et al (2017) Carboxylated-nanoncellulose as a template for the synthesis of silver nanoprism. *Appl Surf Sci* 422:32–38 . doi: 10.1016/j.apsusc.2017.05.242

Collazo-Bigliardi S, Ortega-Toro R, Chiralt Boix A (2018) Isolation and characterisation of microcrystalline cellulose and cellulose nanocrystals from coffee husk and comparative study with rice husk. *Carbohydr Polym* 191:205–215 . doi: 10.1016/j.carbpol.2018.03.022

Correia JADC, Júnior JEM, Gonçalves LRB, Rocha MVP (2013) Alkaline hydrogen peroxide pretreatment of cashew apple bagasse for ethanol production: Study of parameters. *Bioresour Technol* 139:249–256. doi: 10.1016/j.biortech.2013.03.153

Cunha AG, Freire CSR, Silvestre AJD, et al (2007) Highly hydrophobic biopolymers prepared by the surface pentafluorobenzoylation of cellulose substrates. *Biomacromolecules* 8:1347–1352 . doi: 10.1021/bm0700136

Cybulska J, Zdunek A, Konstankiewicz K (2011) Calcium effect on mechanical properties of model cell walls and apple tissue. *J Food Eng* 102:217–223. doi: 10.1016/j.jfoodeng.2010.08.019

da Silva Lacerda V, López-Sotelo JB, Correa-Guimarães A, et al. (2015) Rhodamine B removal with activated carbons obtained from lignocellulosic waste. *J Environ Manage* 155:67–76. doi: 10.1016/j.jenvman.2015.03.007

da Silva Perez D, Montanari S, Vignon MR (2003) TEMPO-Mediated Oxidation of Cellulose III. *Biomacromolecules* 4:1417–1425 . doi: 10.1021/bm034144s

Dai L, Wang B, Long Z, et al (2015) Properties of hydroxypropyl guar/TEMPO-oxidized cellulose nanofibrils composite films. *Cellulose* 22:3117–3126 . doi: 10.1007/s10570-015-0691-2

Davidson TC, Newman RH, Ryan MJ (2004) Variations in the fibre repeat between samples of cellulose I from different sources. *Carbohydr Res* 339:2889–2893 . doi: 10.1016/j.carres.2004.10.005

Davies JT (1957) A quantitative kinetic theory of emulsion type. I. Physical chemistry of the emulsifying agent. In: *Proceedings of 2nd International Congress Surface Activity*. pp 426–438

De France KJ, Hoare T, Cranston ED (2017) Review of Hydrogels and Aerogels Containing Nanocellulose. *Chem Mater* 29:4609–4631 . doi: 10.1021/acs.chemmater.7b00531

de Souza Lima, M. M., & Borsali, R. (2004). Rodlike Cellulose Microcrystals: Structure, Properties, and Applications. *Macromolecular Rapid Communications*, 25(7), 771–787. <https://doi.org/10.1002/marc.200300268>

Dizbay-Onat M, Vaidya UK, Lungu CT (2017) Preparation of industrial sisal fiber waste derived activated carbon by chemical activation and effects of carbonization parameters on surface characteristics. *Ind Crops Prod* 95:583–590. doi: 10.1016/j.indcrop.2016.11.016

Dong H, Snyder JF, Tran DT, Leadore JL (2013a) Hydrogel, aerogel and film of cellulose nanofibrils functionalized with silver nanoparticles. *Carbohydr Polym* 95:760–767 . doi: 10.1016/j.carbpol.2013.03.041

Dong H, Snyder JF, Williams KS, Andzelm JW (2013b) Cation-Induced Hydrogels of Cellulose Nanofibrils with Tunable Moduli. *Biomacromolecules* 14:3338–3345 . doi: 10.1021/bm400993f

Dufresne, A. (2013a). Nanocellulose: a new ageless bionanomaterial. *Materials Today*, 16(6), 220–227. <https://doi.org/10.1016/j.mattod.2013.06.004>

Dufresne, A. (2013b). Nanocellulose: From Nature to High Performance Tailored Materials. Grenoble: Walter de Gruyter. Retrieved from https://books.google.com.co/books/about/Nanocellulose.html?id=6Mfuk_b7gncC&redir_esc=y

Dutra ED, Santos FA, Alencar BRA, et al (2017) Alkaline hydrogen peroxide pretreatment of lignocellulosic biomass: status and perspectives. *Biomass Convers Biorefinery*. doi: 10.1007/s13399-017-0277-3

Faruk O, Bledzki AK, Fink H-P, Sain M (2012) Biocomposites reinforced with natural fibers: 2000–2010. *Prog Polym Sci* 37:1552–1596 . doi: 10.1016/j.progpolymsci.2012.04.003

Feng X, Wang S, Hou J, et al (2011) Effect of hydroxyl content and molecular weight of biodegradable ethylcellulose on demulsification of water-in-diluted bitumen emulsions. *Ind Eng Chem Res* 50:6347–6354 . doi: 10.1021/ie102071q

Ferrer, A., Quintana, E., Filpponen, I., Solala, I., Vidal, T., Rodríguez, A., ... Rojas, O. J. (2012). Effect of residual lignin and heteropolysaccharides in nanofibrillar cellulose and nanopaper from wood fibers. *Cellulose*, 19(6), 2179–2193. <https://doi.org/10.1007/s10570-012-9788-z>

Fras L, Stana-Kleinschek K (2002) Quantitative determination of carboxyl groups in cellulose by complexometric titration. *Lenzinger ...* 80–88 . doi: 10.1080/14328917.2004.11784850

French, A. D. (2013). Idealized powder diffraction patterns for cellulose polymorphs. *Cellulose*, 21(2), 885–896. <https://doi.org/10.1007/s10570-013-0030-4>

Fujisawa S, Okita Y, Fukuzumi H, et al (2011) Preparation and characterization of TEMPO-oxidized cellulose nanofibril films with free carboxyl groups. *Carbohydr Polym* 84:579–583 . doi: 10.1016/j.carbpol.2010.12.029

Fukuzumi H (2012) Studies on structures and properties of TEMPO-oxidized cellulose nanofibril films. 博士論文 98

Fukuzumi H, Saito T, Okita Y, Isogai A (2010) Thermal stabilization of TEMPO-oxidized cellulose. *Polym Degrad Stab* 95:1502–1508 . doi: 10.1016/j.polymdegradstab.2010.06.015

Fukuzumi, H., Saito, T., Okita, Y., & Isogai, A. (2010). Thermal stabilization of TEMPO-oxidized cellulose. *Polymer Degradation and Stability*, 95(9), 1502–1508. <https://doi.org/10.1016/j.polymdegradstab.2010.06.015>

G.Maschio, C. Koufopoulos AL (1992) Pyrolysis, a promising route for biomass utilization. *Bioresour Technol* 42:219–231

Gañán, P., & Mondragon, I. (2002). Surface modification of Figue fibers. Effect on their physico-mechanical properties. *Polymer Composites*, 23(3), 383–394. <https://doi.org/10.1002/pc.10440>

García A, Gandini A, Labidi J, et al (2016) Industrial and crop wastes: A new source for nanocellulose biorefinery. *Ind Crops Prod* 93:26–38 . doi: 10.1016/j.indcrop.2016.06.004

García, A., Gandini, A., Labidi, J., Belgacem, N., & Bras, J. (2016). Industrial and crop wastes: A new source for nanocellulose biorefinery. *Industrial Crops and Products*, 93, 26–38. <https://doi.org/10.1016/j.indcrop.2016.06.004>

Gert E V., Torgashov VI, Zubets O V., Kaputskii FN (2005) Preparation and properties of enterosorbents based on carboxylated microcrystalline cellulose. *Cellulose* 12:517–526 . doi: 10.1007/s10570-005-7134-4

Gómez FN, Combariza MY, Blanco-Tirado C (2017) Facile cellulose nanofibrils amidation using a “one-pot” approach. *Cellulose* 24:717–730 . doi: 10.1007/s10570-016-1174-9

Gopal M, Mathew MD (1986) The scope for utilizing jute wastes as raw materials in various industries: A review. *Agric Wastes* 15:149–158. doi: 10.1016/0141-4607(86)90046-6

Gu J, Hu C, Zhang W, Dichiara AB (2018) Reagentless preparation of shape memory cellulose nanofibril aerogels decorated with Pd nanoparticles and their application in dye discoloration. *Appl Catal B Environ* 237:482–490 . doi: 10.1016/j.apcatb.2018.06.002

Haafiz, M. K. M., Hassan, A., Zakaria, Z., & Inuwa, I. M. (2014). Isolation and characterization of cellulose nanowhiskers from oil palm biomass microcrystalline cellulose. *Carbohydrate Polymers*, 103(1), 119–125. <https://doi.org/10.1016/j.carbpol.2013.11.055>

Habibi Y, Chanzy H, Vignon MR (2006) TEMPO-mediated surface oxidation of cellulose whiskers. *Cellulose* 13:679–687 . doi: 10.1007/s10570-006-9075-y

Habibi Y, Lucia LA, Rojas OJ (2010) Cellulose nanocrystals: chemistry, self-assembly, and applications. *Chem Rev* 110:3479–3500.

Habibi, Y., Chanzy, H., & Vignon, M. R. (2006). TEMPO-mediated surface oxidation of cellulose whiskers. *Cellulose*, 13(6), 679–687. <https://doi.org/10.1007/s10570-006-9075-y>

Habibi, Y., Lucia, L. A., & Rojas, O. J. (2010). Cellulose nanocrystals: chemistry, self-assembly, and applications. *Chemical Reviews*, 110(6), 3479–3500.

Hamou K Ben, Kaddami H, Dufresne A, et al (2018) Impact of TEMPO-oxidization strength on the properties of cellulose nanofibril reinforced polyvinyl acetate nanocomposites. *Carbohydr Polym* 181:1061–1070 . doi: 10.1016/j.carbpol.2017.11.043

Hamou, K. Ben, Kaddami, H., Dufresne, A., Boufi, S., Magnin, A., & Erchiqui, F. (2018). Impact of TEMPO-oxidization strength on the properties of cellulose nanofibril reinforced polyvinyl acetate nanocomposites. *Carbohydrate Polymers*, 181(November), 1061–1070. <https://doi.org/10.1016/j.carbpol.2017.11.043>

Heidarian P, Behzad T, Karimi K (2016) Isolation and characterization of bagasse cellulose nanofibrils by optimized sulfur-free chemical delignification. *Wood Sci Technol* 1–18. doi: 10.1007/s00226-016-0820-6

Heredia-Guerrero JA, Benítez JJ, Domínguez E, et al. (2014) Infrared and Raman spectroscopic features of plant cuticles: a review. *Front Plant Sci* 5:1–14. doi: 10.3389/fpls.2014.00305

Hoyos CG, Alvarez V a., Rojo PG, Vázquez A (2012) Figue fibers: Enhancement of the tensile strength of alkali treated fibers during tensile load application. *Fibers Polym* 13:632–640. doi: 10.1007/s12221-012-0632-8

Hu Y, Tang L, Lu Q, et al. (2014) Preparation of cellulose nanocrystals and carboxylated cellulose nanocrystals from borer powder of bamboo. *Cellulose* 21:1611–1618. doi: 10.1007/s10570-014-0236-0

Iskaleva A, Yimmou BM, Gogate PR, et al (2012) Cavitation assisted delignification of wheat straw: a review. *Ultrason Sonochem* 19:984–93 . doi: 10.1016/j.ultsonch.2012.02.007

Isobe N, Komamiya T, Kimura S, et al (2018) Cellulose hydrogel with tunable shape and mechanical properties: From rigid cylinder to soft scaffold. *Int J Biol Macromol* 117:625–631 . doi: 10.1016/j.ijbiomac.2018.05.071

Isogai A (2013) Wood nanocelluloses : fundamentals and applications as new bio-based nanomaterials. 449–459 . doi: 10.1007/s10086-013-1365-z

Isogai A, Bergström L (2018) Preparation of cellulose nanofibers using green and sustainable chemistry. *Curr Opin Green Sustain Chem* 12:15–21 . doi: 10.1016/j.cogsc.2018.04.008

Isogai A, Saito T, Fukuzumi H (2011) TEMPO-oxidized cellulose nanofibers. *Nanoscale* 3:71–85 . doi: 10.1039/C0NR00583E

Isogai T, Saito T, Isogai A (2010) TEMPO electromediated oxidation of some polysaccharides including regenerated cellulose fiber. *Biomacromolecules* 11:1593–1599 . doi: 10.1021/bm1002575

Isogai, A., Saito, T., & Fukuzumi, H. (2011). TEMPO-oxidized cellulose nanofibers. *Nanoscale*, 3(1), 71–85. <https://doi.org/10.1039/C0NR00583E>

Jiang F, Hsieh Y-L (2013) Chemically and mechanically isolated nanocellulose and their self-assembled structures. *Carbohydr Polym* 95:32–40. doi: 10.1016/j.carbpol.2013.02.022

Johnson RK, Zink-Sharp A, Glasser WG (2011) Preparation and characterization of hydrophobic derivatives of TEMPO-oxidized nanocelluloses. *Cellulose* 18:1599–1609 . doi: 10.1007/s10570-011-9579-y

Kaewprasit C, Hequet E, Abidi N, Gourlot JP (1998) Application of Methylene Blue Adsorption to Cotton Fiber Specific Surface Area Measurement: Part I. Methodology. *J Cotton Sci* 2:164–173

Kallel F, Bettaieb F, Khiari R, et al (2016) Isolation and structural characterization of cellulose nanocrystals extracted from garlic straw residues. *Ind Crops Prod* 87:287–296 . doi: 10.1016/j.indcrop.2016.04.060

Keijsers ERP, Yilmaz G, van Dam JEG (2013) The cellulose resource matrix. *Carbohydr Polym* 93:9–21 . doi: 10.1016/j.carbpol.2012.08.110

Kuramae, R., Saito, T., & Isogai, A. (2014). TEMPO-oxidized cellulose nanofibrils prepared from various plant holocelluloses. *Reactive and Functional Polymers*, 85, 126–133. <https://doi.org/10.1016/j.reactfunctpolym.2014.06.011>

Lamaming J, Hashim R, Leh CP, et al. (2015) Isolation and characterization of cellulose nanocrystals from parenchyma and vascular bundle of oil palm trunk (*Elaeis guineensis*). *Carbohydr Polym* 134:534–540. doi: 10.1016/j.carbpol.2015.08.017

Lasseguette E (2008) Grafting onto microfibrils of native cellulose. *Cellulose* 15:571–580 . doi: 10.1007/s10570-008-9200-1

Lataye DH, Mishra IM, Mall ID (2006) Removal of pyridine from aqueous solution by adsorption on bagasse fly ash. *Ind Eng Chem Res* 45:3934–3943. doi: 10.1021/ie051315w

Lavoine, N., Desloges, I., Dufresne, A., & Bras, J. (2012). Microfibrillated cellulose – Its barrier properties and applications in cellulosic materials: A review. *Carbohydrate Polymers*, 90(2), 735–764. <https://doi.org/10.1016/j.carbpol.2012.05.026>

Leavitt SW, Danzer SR (1993) Method for batch processing small wood samples to holocellulose for stable-carbon isotope analysis. *Anal Chem* 65:87–89. doi: 10.1021/ac00049a017

Lee, B.-M., Jeun, J.-P., Kang, P.-H., Choi, J.-H., & Hong, S.-K. (2017). Isolation and characterization of nanocrystalline cellulose from different precursor materials. *Fibers and Polymers*, 18(2), 272–277. <https://doi.org/10.1007/s12221-017-6548-6>

Li J, Gellerstedt G, Toven K (2009) Steam explosion lignins; their extraction, structure and potential as feedstock for biodiesel and chemicals. *Bioresour Technol* 100:2556–2561 . doi: 10.1016/j.biortech.2008.12.004

Li W, Zhang Y, Li J, et al. (2015) Characterization of cellulose from banana pseudo-stem by heterogeneous liquefaction. *Carbohydr Polym* 132:513–519. doi: 10.1016/j.carbpol.2015.06.066

Li W, Zhao X, Liu S (2013) Preparation of entangled nanocellulose fibers from APMP and its magnetic functional property as matrix. *Carbohydr Polym* 94:278–285 . doi: 10.1016/j.carbpol.2013.01.052

Lichtenstein K, Lavoine N (2017) Toward a deeper understanding of the thermal degradation mechanism of nanocellulose. *Polym Degrad Stab* 146:53–60 . doi: 10.1016/j.polymdegradstab.2017.09.018

Lichtenstein, K., & Lavoine, N. (2017). Toward a deeper understanding of the thermal degradation mechanism of nanocellulose. *Polymer Degradation and Stability*, 146, 53–60. <https://doi.org/10.1016/j.polymdegradstab.2017.09.018>

Lif A, Stenstad P, Syverud K, et al (2010) Fischer-Tropsch diesel emulsions stabilised by microfibrillated cellulose and nonionic surfactants. *J Colloid Interface Sci* 352:585–592 . doi: 10.1016/j.jcis.2010.08.052

Liu C, Li B, Du H, et al (2016) Properties of nanocellulose isolated from corncob residue using sulfuric acid, formic acid, oxidative and mechanical methods. *Carbohydr Polym* 151:716–724 . doi: 10.1016/j.carbpol.2016.06.025

Liu C-F, Ren J-L, Xu F, et al. (2006) Isolation and characterization of cellulose obtained from ultrasonic irradiated sugarcane bagasse. *J Agric Food Chem* 54:5742–5748. doi: 10.1021/jf060929o

López-Carballo G, Higuera L, Gavara R, Hernández-Muñoz P (2013) Silver Ions Release from Antibacterial Chitosan Films Containing in Situ Generated Silver Nanoparticles. *J Agric Food Chem* 61:260–267 . doi: 10.1021/jf304006y

Lu H, Gui Y, Zheng L, Liu X (2013) Morphological, crystalline, thermal and physicochemical properties of cellulose nanocrystals obtained from sweet potato residue. *Food Res Int* 50:121–128. doi: 10.1016/j.foodres.2012.10.013

Lu Q, Tang L, Lin F, et al. (2014) Preparation and characterization of cellulose nanocrystals via ultrasonication-assisted FeCl₃-catalyzed hydrolysis. *Cellulose* 21:3497–3506. doi: 10.1007/s10570-014-0376-2

Ludueña, L. N., Vecchio, A., Stefani, P. M., & Alvarez, V. A. (2013). Extraction of cellulose nanowhiskers from natural fibers and agricultural byproducts. *Fibers and Polymers*, 14(7), 1118–1127. <https://doi.org/10.1007/s12221-013-1118-z>

Luzi F, Fortunati E, Puglia D, et al. (2014) Optimized extraction of cellulose nanocrystals from pristine and carded hemp fibres. *Ind Crops Prod* 56:175–186. doi: 10.1016/j.indcrop.2014.03.006

Maestri CA, Abrami M, Hazan S, et al (2017) Role of sonication pre-treatment and cation valence in the sol-gel transition of nano-cellulose suspensions. *Sci Rep* 7:11129 . doi: 10.1038/s41598-017-11649-4

Malucelli LC, Lacerda LG, Dziedzic M, da Silva Carvalho Filho MA (2017) Preparation, properties and future perspectives of nanocrystals from agro-industrial residues: a review of recent research. *Rev Environ Sci Bio/Technology* 16:131–145. doi: 10.1007/s11157-017-9423-4

Mandal A, Chakrabarty D (2011) Isolation of nanocellulose from waste sugarcane bagasse (SCB) and its characterization. *Carbohydr Polym* 86:1291–1299.

Maran JP, Priya B (2015) Ultrasound-assisted extraction of pectin from sisal waste. *Carbohydr Polym* 115:732–738. doi: 10.1016/j.carbpol.2014.07.058

Mazeau K (2015) The hygroscopic power of amorphous cellulose: A modeling study. *Carbohydr Polym* 117:585–591. doi: 10.1016/j.carbpol.2014.09.095

Melo BC, Paulino FAA, Cardoso VA, et al (2018) Cellulose nanowhiskers improve the methylene blue adsorption capacity of chitosan-g-poly(acrylic acid) hydrogel. *Carbohydr Polym* 181:358–367 . doi: 10.1016/j.carbpol.2017.10.079

Miranda MIG, Bica CID, Nachtigall SMB, et al. (2013) Kinetic thermal degradation study of maize straw and soybean hull celluloses by simultaneous DSC–TGA and MDSC techniques. *Thermochim Acta* 565:65–71. doi: 10.1016/j.tca.2013.04.012

Mishra SP, Manent A-S, Chabot B, Daneault C (2012) The Use of Sodium Chlorite in Post-Oxidation of TEMPO-Oxidized Pulp: Effect on Pulp Characteristics and Nanocellulose Yield. *J Wood Chem Technol* 32:137–148 . doi: 10.1080/02773813.2011.624666

Mishra, S. P., Manent, A.-S., Chabot, B., & Daneault, C. (2012). Production of nanocellulose from native cellulose - various options utilizing ultrasound. *Bioresources*, 7(1), 422–436.

Mishra, S. P., Thirree, J., Manent, A., & Chabot, B. (2011). Ultrasound-catalyzed tempo-mediated oxidation of native cellulose for the production of nanocellulose: effect of process variables, 6(Brown 2010), 121–143.

Missoum K, Bras J, Belgacem MN (2012) Organization of aliphatic chains grafted on nanofibrillated cellulose and influence on final properties. *Cellulose* 19:1957–1973 . doi: 10.1007/s10570-012-9780-7

Missoum, K., Bras, J., & Belgacem, M. N. (2012). Water Redispersible Dried Nanofibrillated Cellulose by Adding Sodium Chloride. *Biomacromolecules*, 13(12), 4118–4125. <https://doi.org/10.1021/bm301378n>

Mittal A, Katahira R, Donohoe BS, et al (2017) Alkaline Peroxide Delignification of Corn Stover. *ACS Sustain Chem Eng* 5:6310–6321 . doi: 10.1021/acssuschemeng.7b01424

Montanari S, Roumani M, Heux L, Vignon MR (2005) Topochemistry of Carboxylated Cellulose Nanocrystals Resulting from TEMPO-Mediated Oxidation. *Macromolecules* 38:1665–1671. doi: 10.1021/ma048396c

Moon, R. J., Martini, A., Nairn, J., Simonsen, J., & Youngblood, J. (2011). Cellulose nanomaterials review: structure, properties and nanocomposites. *Chemical Society Reviews*, 40(7), 3941–3994. <https://doi.org/10.1039/c0cs00108b>

Morais JPS, Rosa M de F, Filho M de sá M de S, et al. (2013) Extraction and characterization of nanocellulose structures from raw cotton linter. *Carbohydr Polym* 91:229–235.

Morán JI, Alvarez VA, Cyras VP, Vázquez A (2008) Extraction of cellulose and preparation of nanocellulose from sisal fibers. *Cellulose* 15:149–159. doi: 10.1007/s10570-007-9145-9

Morán, J. I., Alvarez, V. A., Cyras, V. P., & Vázquez, A. (2008). Extraction of cellulose and preparation of nanocellulose from sisal fibers. *Cellulose*, 15(1), 149–159. <https://doi.org/10.1007/s10570-007-9145-9>

Moriana R, Vilaplana F, Ek M (2015) Forest residues as renewable resources for bio-based polymeric materials and bioenergy: chemical composition, structure and thermal properties. *Cellulose* 22:3409–3423 . doi: 10.1007/s10570-015-0738-4

Muthulakshmi L, Rajini N, Nellaiah H, et al (2017) Experimental Investigation of Cellulose/Silver Nanocomposites Using In Situ Generation Method. *J Polym Environ* 25:1021–1032 . doi: 10.1007/s10924-016-0871-7

Ogundare SA, van Zyl WE (2018) Nanocrystalline cellulose as reducing- and stabilizing agent in the synthesis of silver nanoparticles: Application as a surface-enhanced Raman scattering (SERS) substrate. *Surfaces and Interfaces* 13:1–10 . doi: 10.1016/j.surfin.2018.06.004

Okita Y, Fujisawa S, Saito T, Isogai A (2011) TEMPO-Oxidized Cellulose Nanofibrils Dispersed in Organic Solvents. *Biomacromolecules* 12:518–522 . doi: 10.1021/bm101255x

Okita Y, Saito T, Isogai A (2010) Entire surface oxidation of various cellulose microfibrils by TEMPO mediated oxidation. 1696–1700

Okita, Y., Saito, T., & Isogai, A. (2010). Entire Surface Oxidation of Various Cellulose Microfibrils by TEMPO-Mediated Oxidation. *Biomacromolecules*, 11(6), 1696–1700. <https://doi.org/10.1021/bm100214b>

Osong SH, Norgren S, Engstrand P (2016) Processing of wood-based microfibrillated cellulose and nanofibrillated cellulose , and applications relating to papermaking : a review. *Cellulose* 23:93–123 . doi: 10.1007/s10570-015-0798-5

Ouchi, A. (2008). Efficient total halogen-free photochemical bleaching of kraft pulps using alkaline hydrogen peroxide. *Journal of Photochemistry and Photobiology A: Chemistry*, 200(2–3), 388–395. <https://doi.org/10.1016/j.jphotochem.2008.09.006>

Oudiani, a. El, Chaabouni, Y., Msahli, S., & Sakli, F. (2011). Crystal transition from cellulose I to cellulose II in NaOH treated *Agave americana* L. fibre. *Carbohydrate Polymers*, 86(3), 1221–1229. <https://doi.org/10.1016/j.carbpol.2011.06.037>

Ovalle-Serrano SA, Blanco-Tirado C, Combariza MY (2013) Síntesis in situ de nanopartículas de plata sobre fibras de Fique. *Rev Colomb Química* 42:30–37.

Ovalle-Serrano SA, Blanco-Tirado C, Combariza MY (2018a) Exploring the composition of raw and delignified Colombian fique fibers, tow and pulp. *Cellulose* 25:151–165 . doi: 10.1007/s10570-017-1599-9

Ovalle-Serrano SA, Carrillo VS, Blanco-Tirado C, et al. (2015) Controlled synthesis of ZnO particles on the surface of natural cellulosic fibers: effect of concentration, heating and sonication. *Cellulose* 22:1841–1852. doi: 10.1007/s10570-015-0620-4

Ovalle-Serrano SA, Gómez FN, Blanco-Tirado C, Combariza MY (2018b) Isolation and characterization of cellulose nanofibrils from Colombian Fique decortication by-products. *Carbohydr Polym* 189:169–177 . doi: 10.1016/j.carbpol.2018.02.031

Ovalle-Serrano, S. A., Blanco-Tirado, C., & Combariza, M. Y. (2018). Exploring the composition of raw and delignified Colombian Fique fibers, tow and pulp. *Cellulose*, 25(1), 151–165. <https://doi.org/10.1007/s10570-017-1599-9>

Peinado, J. E., Ospina, L. F., Rodríguez, L., Miller, J., Carvajal, C., & Negrete, R. (2006). *Guía Ambiental del Subsector Fiquero*. Bogotá: Cadena Productiva Nacional del Fique.

Perez-Pimienta J a., Lopez-Ortega MG, Chavez-Carvayar J a., et al. (2015) Characterization of agave bagasse as a function of ionic liquid pretreatment. *Biomass and Bioenergy* 75:180–188. doi: 10.1016/j.biombioe.2015.02.026

Perez-Pimienta JA, Poggi-Varaldo HM, Ponce-Noyola T, et al (2016) Fractional pretreatment of raw and calcium oxalate-extracted agave bagasse using ionic liquid and alkaline hydrogen peroxide. *Biomass and Bioenergy* 91:48–55 . doi: 10.1016/j.biombioe.2016.05.001

Pretsch, E., Bühlmann, P., & Badertscher, M. (2009). Structure Determination of Organic Compounds. *Structure Determination of Organic Compounds: Tables of Spectral Data*. Berlin, Heidelberg: Springer Berlin Heidelberg. <https://doi.org/10.1007/978-3-540-93810-1>

Prozil SO, Evtuguin D V, Lopes LPC (2012) Chemical composition of grape stalks of *Vitis vinifera* L. from red grape pomaces. *Ind Crops Prod* 35:178–184. doi: 10.1016/j.indcrop.2011.06.035

Puangsin, B., Yang, Q., Saito, T., & Isogai, A. (2013). Comparative characterization of TEMPO-oxidized cellulose nanofibril films prepared from non-wood resources. *International Journal of Biological Macromolecules*, 59, 208–213. <https://doi.org/10.1016/j.ijbiomac.2013.04.016>

Quintero, M., Castro, L., Ortiz, C., Guzmán, C., & Escalante, H. (2012). Enhancement of starting up anaerobic digestion of lignocellulosic substrate: Figue's bagasse as an example. *Bioresource Technology*, 108, 8–13. <https://doi.org/10.1016/j.biortech.2011.12.052>

Ramadoss G, Muthukumar K (2014) Ultrasound assisted ammonia pretreatment of sugarcane bagasse for fermentable sugar production. *Biochem Eng J* 83:33–41. doi: 10.1016/j.bej.2013.11.013

Ramadoss, G., & Muthukumar, K. (2015). Influence of dual salt on the pretreatment of sugarcane bagasse with hydrogen peroxide for bioethanol production. *Chemical Engineering Journal*, 260, 178–187. <https://doi.org/10.1016/j.cej.2014.08.006>

Ramadoss, G., & Muthukumar, K. (2016). Mechanistic study on ultrasound assisted pretreatment of sugarcane bagasse using metal salt with hydrogen peroxide for bioethanol production. *Ultrasonics Sonochemistry*, 28, 207–217. <https://doi.org/10.1016/j.ultsonch.2015.07.006>

Rattaz, A., Mishra, S. P., Chabot, B., & Daneault, C. (2011). Cellulose nanofibres by sonocatalysed-TEMPO-oxidation. *Cellulose*, 18(3), 585–593. <https://doi.org/10.1007/s10570-011-9529-8>

Rehman N, de Miranda MIG, Rosa SML, et al. (2013) Cellulose and Nanocellulose from Maize Straw: An Insight on the Crystal Properties. *J Polym Environ* 22:252–259. doi: 10.1007/s10924-013-0624-9

Renard CMGC, Rohou Y, Hubert C, et al. (1997) Bleaching of Apple Pomace by Hydrogen Peroxide in Alkaline Conditions: Optimisation and Characterisation of the Products. *LWT - Food Sci Technol* 30:398–405. doi: 10.1006/fstl.1996.0195

Rohaizu, R., & Wanrosli, W. D. (2017). Sono-assisted TEMPO oxidation of oil palm lignocellulosic biomass for isolation of nanocrystalline cellulose. *Ultrasonics Sonochemistry*, 34, 631–639. <https://doi.org/10.1016/j.ultsonch.2016.06.040>

Saito T, Isogai A (2004) TEMPO-Mediated Oxidation of Native Cellulose. The Effect of Oxidation Conditions on Chemical and Crystal Structures of the Water-Insoluble Fractions. *Biomacromolecules* 5:1983–1989 . doi: 10.1021/bm0497769

Saito T, Kimura S, Nishiyama Y, Isogai A (2007) Cellulose Nanofibers Prepared by TEMPO-Mediated Oxidation of Native Cellulose. *Biomacromolecules* 8:2485–2491 . doi: 10.1021/bm0703970

Saito T, Okita Y, Nge TT, et al (2006) TEMPO-mediated oxidation of native cellulose: Microscopic analysis of fibrous fractions in the oxidized products. *Carbohydr Polym* 65:435–440 . doi: 10.1016/j.carbpol.2006.01.034

Saito, T., & Isogai, A. (2004). TEMPO-Mediated Oxidation of Native Cellulose. The Effect of Oxidation Conditions on Chemical and Crystal Structures of the Water-Insoluble Fractions. *Biomacromolecules*, 5(5), 1983–1989. <https://doi.org/10.1021/bm0497769>

Saito, T., Kimura, S., Nishiyama, Y., & Isogai, A. (2007). Cellulose Nanofibers Prepared by TEMPO-Mediated Oxidation of Native Cellulose. *Biomacromolecules*, 8(8), 2485–2491. <https://doi.org/10.1021/bm0703970>

Saito, T., Nishiyama, Y., Putaux, J.-L., Vignon, M., & Isogai, A. (2006). Homogeneous Suspensions of Individualized Microfibrils from TEMPO-Catalyzed Oxidation of Native Cellulose. *Biomacromolecules*, 7(6), 1687–1691. <https://doi.org/10.1021/bm060154s>

Salas C, Nypelö T, Rodriguez-Abreu C, et al (2014) Nanocellulose properties and applications in colloids and interfaces. *Curr Opin Colloid Interface Sci* 19:383–396 . doi: 10.1016/j.cocis.2014.10.003

Santos JDG, Espeleta AF, Branco A, de Assis SA (2013) Aqueous extraction of pectin from sisal waste. *Carbohydr Polym* 92:1997–2001. doi: 10.1016/j.carbpol.2012.11.089

Satyanarayana KG, Flores-Sahagun THS, Dos Santos LP, et al. (2013) Characterization of blue agave bagasse fibers of Mexico. *Compos Part A Appl Sci Manuf* 45:153–161. doi: 10.1016/j.compositesa.2012.09.001

Sèbe, G., Ham-Pichavant, F., Ibarboure, E., Koffi, A. L. C., & Tingaut, P. (2012). Supramolecular structure characterization of cellulose II nanowhiskers produced by acid hydrolysis of cellulose I substrates. *Biomacromolecules*, 13(2), 570–8. <https://doi.org/10.1021/bm201777j>

Segal L, Creely JJ, Martin AE, Conrad CM (1959) An Empirical Method for Estimating the Degree of Crystallinity of Native Cellulose Using the X-Ray Diffractometer. *Text Res J* 29:786–794. doi: 10.1177/004051755902901003

Senthil Muthu Kumar T, Rajini N, Obi Reddy K, et al (2018) All-cellulose composite films with cellulose matrix and Napier grass cellulose fibril fillers. *Int J Biol Macromol* 112:1310–1315 . doi: 10.1016/j.ijbiomac.2018.01.167

Silkin PP, Ekimova NV (2012) Relationship of strontium and calcium concentrations with the parameters of cell structure in Siberian spruce and fir tree-rings. *Dendrochronologia* 30:189–194. doi: 10.1016/j.dendro.2011.06.003

Silva FDA, Chawla N, Filho RDDT (2008) Tensile behavior of high performance natural (sisal) fibers. *Compos Sci Technol* 68:3438–3443. doi: 10.1016/j.compscitech.2008.10.001

Smith KC, Edionwe E, Michel B (2010) Conductimetric titrations: A predict-observe-explain activity for general chemistry. *J Chem Educ* 87:1217–1221 . doi: 10.1021/ed100538q

Stelte W, Sanadi AR (2009) Preparation and Characterization of Cellulose Nanofibers from Two Commercial Hardwood and Softwood Pulps. *Ind Eng Chem Res* 48:11211–11219 . doi: 10.1021/ie9011672

Su Y, Du R, Guo H, et al (2015) Fractional pretreatment of lignocellulose by alkaline hydrogen peroxide: Characterization of its major components. *Food Bioprod Process* 94:322–330 . doi: 10.1016/j.fbp.2014.04.001

Subhedar PB, Gogate PR (2014) Alkaline and ultrasound assisted alkaline pretreatment for intensification of delignification process from sustainable raw-material. *Ultrason Sonochem* 21:216–25. doi: 10.1016/j.ultsonch.2013.08.001

Sul'man EM, Sul'man MG, Prutenskaya EA (2011) Effect of ultrasonic pretreatment on the composition of lignocellulosic material in biotechnological processes. *Catal Ind* 3:28–33. doi: 10.1134/S2070050411010120

Sun JX, Sun R, Sun XF, Su Y (2004) Fractional and physico-chemical characterization of hemicelluloses from ultrasonic irradiated sugarcane bagasse. *Carbohydr Res* 339:291–300. doi: 10.1016/j.carres.2003.10.027

Sun R, Tomkinson J (2002) Comparative study of lignins isolated by alkali and ultrasound-assisted alkali extractions from wheat straw. *Ultrason Sonochem* 9:85–93. doi: 10.1016/S1350-4177(01)00106-7

Sun RC, Fang JM, Tomkinson J (2000) Delignification of rye straw using hydrogen peroxide. *Ind Crops Prod* 12:71–83. doi: 10.1016/S0926-6690(00)00039-X

Sundaram V, Muthukumarappan K, Kamireddy SR (2015) Effect of ammonia fiber expansion (AFEX™) pretreatment on compression behavior of corn stover, prairie cord grass and switchgrass. *Ind Crops Prod* 74:45–54 . doi: 10.1016/j.indcrop.2015.04.027

Tang L, Tang F, Li M, Li L (2018) Facile synthesis of Ag@AgCl-contained cellulose hydrogels and their application. *Colloids Surfaces A Physicochem Eng Asp* 553:618–623 . doi: 10.1016/j.colsurfa.2018.06.016

Tang Z, Li W, Lin X, et al (2017) TEMPO-Oxidized cellulose with high degree of oxidation. *Polymers (Basel)* 9:3–4 . doi: 10.3390/polym9090421

Ten, E., Jiang, L., & Wolcott, M. P. (2012). Strategies for Preparation of Oriented Cellulose Nanowhiskers Composites. In ACS Symposium Series (Vol. 1107, pp. 17–36). <https://doi.org/10.1021/bk-2012-1107.ch002>

Teow YH, Kam LM, Mohammad AW (2018) Synthesis of cellulose hydrogel for copper (II) ions adsorption. *J Environ Chem Eng* 6:4588–4597 . doi: 10.1016/j.jece.2018.07.010

Thoniyot P, Tan MJ, Karim AA, et al (2015) Nanoparticle-Hydrogel Composites: Concept, Design, and Applications of These Promising, Multi-Functional Materials. *Adv Sci* 2:1400010 . doi: 10.1002/advs.201400010

Tojo G, Fernández M (2007) Oxidation of primary alcohols to carboxylic acids: a guide to current common practice

Trinh ND, Nguyen TTB, Nguyen TH (2015) Preparation and characterization of silver chloride nanoparticles as an antibacterial agent. *Adv Nat Sci Nanosci Nanotechnol* 6:1–6 . doi: 10.1088/2043-6262/6/4/045011

Wada M, Kondo T, Okano T (2003) Thermally Induced Crystal Transformation from Cellulose I[alpha] to I[beta]. *Polym J* 35:155–159 . doi: 10.1295/polymj.35.155

Wang B, Wang X, Feng H (2010) Deconstructing recalcitrant Miscanthus with alkaline peroxide and electrolyzed water. *Bioresour Technol* 101:752–760 . doi: 10.1016/j.biortech.2009.08.063

Wang, B., Sain, M., & Oksman, K. (2007). Study of Structural Morphology of Hemp Fiber from the Micro to the Nanoscale. *Applied Composite Materials*, 14(2), 89–103. <https://doi.org/10.1007/s10443-006-9032-9>

Wen JL, Sun SL, Yuan TQ, et al. (2013) Structural elucidation of lignin polymers of eucalyptus chips during organosolv pretreatment and extended delignification. *J Agric Food Chem* 61:11067–11075. doi: 10.1021/jf403717q

Wertz, J. L., Bédué, O., & Mercier, J. P. (2010). Structure and Properties of Cellulose. In *Cellulose Science and Technology* (pp. 87–140). EPFL Press. Retrieved from <http://books.google.pt/books?id=XI4nfkRyfGQC>

Wicaksono, R., Syamsu, K., Yuliasih, I., & Nasir, M. (2013). Cellulose Nanofibers from Cassava Bagasse: Characterization and Application on Tapioca-Film. *Chemistry and Materials Research*, 3(13), 79–87.

Williams DR, Nishitani K (1980) A mild oxidation of aldehydes to α,β -unsaturated aldehydes. *Tetrahedron Lett* 21:4417–4420 . doi: 10.1016/S0040-4039(00)92188-9

Wójciak A, Kasprzyk H, Sikorska E, et al. (2014) FT-Raman, FT-infrared and NIR spectroscopic characterization of oxygen-delignified kraft pulp treated with hydrogen peroxide under acidic and alkaline conditions. *Vib Spectrosc* 71:62–69. doi: 10.1016/j.vibspec.2014.01.007

Xiang Q, Lee YY (2000) Oxidative Cracking of Precipitated Hardwood Lignin by Hydrogen Peroxide. *Appl Biochem Biotechnol* 84–86:153–162 . doi: 10.1385/ABAB:84-86:1-9:153

Xu Y, Kawata S, Hosoi K, et al (2009) Thermomechanical properties of the silanized-kenaf/polystyrene composites. *Express Polym Lett* 3:657–664 . doi: 10.3144/expresspolymlett.2009.82

Yang H (2011) Investigation and characterization of oxidized cellulose and cellulose nanofiber films

Yang H, Yan R, Chen H, et al (2007) Characteristics of hemicellulose, cellulose and lignin pyrolysis. *Fuel* 86:1781–1788 . doi: 10.1016/j.fuel.2006.12.013

Yao Q, Fan B, Xiong Y, et al (2017) Stress sensitive electricity based on Ag/cellulose nanofiber aerogel for self-reporting. *Carbohydr Polym* 168:265–273 . doi: 10.1016/j.carbpol.2017.03.089

Yu H, You Y, Lei F, et al. (2015) Comparative study of alkaline hydrogen peroxide and organosolv pretreatments of sugarcane bagasse to improve the overall sugar yield. *Bioresour Technol* 187:161–166. doi: 10.1016/j.biortech.2015.03.123

Zhu C, Xue J, He J (2009) Controlled In-Situ Synthesis of Silver Nanoparticles in Natural Cellulose Fibers Toward Highly Efficient Antimicrobial Materials. *J Nanosci Nanotechnol* 9:3067–3074 . doi: 10.1166/jnn.2009.212